INVESTIGATING THE CHARGE SEPARATION AND TRANSPORT IN IRON BASED PHOTOANODES FOR SOLAR-DRIVEN WATER SPLITTING

PRINCE SAURABH BASSI

SCHOOL OF MATERIALS SCIENCE AND ENGINEERING

2015

INVESTIGATING THE CHARGE SEPARATION AND TRANSPORT IN IRON BASED PHOTOANODES FOR SOLAR-DRIVEN WATER SPLITTING

PRINCE SAURABH BASSI

School of Materials Science and Engineering

A thesis submitted to the Nanyang Technological University in partial fulfilment of the requirement for the degree of Doctor of Philosophy

2015

Abstract

Solar fuel production using Photoelectrochemical Cell has developed after Fujishima and Honda demonstrated in 1972, for the first time, solar water splitting using Titanium Dioxide (TiO_2) as photoanode. After that, efforts have been made to employ cheap, abundant and non-toxic semiconducting materials as photoanodes and to improve overall efficiency and performance of PEC devices. In the last decade, hematite (α-Fe_2O_3) based PEC devices have attracted many scientists in exploiting its advantages like good visible light absorption and stability but the efficiency achieved (only 1-2%) is still far from the theoretical limit of Solar-to-Hydrogen (STH) efficiency (15%). This is due to the limitations of hematite like small minority carrier diffusion length, poor charge transport properties, slow water oxidation kinetics etc. To counter this, hematite nanostructures with elemental doping are used in PEC devices and are thermally activated through sintering at high temperature to achieve significant photocurrent. But high temperature annealing also deforms the substrate morphology which in turn degrades the conductivity and hence trade-offs with overall performance of PEC device.

Here, we have demonstrated annealing profile which proves optimal in tackling bulk recombination and simultaneously keeping intact the crystallinity of Fe_2O_3 nanorods and conductivity of FTO substrates. Through measurements performed under frontside and backside illumination, we have shown electron transport drives the photocurrent under backside illumination for the optimized annealing profile. To inhibit the surface recombination probability, we employed surface passivation technique by coating hematite nanorods with a very thin Atomic Layer Deposition (ALD) grown TiO_x overlayer which resulted in manifold enhancement in its performance.

Owing to inability of Fe_2O_3 to reduce water due to its lower conduction band level than the water reduction potential, iron based photoanodes based on Fe-Ti-O systems were explored. Crystalline nanoporous single phase Fe_2TiO_5 (without secondary phases) thin films are obtained and characterized for the first time. This material is stable in water and has a bandgap suitable for visible light absorption (2.1eV). Using XPS, the work function was calculated to lay around 4.77 eV with respect to vacuum level and the conduction band is estimated to lie or higher than water reduction level based on XPS data. Hall measurement showed a mobility of around 6 $cm^{-2}V^{-1}s^{-1}$ which demonstrate good charge transport properties of Fe_2TiO_5 thin films.

To enhance charge separation and transport in pristine Fe_2O_3 nanorods, it was coupled with Fe_2TiO_5 thin films to form a Fe_2O_3/Fe_2TiO_5 heterojunction, which according to their band level positions share a type II band alignment. Synthesized using low-cost hydrothermal technique, these heterojunction films show high photocurrent, reaching 1.4 mA/cm^2, as compared to pristine Fe_2O_3 and Fe_2TiO_5 films. Characterization techniques like impedance spectroscopy and PEC characterization with hole scavenger revealed the charge dynamics of the system. It is proposed that surface mediated water oxidation was enhanced for the heterojunction films which allowed firstly the trapping of holes in the surface states and secondly facile transfer of these holes into the electrolyte for water oxidation. In sum, the favorable band alignment and the improvement in catalytic activity due to integration of Fe_2TiO_5 film with Fe_2O_3 nanorods was beneficial in providing low onset voltages and higher photocurrent density for heterojunction based PEC devices.

Acknowledgements

First and foremost, I would like to pay my deepest gratitude to my supervisor, Associate Professor Lydia Helena Wong for her invaluable guidance throughout the progress of my research work. She motivated me to pursue research ideas and enthusiastically supported me in every stage of my PhD. In addition to her advice and wisdom in defining the project direction, her calm demeanor and optimistic attitude enthused and inspired me throughout my studies at NTU. It has been a great experience to learn and work with her.

I am grateful to Prof. James Barber whose research acumen, humility and enthusiasm always inspire me to become a good scientist and a better person. I am grateful to Dr. Xi Lifei with whom I worked and developed a strong understanding of research work just after joining NTU. I would like to thank Dr. Rajini and Gurudayal with whom I have shared fruitful discussions and insight into research. I would like to thank my colleagues Dr. Hu Peng, Dr. Phong, Dr. Fang Jun, Dr. Chao, Dr. Jian, Chen Yang, Chee Keong, Rui Lin, Lisha, Yusen, Joel and Wang Zheng in Solar Fuels Lab who helped me in one way or the other while working in the laboratory. I am also thankful to my collaborators: Dr. Pablo, Dr. Xianglin, Dr. Yanan and Dr. Sing Yang. I would like to give my hearty wishes and gratitude to my friends Ankit, Anurag, Apoorva, Deepak, Manu, Prashant, Ravi, Sujit, Shantanu, Shailesh, Shrish, Varun, Venkat, Vipin, Vishal, Vishesh, Vivek and many more who stayed with me throughout this important phase of life and made my life in Singapore wonderful.☺

This thesis is dedicated to my family for their unconditional love and continuous encouragement during my research at NTU which motivated me to work harder to achieve this accomplishment.

Table of Contents

List of Figures

List of Abbreviations

PEC: Photoelectrochemical Cell

FTO: Fluorine Doped Tin Oxide

WE: Working Electrode

RE: Reference Electrode

CE: Counter Electrode

RHE: Reversible Hydrogen Electrode

E_{VAC}: Energy Level with respect to Vacuum Level

E_{NHE}: Energy Level with respect to Normal Hydrogen Electrode Level

Ec: Conduction Band Edge of a Semiconductor

Ev: Valence Band Edge of a Semiconductor

EDS: Energy Dispersive Spectroscopy

EIS: Electrochemical Impedance Spectroscopy

UPS: Ultraviolet Photoelectron Spectroscopy

XPS: X-Ray Photoelectron Spectroscopy

FESEM: Field Emission Scanning Electron Microscopy

HRTEM: High Resolution Transmission Electron Microscopy

IPCE: Incident Photon to Current Efficiency

PCE: Power Conversion Efficiency

Chapter 1.

Introduction

1.1 Background

Owing to great technological advancements in 21st Century, in spite of the many differences among developed and developing economies of this world, one issue which all of them share is the energy crisis. While developing countries are in dire need of energy to uplift their economy, developed countries need it to sustain their grown economy. Under pressure from the climate change community and limited availability of current non-renewable energy sources like fossil fuels, the world is looking for various renewable energy options. Among them it is believed that solar energy could pave the way to supply more than enough energy if utilized to its true potential. An extensive analysis of current energy needs and the huge contribution that solar power could make has been presented by MacKay [1]. It states the rate of current energy consumption by the global population, is around 16 Terawatts, averaged over a year, while the sun provides energy at an average annual rate of 120,000 Terawatts at the Earth's surface. There is no doubt that solar energy is available far in excess of the needs of mankind, but the challenge is to utilize it using low-cost manufacturing ways and store it by simple, cost effective and efficient methods on a large scale. Solar energy could be stored in the form of solar fuels which could be used anytime and can also be transported easily. Solar fuels could be produced using the process called artificial photosynthesis or solar water splitting which aims at utilizing solar energy to perform electrolysis on water to yield hydrogen gas, which is visualized as next form of clean energy.

Similar to natural photosynthesis, artificial photosynthesis also require solar light driven water splitting catalyst, or photoelectrode, to provide high energy electrons which can reduce protons to hydrogen or CO_2 to carbon-based energy molecules. These cathodic reduction reactions can be facilitated by many suitable catalysts [2]. Another reaction of water oxidation is also equally important for development of an artificial photosynthetic system. It is a kinetically (4 electron process) and thermodynamically difficult reaction, which need a minimum energy corresponding to a potential of 1.23 V vs Normal Hydrogen Electrode (NHE) at pH 0 [3]. However, various energy intermediates are involved in this multi-step oxygen evolution reaction which requires a significant overpotential [2-4].

One fascinating approach to replicate a photosynthetic light harvesting system integrated with a reaction center is by employing photoabsorbing semiconductors which generate charge carriers. Here, photon absorption leads to the formation of charge carriers as negatively charged electrons in the conduction and positively charged holes in the valence band of the semiconductor. For solar water splitting, water oxidation is mainly driven by photogenerated holes present in the valence band while the excited electrons in conduction band take part in reducing protons to hydrogen as represented by the following equations [5-7];

$$2H_2O + light \rightarrow 4H^+ + O_2 + 4e^- \qquad (1a)$$

$$4H^+ + 4e^- \rightarrow 2H_2 \qquad (1b)$$

Thus, photocatalytic water splitting constitutes four steps: (1) absorption of photons from the solar spectrum, (2) Generation of electron-hole pairs, (3) separation and stabilization of these pairs, and finally, (4) utilization of the separated charge carriers for hydrogen and oxygen evolution [2, 8]. A single photocatalyst material that can carry out all these steps efficiently would be the holy grail of this field [7]. In fact, till now it has been a challenge to find such material or system that can prove as efficient as natural photosynthesis. Such photocatalytic systems must have good stability in aqueous solutions, favourable band energies with respect to water redox levels, appreciable light absorption in visible range of solar spectrum, good conductivity, good thermodynamic stability and be robust, abundant and non-toxic. Appropriate band levels of a semiconductor would be such that could straddle water reduction and water oxidation levels. This means the valence band should have more positive value as compared to water oxidation (H_2O/O_2) and conduction band negative than water reduction (H_2O/H_2) level. There have been major developments in exploration of wide range of photocatalytic materials and optimization of their energy band configurations for different applications [2, 9-10]. Domen et al demonstrated synthesis and characterization of oxynitride materials with optimum band gaps and which can undergo both water oxidation and proton reduction reactions but with relatively low quantum yield of ~ 5-6% [11]. In many such types of photocatalytic systems, charge recombination can be very high due to poor charge separation which limits the photon-to-electron quantum yield. Hence, photoelectrochemical (PEC) cells with semiconductor/electrolyte interface or homojunctions/heterojunctions of two complementary semiconductors are more efficient due to presence of electric field or built in voltage due to band levels alignment which improves charge separation and hence limits the probability of recombination [6].

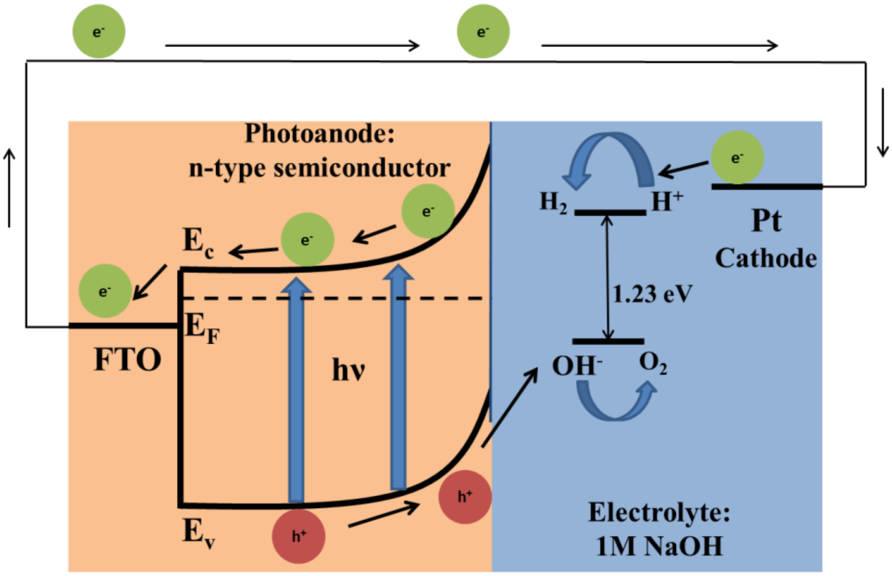

Figure 1.1.1 A Standard Photoelectrochemical Cell with an n-type semiconductor as a Working Photoanode for Solar Water Splitting

A typical PEC Cell with an n-type semiconductor as the photoanode (a working electrode) immersed in an electrolyte (generally 1M NaOH for oxide based photoanodes) is shown in **Figure 1.1.1.** A 3-electrode system is generally used in PEC with a reference electrode like Ag/AgCl or Saturated Calomel Electrode (SCE) and Counter electrode as a Platinum coil/mesh/wire. Once the working electrode i.e. n-type semiconductor is immersed in electrolyte, due to the difference in chemical potential of electrons in semiconductor and electrolyte or in other words, the difference in Fermi level of semiconductor and electrolyte, the transfer of electrons from semiconductor to electrolyte takes place. This results in a positive space charge layer formation also known as depletion region due to depletion of majority carriers from this region. This is the typical semiconductor-electrolyte interface or junction which defines the charge transfer phenomenon after the semiconductor layer is irradiated with simulated solar spectrum (AM 1.5G). This potential barrier allows the minority carrier injection into the electrolyte and provides electric field to facilitate movement of electrons into the back contact (here FTO). Electrons through outer circuit move to the counter electrode

(Pt) to reduce H^+ ions into H_2 whereas holes oxidize OH^- ions which evolve oxygen on the semiconductor-electrolyte surface.

In 1972, Fujishima and Honda discovered the hydrogen generation using TiO_2 as the photocatalyst in a PEC Cell [12]. After that discovery, the field of solar fuel production has developed immensely. Various photocatalytic and other hybrid material systems have been extensively studied for water splitting over the past decades and many good review papers have been published [2, 11, 13-20]. Other materials with better band gaps for water splitting like WO_3 [21-22], $BiVO_4$ [23-25] have also been studied in some depth. Of all the candidates studied as a photoanode in PEC, one of the most attractive and well researched is Hematite, Fe_2O_3 [19-20, 26-27] due to its remarkable performance as a photoanode in water splitting PEC cells. It has been extensively studied, due to its favourable band gap of 2.2 eV that allows wide absorption of visible part of solar spectrum, because it possess good aqueous stability and is low cost and abundant in nature [26]. Fe_2O_3 is theoretically estimated to achieve a water oxidation efficiency of 15% [14]. However, Solar-to-Hydrogen (STH) efficiencies reported for hematite are much lower due to the small hole diffusion length (2-4 nm), poor mobility/conductivity and slow oxygen evolution kinetics [27-29]. To achieve higher efficiencies, modification of hematite electrodes through nanostructuring [20, 30], elemental doping [31], surface modification with surface passivation layers [32-34] or introduction of cocatalysts [35-37] or by designing heterojunctions have been successful approaches in recent times [38].

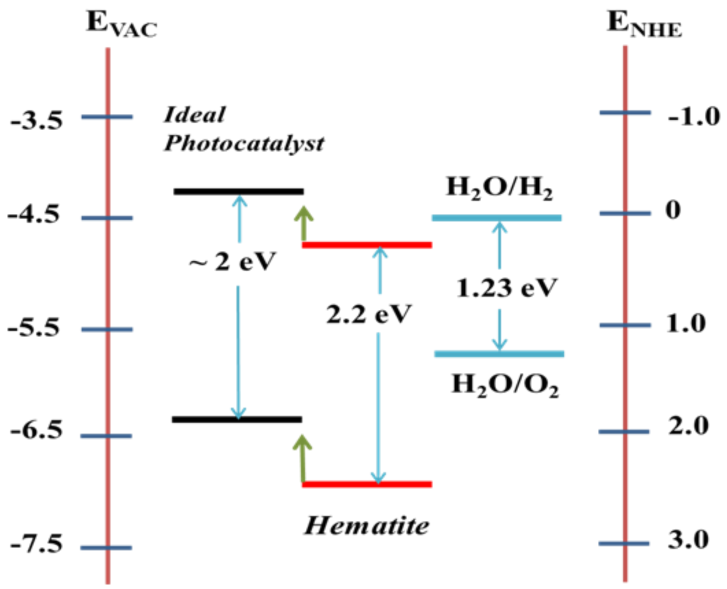

Figure 1.1.2 Schematic diagram of Band levels for Hematite and for an ideal photocatalyst for overall water splitting. Adapted from Bassi P.S.; Gurudayal; Wong L. H.; Barber J.; "Iron Based Photoanodes for Solar Fuel Production"; *Phys. Chem. Chem. Phys., 2014,16, 11834-11842*. Reproduced by permission of the PCCP Owner Societies

Although hematite is a good performing photoanode in terms of photocurrent and efficiency but it is still far from its maximum photocurrent of 12.5 mA/cm^2. Its band levels are also not favourable for hydrogen production which limits its prospect for bias free solar water splitting. Hence, there is a need to keep exploring for a more robust, abundant and non-toxic stable oxide-based photoanode (as shown in **Figure 1.1.2** as Ideal Photocatalyst) with better band positions and good charge transport properties for application in overall water splitting or PEC cell applications. A plethora of hybrid photocatalysts with appropriate band level positions have been developed with complex stoichiometry or anionic tailoring for solar water splitting [8, 11]. Kudo et al reported titanates and tantalates for solar water splitting [2]. There are some systems reported like Fe-Ti-O or Ti-V-O or Ti-Ni-O with optimum band gaps to be used in photocatalytic water splitting [39]. Hematite and TiO_2 are extensively used as photocatalysts and are abundant, non-toxic and inexpensive oxides. The hybrid of Fe_2O_3 and TiO_2 could be advantageous in tackling poor charge transport properties exhibited by hematite and low absorption of solar spectrum due to wide band gap of TiO_2. Hence, this Fe-Ti-O system comprising of many iron-titanates like $FeTiO_3$, Fe_2TiO_5 or $FeTi_2O_5$ is worth exploring as they could have favourable conduction band and valence band levels as compared to hematite [7, 40].

To improve charge separation or transport of a photoanode, various strategies could be employed. Bulk recombination could be tackled using nanostructuring of photoelectrodes and doping them with n-type elements[18]. Surface recombination occurring due to surface defects like dangling bonds, adsorbed ions, lattice disordering etc. could be inhibited by using surface overlayers or co-catalysts [41-42]. There are other techniques like heterojunction or tandem cells or Z-Schemes where the photoanode limitation is tackled using another complementary photoanode to enhance the overall performance of the PEC as compared to their individual counterparts [26, 43-44]. In Heterojunction, when two different semiconductor materials are coupled with each other, due to the difference in their respective valence and conduction band positions, a potential difference is developed between the two. This leads to electric field which could separate electrons and holes more efficiently and hence the performance of PEC devices.

In sum, there is a need to enhance the charge separation and transport of prevailing hematite photoanodes and to explore novel stable photoanodes with favorable band level positions and good charge transport properties. Strategies like nanostructuring, doping, surface treatment or heterojunction could then be employed on these photoanode systems to achieve overall higher performance in PEC Cells.

1.2 Thesis Objectives and Scopes

The objective of this work is to investigate and enhance charge transport and separation in pristine iron based photoanode materials for solar water oxidation. To fulfill these objectives, the scope of the thesis is as follows:

a) **Investigation of charge transport in Pristine and TiO_x Coated Hematite (Fe_2O_3) Nanorods as photoanode:** Hematite photoanodes on FTO substrates are thermally activated to achieve a significant photocurrent density. But there is a trade-off between crystallinity and conductivity of Fe_2O_3, and conductivity of FTO which reduces with high annealing temperature (>750°C) due to deformation in its morphology. A systematic study into the effect of annealing temperature of Fe_2O_3 based photoanodes would be done under different side of illumination to find the optimum annealing profile which can yield active and crystalline hematite nanorods based photoelectrode. Bulk/surface charge separation efficiency of differently annealed pristine Fe_2O_3 nanorods would be evaluated to observe the limiting factor of performance. Surface charge separation efficiency would be improved by passivating hematite nanorods with ALD grown TiO_x overlayer. Bulk/surface charge separation efficiency would then be evaluated to observe the change in efficiency after surface passivation.

b) **Introducing Iron Titanate (Fe_2TiO_5), with better band energetics than Fe_2O_3, as Photoanode:** It has been hypothesized that Fe-Ti-O systems could possess favorable band levels as compared to hematite. Hence, an air-stable phase Fe_2TiO_5, hybrid of Fe_2O_3 and TiO_2, with a band gap of 2.1 eV will be explored. Synthesis of nanoporous Fe_2TiO_5 thin films with feature size of 30-50 nm through low-cost hydrothermal technique is reported. Ultraviolet Photoelectron Spectroscopy (UPS) of pristine films to get an insight into band level positions and Hall Measurement to compare electron mobility and carrier concentration of Fe_2TiO_5 with Fe_2O_3 will also be performed. To improve the photocurrent density of pristine films, surface passivation using thin SnO_x overlayer will be performed and its characterization will be presented.

c) **Improving charge separation and transport by using Fe_2O_3/Fe_2TiO_5 Heterojunction as a photoanode:** From the determination of band level positions of Fe_2TiO_5 mentioned in last section, it was realized that integration of Fe_2O_3 and Fe_2TiO_5 could lead to type II band alignment which could lead to better charge separation and transport in Fe_2O_3 nanorods. Fe_2O_3/Fe_2TiO_5 heterojunction synthesized with varied reaction conditions would be demonstrated here and comparison of performance exhibited by heterojunction would be compared with its pristine constituents. To further improve photocurrent and onset potential, coupling of optimized heterojunction with CoO_x will be presented. Photoelectrochemical characterizations in presence of hole scavenger H_2O_2 and Electrochemical Impedance Spectroscopic Analysis would be utilized to get an insight into bulk/surface charge carrier efficiencies for heterojunction and pristine films and reason for better charge transfer kinetics in heterojunction thin films.

1.3 Thesis Organization

The thesis consists of 6 chapters. Chapter 1 introduces the field of solar water splitting and background of the materials commonly used as photoanodes in photoelectrochemical cells followed by the objective and scope of thesis. It then presents how the thesis is organized to investigate the problem of charge transport and separation in iron based photoanodes.

Chapter 2 discusses about the literature review of application of Hematite (Fe_2O_3) and Iron Titanate (Fe_2TiO_5) as a photoanode. It then presents surface passivation and introduction of heterojunction as the strategies to improve charge separation and transport which greatly affects in improving the performance of PEC devices. It also showcases a theoretical background of important measurements that are useful in understanding the internal dynamics of photoelectrochemical cell.

Chapter 3 includes methodology of preparation of photoanodes using techniques like hydrothermal techniques or spray techniques and their surface treatment by drop casting or Atomic Layer Deposition method. It also demonstrates details about material characterization of thin films and photoelectrochemical characterization of photoanodes to observe structural/morphological properties and performance of thin film electrodes.

In the first section of Chapter 4, the results and discussion of pristine and TiO_x coated Fe_2O_3 photoanodes characterized under front and back illumination are presented. In second section, it reports pristine Fe_2TiO_5 nanoporous thin films and SnO_x coated films as photoanode for solar water splitting. It then discusses the intrinsic (band level positons, electron mobility) and PEC characterization of Fe_2TiO_5 thin films. Finally, in the last section, Fe_2O_3/Fe_2TiO_5 Nano- heterojunctions synthesized and characterized as photoanodes are reported. Bulk/charge carrier separation efficiency and impedance spectroscopy results are discussed to propose the charge transport model owing to which the manifold enhancement in photocurrent was observed in these PEC devices.

Chapter 5 concludes the study of Fe_2O_3 nanorods, Fe_2TiO_5 nanoporous thin films and their heterojunction (Fe_2O_3/Fe_2TiO_5) based PEC devices presented in the thesis.

Chapter 6 presents the recommended future work, i.e. enhancing the performance of pristine Fe_2TiO_5 thin films and morphological improvement of Fe_2O_3/Fe_2TiO_5 Heterojunction

1.4 Thesis Contribution

The original contributions of thesis are as follows:

1. An investigative study into the effect of annealing temperature used in fabrication of pristine hematite nanorods and characterization under frontside and backside illumination for application as photoanodes in photoelectrochemical cell. A favorable annealing profile is proposed to avoid damage to FTO and achieve appreciable crystallinity of Fe_2O_3 nanorods which are a trade-off to achieve efficient electron transport.
2. Impact of surface passivating layer i.e. ALD grown TiO_x coating, on Fe_2O_3 nanorods in minimizing surface recombination, which is the limiting factor for pristine Fe_2O_3 nanorods.
3. Demonstration of the state-of-the-art material, Fe_2TiO_5, which is thermally stable, abundant, non-toxic, possesses good absorption band edge along-with favorable band level positioning with respect to water redox levels and shows appreciable charge transport properties. Synthesis of pure phase Fe_2TiO_5 nanoporous thin films through simple hydrothermal technique has been shown for the first time to the best of our knowledge. Morphological, Electrical, Spectroscopic and Photoelectrochemical Characterizations have been performed to highlight its intrinsic properties and to establish it as a promising photoanode for PEC.
4. A comprehensive study of Fe_2O_3/Fe_2TiO_5 Heterojunction between pristine Fe_2O_3 nanorods and Fe_2TiO_5 nanoporous thin films. Demonstration of influence of type II band alignment of two abundant, low-cost stable oxides to achieve thermal and aqueous stable heterojunction based photoanode with better charge separation and transport for application in PEC devices.

Chapter 2.

Literature Review

This chapter presents different aspects of application of iron based photoanodes for solar water splitting. **Section 2.1** covers the development of hematite as one of the most suitable candidates for use in PEC Cell. It presents tackling of bulk recombination through employment of nanostructuring and doping techniques. **Section 2.2** introduces another iron based photoanode namely pseudobrookite, Fe_2TiO_5 which could be a promising iron based photocatalyst for future applications in PEC devices. **Section 2.3** elaborates on the surface treatment of photoanodes which could prove beneficial in inhibiting surface recombination which is a major limiting factor in performance of porous electrodes. **Section 2.4** investigates on heterojunction photoelectrodes constituted of stable oxides possessing favorable band positions for improved charge separation and transport. Last **Section 2.5** briefly covers the theoretical background of photoelectrochemical measurements and the information extracted from them to get an insight into the performance of photoanodes.

2.1 Hematite as a Photoanode for Solar Water Splitting

Hematite, Fe_2O_3 is an abundant iron ore found which is abundant in the Earth's crust. It is a non-toxic, low cost, thermal and aqueous stable material with an optimum band gap energy which makes it a promising candidate for application as photocatalyst for solar water splitting [26]. Fe_2O_3 has a crystal structure similar to Al_2O_3, which is trigonal (hexagonal scalenohedral, $\overline{3}$ 2/m). It possesses space group R3c and lattice parameters of a = 5.0356 Å , c = 13.7489 Å , with six molecules per unit cell [26]. It is an n-type semiconductor with a band gap of 2.2 eV that covers most part of solar light spectrum. Its valence band level allows the oxidation of water whereas the conduction band positioning is not favourable for water reduction i.e. hydrogen evolution. Due to this, an external voltage bias is required to overcome this potential (~0.4V) for simultaneous oxygen and hydrogen evolution. Due to high recombination of photogenerated charge carriers in bulk and on the surface, the efficiencies reported are generally very low than their theoretical water splitting efficiency (~15%). This recombination plays an important role in limiting photocurrent density in hematite which can go to a theoretical maximum of 12.6mA/cm^2 [26]. Large bulk recombination in hematite is primarily due to its low minority carrier diffusion length (2-4 nm) and secondarily owing to its large absorption depth, the depth at which 63% photons get absorbed. These factors result in photons being absorbed outside thin space charge layer due to which majority of photons get dissipated before getting converted into charge carriers [26, 45]. Another major limitation of using hematite is the requirement for a voltage bias to overcome the overpotential required for water splitting. This is due to, firstly, the positioning of its conduction band level, which is positive by 0.4-0.5V to allow the reduction of water to hydrogen. Secondly, due to the slow hole transport across the semiconductor-electrolyte interface owing to its poor water oxidation kinetics, which eventually causes the accumulation of photogenerated holes near the semiconductor/electrolyte interface.

Owing to limitations mentioned above, most of the works reported on hematite use it as a working photoanode in PEC devices (as mentioned in **Section 1.1)** with an applied voltage bias in highly basic electrolyte (1M NaOH). This bias allows to overcome the drawbacks that hematite possesses. **Figure 2.1.1** shows the typical current density vs potential (J-V) plot for a photoanode, like hematite, in a PEC device with high onset potential (as compared to its flat band potential) and low plateau/saturation current denoted as black curve. Whereas a high efficiency photoanode based PEC cell (represented as red curve) would have a low onset potential and a high plateau current. The main emphasis of research on hematite as a photoanode is to minimize the gap between the two curves and emulate the red curve. To achieve this, various strategies have been employed as shown in **Figure 2.1.1** and discussed below.

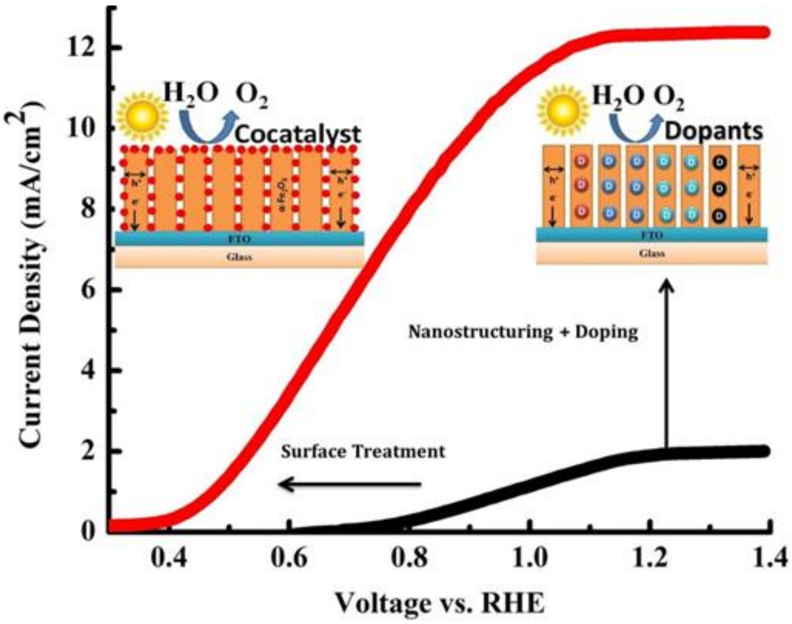

Figure 2.1.1 Desired performance (red) as compared to existing performance (black) for Hematite Photoanode. Adapted from Bassi P.S.; Gurudayal; Wong L. H.; Barber J.; "Iron Based Photoanodes for Solar Fuel Production"; *Phys. Chem. Chem. Phys., 2014, 16, 11834-11842*. Reproduced by permission of the PCCP Owner Societies

To enhance the plateau photocurrent, advancements in doping and nanostructuring is required, whereas to cathodically shift the onset potential, the improvement in surface properties of photoactive layer through surface treatments is needed. In the following section, different approaches in nanostructuring and doping, to improve the light absorption and photon-to-electron conversion efficiency will be discussed. To tackle another limitation of hematite i.e. the sluggish hole injection from semiconductor into the electrolyte which increases the overpotential, strategies like surface passivation with ultrathin thin metal oxide overlayer or integration with co-catalysts are employed which will be reviewed in subsequent section.

Influence of Nanostructuring in tackling Bulk Recombination in Fe_2O_3 photoanodes

As discussed earlier, the requirement for nanostructuring in hematite arises due to the trade-off between the low absorption coefficient, which needs 400-500 nm photoabsorbing films for complete solar spectrum absorption and the small minority carrier (hole) diffusion length (2-4nm) which need 5-10 nm of feature size (carrier harvesting width) for efficient hole injection into the electrolyte [18, 20, 46-47]. Therefore, nanowire/nanorod array with radii of 5-10 nm and length of 400-500 nm could be the ideal nanostructure which fulfil above criteria and is as shown schematically in **Figure 2.1.2.** With the same absorption depth of hematite for nanorods as for the planar film, the former could participate more efficiently in hole injection due to a small radial feature size and the proximity of the nanorod surface with electrolyte. This enhances the photocurrent density by inhibiting the bulk electron-hole recombination. It is notable that the introduction of cauliflower-like nanostructures by Graetzel et al renewed the interest in hematite [30]. Since then, immense efforts in nanostructuring of hematite have been reported which are very well documented by Sivula et al [26]. In this section, a brief review on the recent advancements in hematite nanostructuring for application in PEC device would be presented.

An important development in fabricating hematite nanorods on large area substrates has been the application of a simple solution-based hydrothermal technique for growing nanorods on fluorine-doped tin oxide (FTO) substrates [48-49]. The perpendicular alignment of one-dimensional nanorod arrays on FTO substrates in [110] direction is instrumental since the anisotropic conductivity along this direction has been found to be four fold higher as compared to that in the orthogonal direction which eventually enhances the electron transport along the nanrods and hence the photocurrent density [30].

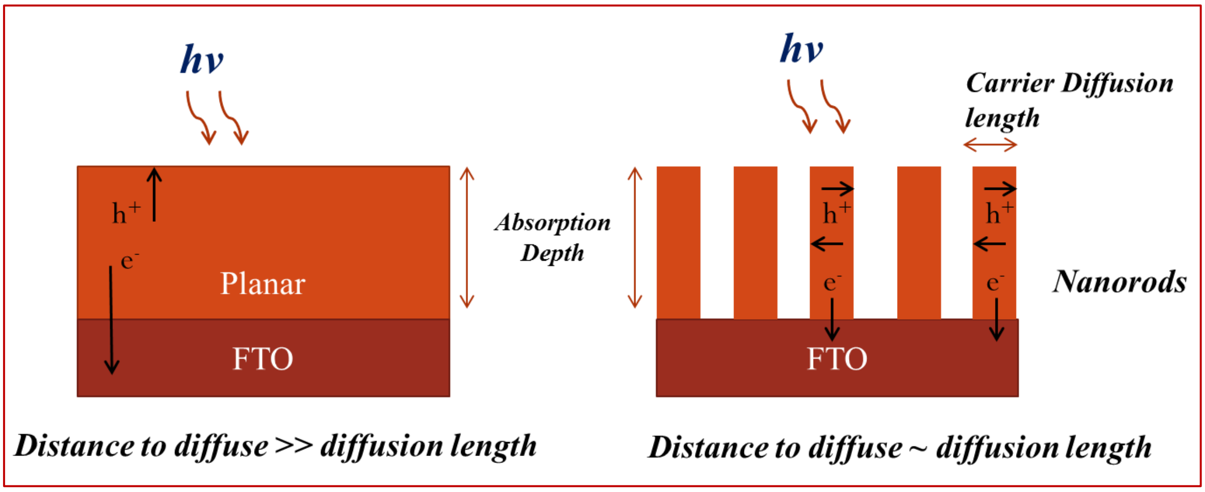

Figure 2.1.2 Schematic diagram of Planar Photoanode and Nanorods based Photoanode

Other reports on fabrication of hematite on large area substrates include thermal or plasma based oxidation of Fe foils into hematite [50-51] or the facile solution synthesis of α-$FeF_3 \cdot 3H_2O$ nanowires and their subsequent conversion to α-Fe_2O_3 nanowires [52]. Another influential strategy in nanostructuring is the development of branched/dendritic structures which enhance surface area of hematite nanorods or nanowires. The enhanced surface area exposed to electrolyte should increase the rate of injection of photogenerated holes into the electrolyte. Zheng et al demonstrated dendritic Fe_2O_3 nanowire arrays prepared by thermal oxidation of electrodeposited dendritic Fe nanowires [53]. In spite of the larger surface area in dendritic structure than the nanowires, the former showed lower photocurrent density than the other reported nanowires and nanotubes which could be due to higher electron/hole recombination probability or due to the presence of higher density of surface defects. These results highlight the trade-off associated with increasing surface area, i.e. increasing the probability of charge carrier separation while increasing the amount of surface defects which increases the surface recombination. Yang et al [54] reported a unique hematite photoanode composed of nano-branches of β-FeOOH on Ti-doped hematite nanorod array grown on an undoped hematite underlayer using hydrothermal technique. The combined Ti-doped nanorods and the underlayer structure enhanced the charge separation and lowered the onset potential. After employing β-FeOOH nano-branches, the photocurrent density further enhanced but the onset potential shifted positively due to increase in flat band potential as confirmed by Electrochemical Impedance Spectroscopic analysis. Deng et al demonstrated Ti-doped hematite nanostructures of an urchin-like morphology, which significantly enhanced the surface area as compared to untreated nanostructures [55]. A remarkable plateau photocurrent density of 3.76 mA/cm^2 was observed under standard AM 1.5G condition at 1.74V vs. RHE in 1M NaOH electrolyte, which was around 2.5 times higher as compared to pristine nanostructures (1.48 mA/cm^2). Hematite of Worm-like morphology and doped with Pt was presented by Kim et al which yielded a very high photocurrent density 4.32 mA/cm^2 at 1.23 V vs. RHE [56] In sum, nanostructuring has proven to be a beneficial way of improving overall performance of photoanodes by increasing the effective surface area and hence the charge separation.

Influence of Doping on the conductivity and performance of Fe_2O_3 photoanodes:

Doping of impurities has been used in many semiconductor systems for enhancing the bulk charge carrier concentration and hence the overall conductivity. Pure hematite possess low electrical conductivity of the order of 10^{-14} $\Omega^{-1}cm^{-1}$ [57], charge carrier concentration around 10^{18} cm^{-3} and electron mobility of around 10^{-2} cm^2 V^{-1} s^{-1} [58]. Since the conductivity of a semiconductor is given by $\sigma = ne\mu_e + pe\mu_p$, increasing charge carrier concentration (i.e. n or p type) by electronic doping is often utilized to compensate for the low electron and hole mobilities. Hematite is an n-type semiconductor owing to oxygen vacancies present in the bulk. When divalent metal like Mg, Cu or Ni, replace Fe^{3+} sites in the lattice, hole carriers are generated and hematite becomes a p-type material [4, 59-60]. Whereas doping of tetravalent metal like Sn, Ti, Zr and Si, extra electrons are generated and hematite remains n-type with enhanced electron density [27, 30, 55, 61-62].

Ling et al demonstrated the dependence of high temperature sintering of hematite nanowires on the photocurrent density [27]. The enhancement in photoactivity of nanowires was due to the presence of Sn^{+4} ions resulting in increase in charge carrier concentration from 1.89 x 10^{19} to 5.38 x 10^{19} cm^{-3} with annealing of nanowires at 650°C and 800°C respectively in air. The Sn^{4+} ions from the FTO substrate diffused into Fe_2O_3 nanostructure during high temperature annealing which acted as an electron donor and hence increased the charge carrier density in hematite nanowires. Graetzel et al developed cauliflower-like nanostructures of Si-doped Fe_2O_3 with high surface area and feature size of 10-20 nm which yielded appreciable photocurrent of 2.2 mA/cm^2 @ 1.23V versus RHE. This enhanced performance was attributed to the high donor density of Si-doped Fe_2O_3 of around 1.7 x 10^{20} cm^{-3} extracted by Mott-Schottky analysis. It is also worth noting that in this specific case, Si was also instrumental in developing the cauliflower nanostructure with very small feature size [30].

An insight into Cu and Ti doped hematite through theoretical measurements was reported by Meng et al [60]. Using density function theory (DFT) calculations, they showed that the conduction band minimum (CBM) of Cu-doped Fe2O3 was favorable to facilitate hydrogen evolution which is not possible for pristine hematite. Hence, the valence and conduction band levels could be able to facilitate both oxygen and hydrogen evolution from water without any application of voltage bias. With Ti doping in hematite, the DFT calculations showed enhancement of conductivity and slight change in band gap due to creation of shallow donor levels which shifts the Fermi level towards the conduction band edge of hematite [60]. Shen et al investigated Ti-doped hematite experimentally and found an increase in photocurrent density after Ti doping to 14 times as compared to pristine hematite [63]. These and other works reported earlier [55, 64-65] further strengthen the importance of Ti doping which enhance the charge carrier density in hematite and hence increases its performance.

A hematite nanorods based photoanode doped with Pt and surface treated with Co-Pi, yielded a remarkable photocurrent of 4.32 mA/cm^2 at 1.23 V vs. RHE under standard simulated 1-sun (100 mW/cm^2) solar spectrum [56]. These nanorods had a ''wormlike'' morphology formed with two steps annealing process, firstly at 550°C and finally at 800°C in air. Pt doping was influential in improving the charge transport characteristics in the bulk of hematite nanorods whereas Co-Pi, commonly used as an oxygen evolution cocatalyst, enhanced the hole transport kinetics on the semiconductor-electrolyte interface. Pt doping yielded an improvement in the electrical conductivity of hematite by increasing the donor density from 3.27 x 10^{17} cm^{-3} for pristine Fe_2O_3 to 2.77 x 10^{18} cm^{-3} for Pt-doped Fe_2O_3 and further to 3.91 x 10^{18} $cm^{-3}$for Pt-doped Fe_2O_3/Co-Pi [56]. Gurudayal et al reported solution based methodology to synthesize Mn-doped Fe_2O_3 nanorods which yielded improved oxygen evolution activity as compared to pristine Fe_2O_3 nanorods [31]. It was found that doping of 5 mol % Mn precursor was optimum to improve the photocurrent densities at 1.23 V vs. RHE by upto 3 times. Doping also cathodically shifted the onset potential by 30 mV as compared to the pristine nanorods. Through Mott-Schottky analysis, the improvement in photocurrent density was attributed to increase in the donor densities. The decrease in transient photocurrent for Mn doped samples as observed by Chronoamperometry, indicated the beneficial effects of Mn doping which led to a suppression in electron-hole recombination and a reduction in the energy barrier for hole transport. It was claimed to be due to the presence of multivalent oxidation states of Mn leading to a low (O-Mn-O) energy barrier for hole transport.

Another type of doping strategy reported is the generation of oxygen vacancies in the bulk which act as shallow donors and hence increase the donor density. Ling et al demonstrated the incorporation of oxygen vacancies in hematite [66]. They fabricated hematite nanowires with enhanced concentration of oxygen vacancy resulting in improved photoactivity for water oxidation. Due to the release of oxygen during inert atmosphere annealing of hematite, oxygen vacancies carried an extra electron which increased the donor density as corroborated by Mott-Schottky analysis. This report was also the first demonstration of highly photoactive hematite nanowires, without any elemental doping, by using low post-annealing temperature (550°C). An investigative study to decouple the interaction between extrinsic Sn dopants and oxygen vacancies was reported by Yang et al [67]. They demonstrated that electronic dopants and oxygen vacancy complement each other to reduce the onset potential and enhance the electrical conductivity eventually increasing the photocurrent density. Recently, a study of oxygen deficient Fe_2O_3 photoelectrodes through Transient Absorption Spectroscopy has been reported by Forster et al [68]. It was shown that the inclusion of oxygen vacancies block the slow surface hole-bulk electron recombination pathways which enhances the performance of PEC.

Zandi et al reported an unconventional role of Ti doping in enhancing the photoactivity of hematite [69]. Instead of increasing charge carrier density, Ti was suspected to increase the efficiency of hole transport properties across the hematite/electrolyte interface. Even though some preliminary data was presented, further experimental evidence is still required to support this theory. Recently, Kronawitter et al through in-depth theoretical and experimental observations illustrated that the role of Ti incorporation is not limited to electronic doping but also in distorting the unoccupied Fe 3d - O 2p band of Fe_2O_3 [70]. To summarize, nanostructuring and doping strategies have been reported by many authors to be beneficial in altering the electronic properties of pristine hematite and eventually enhancing the performance of hematite based PEC devices. But the enhancement in performance is still far from the desired performance i.e. around 10% STH efficiency which paves the way for deployment of other techniques like heterojunction between two complementary properties which can yield an extra built-in voltage to allow better charge separation and transport in the bulk. This is going to be discussed further in **Section 2.4**.

2.2 Alternate Materials for Solar Water Splitting: Fe_2TiO_5 as Photoanodes

One of the biggest challenges faced by the scientific community is to explore a photocatalyst whose band levels straddle the water redox levels, as shown in **Figure 1.1.2** and possesses good charge transport properties to minimize electron/hole recombination probability. In spite of many fascinating features of nano-structured and surface treated hematite, it is imperative to keep striving for different classes of iron-based materials as photoanode for water oxidation which are low-cost, non-toxic and possess more favourable intrinsic properties than hematite. More importantly, the need to find semiconducting materials possessing band levels that straddles water redox levels is immense. Theoretically, this improvement could be achieved by changing the band structures of the material by solid solution or composites of two or more systems. Experimentally, hybrid materials have been reported but have had little impact owing to the difficulty in fabricating crystalline single phase electrodes with appreciable porosity for enhanced photoactivity. There have been research on a plethora of hybrid photocatalysts with complex stoichiometry that possess favourable band level positions that could be used for solar water splitting [8, 11].

Iron based ferrites are fascinating class of materials to study as an alternative to hematite or for integration with the latter. Boumaza et al reported $ZnFe_2O_4/SrTiO_3$ system for hydrogen production as $ZnFe_2O_4$ has a conduction band level higher than that for water reduction [71]. Utilizing such conduction band energy favourable for hydrogen evolution, Mcdonald et al coupled $ZnFe_2O_4$ with Fe_2O_3 as a photoanode [72]. It was shown that

$ZnFe_2O_4$ has a band gap of around 2 eV and is stable in aqueous solutions. Its conduction and valence band edges are shifted in negative direction by around 200mV as compared to hematite which resulted in better photocurrent density in $Fe_2O_3/ZnFe_2O_4$ composite as compared to pristine hematite due to good band level alignment which results in efficient electron-hole separation. Miao et al [73] reported a similar approach heterojunction of Ti-doped Fe_2O_3 and $ZnFe_2O_4$ was shown to enhance photoelectrochemical performance owing to the better charge separation. Recently, Kim et al reported a manifold increase in photocurrent density for $ZnFe_2O_4$ based photoanodes activated using Hybrid Microwave annealing (HMA) as compared to conventional thermal annealed samples [74]. The HMA treatment was effective in supressing charge carrier recombination and enhancing the performance of these photoanodes. Rekhila et al demonstrated that $NiFe_2O_4$ can be used as a photocathode for solar hydrogen production in the presence of a sacrificial electron donor [75]. The physical characterization of the material showed the p-type behaviour with a band gap of 1.56 eV which also opens a possibility of integrating it with hematite as a p-n junction in future.

Another class of materials, the titanates, have also been shown to possess promising qualities for solar water splitting catalysis [76-77]. Kudo et al has enumerated a number of diverse heterogeneous photocatalysts, including titanates and tantalates, for solar water splitting [2]. They demonstrated that through solid solution of two materials, with not so favourable band levels, efficient photocatalytic water splitting materials could be prepared. A similar idea was proposed by Thimsel et al where the conditions to prepare mixed transition metal oxides with optimum band gaps was demonstrated [39]. Although they focussed on Fe-Ti-O system, it was further claimed that it could also be extrapolated to Ti-V-O or Ti-Ni-O systems. Stoichiometric changes in TiO_2 through incorporation of Fe were shown to effectively tune band gaps. They showed experimentally and theoretically, that iron titanates have better band gap for visible light excitation as compared to TiO_2. It was also claimed that with valence band level already being favourable for water oxidation, the shift in conduction band level towards hydrogen generation could in turn result in the reduction of the overpotential.

Ginley et al synthesized and characterized crystals for different iron titanates $FeTiO_3$, Fe_2TiO_4 and Fe_2TiO_5 for application as anodes for photoelectrolysis of water [78]. Among these titanates, $FeTiO_3$ with a band gap of 2.5-2.9 eV has been studied mainly with TiO_2 as an absorber for photocatalytic applications [79]. Kim et al reported nanodiscs of $FeTiO_3$ prepared by hydrothermal treatment which were then exposed to TiO_2 nanoparticles to integrate them [80]. They reported $FeTiO_3/TiO_2$ as water oxidizing visible light photocatalyst where $FeTiO_3$ acts as the light absorber and TiO_2 as electron transporter. Similar work has been conducted where $FeTiO_3$ is utilized as an absorption enhancing layer on TiO_2 for photochemical processes where it is also shown that valence band matching between them increases the hole transport across the semiconductor/electrolyte interface and hence enhances the photocatalytic activity [79, 81].

It is the theoretical and experimental studies by diverse groups in tuning the band gap or levels, through solid solution of two oxides which displays the potential of Fe-Ti-O system. It is also constituted of Fe and Ti which are abundant, non- toxic and widely explored as Fe_2O_3 and TiO_2. It is likely that conduction band and valence band levels in iron titanate would be more favourable for water splitting as compared to hematite [7, 40]. Among titanates, $FeTiO_3$ has been used in Photocatalysis as an absorber with TiO_2 as mentioned earlier. But oxidation state of Fe as +2 limits its use as a photoanode, which requires thermal activation through sintering, which could produce mixed phases of Fe^{+2} and Fe^{+3} ions and hence could hamper their performance in PEC. There has also been reported a possible intervalence charge transfer from Fe^{+2}, Ti^{+4} to Fe^{+3}, Ti^{+3} which could potentially lower its photoactivity due to higher recombination of photogenerated charge carriers to these variable valence states [82]. This limitation is also applicable to Fe_2TiO_4 which shares a similar oxidation state of Fe as +2. Another mineral pseudobrookite, Fe_2TiO_5 is an abundant iron titanium oxide found in post-volcanic or young volcanic rocks. The crystal structure of Fe_2TiO_5 is orthorhombic (Space Group: Cmcm) containing four molecules, with lattice constants of a= 0.997, b=0.993, and c =0.372 nm with Fe and Ti atoms occupying (8f) and (4c) sites respectively [83]. With a favourable indirect band gap of around 2.1 eV, it has good solar spectrum absorbing qualities and is also stable thermodynamically as well as in aqueous solutions [40, 84-85]. It's electronic and photocatalytic properties have been largely unexplored. Recently, nanoheterostructures based Fe_2TiO_5 thin films have been shown to possess favourable visible light responses even though it is hard to attribute the photoactivity to the Fe_2TiO_5 only as the produced compound contains traces of hematite as well [86]. Hence, investing the effort in synthesizing and characterising a pure phase Fe_2TiO_5 thin films is worthwhile which could open new avenues to the solar fuel production.

2.3 Surface Treatment of photoanodes with surface overlayer and cocatalyst

As mentioned in earlier sections, there is a need to develop photoanode materials that have optimum band level positions and possess good charge transport properties. In a typical photoanode system, after absorption of photons from illuminated solar spectrum, they have to be utilized to convert them into charge carriers effectively. This is limited by recombination processes that happen in bulk, in depletion region or on surface in a photoanode. Walter et al reported on recombination pathways the photogenerated charge carriers could undergo during hole injection into electrolyte and electron transport to the back contact as shown in **Figure 2.3.1** [7].

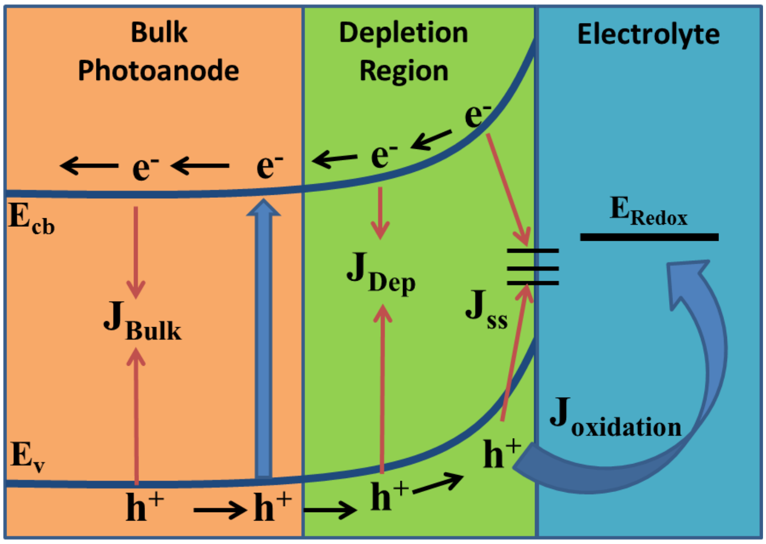

Figure 2.3.1 Schematic representation of Recombination pathways that charge carriers can undergo in an n-type semiconductor [7]

J_{bulk}, as shown in **Figure 2.3.1** above, is the electron-hole recombination pathway affiliated to bulk semiconductor. Since, depletion width formed after the contact with electrolyte is very small as compared to the overall thickness of the semiconductor (which has to be large to allow complete absorption of solar spectrum), the carriers do not witness electric field in the bulk. Hence, the diffusion of the photogenerated charge carriers to their respective contacts is the limiting factor.

As discussed earlier, nanostructuring allows to tackle the problem of bulk recombination which is not only limited to hematite but also for the photoanode systems with short minority carrier diffusion length. It allows a thin feature size like in nanorods, where photons are absorbed near the depletion region and hence the transport of minority charge carriers is efficient. The other strategy that is effective in improving charge transport properties of bulk is doping. Similar to hematite, in any photoanode system, it is required that the conductivity of the bulk is large to assist the effective charge transport. Doping the extravalent elements in the n-type photoanodes allows the enhancement of charge density inside the bulk which increases the overall conductivity. The other pathway that could lead to loss in photocurrent is J_{dep} which is due to the shallow or deep traps present in the depletion region that limits the transport of charge carriers. It has been observed that this recombination is not a major contributing factor in n-type doped semiconducting photoanodes. With doping, the deep energy levels, which act as the recombination centers, could be diminished [87].

Most influential recombination pathway which limits the performance of a nanostructured photoanode is J_{ss}, the surface recombination, which is highly rampant in photoanodes, especially in hematite. To tackle bulk recombination, high surface area electrodes based on nanostructures are fabricated but this increases the density of surface defects as well. These surface defects are either lattice disordering or dangling bonds or the adsorbed ions [87]. These defects act as an inhibitor to the hole injection into the electrolyte leading to hole accumulation. Due to holes accumulation, electrons undergo a back electron-hole recombination reaction which drastically lowers the performance of photoanodes.

The sluggish hole transport owing to these surface defects could be improved by surface treatment with a metal oxide either for surface passivation or as co-catalysts. These two phenomena play different roles in assisting hole injection into the electrolyte. Surface passivation facilitates the reduction of surface defects on porous hematite which reduces the hole-electron recombination rate by forming an ultrathin overlayer on top of photoanode. Use of co-catalyst allows the fast oxidation of its metallic element which readily assists hole transport from photoanode surface into the electrolyte. These co-catalysts could also improve the charge transfer by introducing a mid-gap state between the valence band of semiconductor and water oxidation level to enhance hole transfer and hence water oxidation. An in-detailed perspective article by Guijarro et al highlights and discusses the beneficial effects of surface treatment in enhancing the light harvesting efficiency [88].

Many surface passivation strategies, with hematite or other photoanodes, such as employing CoF_3 [89], Al_2O_3 [32], Ga_2O_3 [90], SnO_2 [34] and ZnO [33] have been reported. A favourable flat band shift in Ti-doped Fe_2O_3 thin films after surface treatment with CoF_3 solution have been shown by Hu et al [89]. This work was fascinating as the photogenerated electrons, due to the shift in Fermi level, were able to generate hydrogen without any applied bias, which emphasised the importance of surface modification in shifting band levels. Formal et al deposited an ultra-thin film of Al_2O_3 on hematite photoanodes using Atomic Layer Deposition (ALD) technique which reduced the overpotential by 100 mV [32]. The alumina overlayer also enhanced photocurrent to a value of 0.85 mA/cm^2 at 1.0 V vs. RHE as compared to 0.24 mA/cm^2 for pristine hematite. Through optical spectroscopy and electrochemical studies, the role of the alumina overlayer was confirmed as a surface passivating layer. Hisatomi et al [90] reported that surface passivation of hematite photoanodes using corundum-type overlayers decreases the lattice strain and eventually decreases the density of surface defects. A negative shift of 200mV in overpotential was observed after using Al_2O_3 and Ga_2O_3 overlayers on hematite. Xi et al showed surface passivation using ZnO overlayer on spray pyrolyted hematite photoanodes [33]. A shift of -170 mV and enhanced photocurrent of 1.08 mA/cm^2 was subjected to change in flat band potential and reduction in surface defects due to ZnO overlayer.

Various oxygen evolution catalysts like Co-Pi [36, 91], IrO_2 [92], Cobalt oxides [30, 93] have also been coupled with hematite photoanodes because of their fast hole transfer kinetics for water oxidation. A cocatalyst present on the semiconductor/electrolyte interface can act as a mediator to ease hole transfer from the interface due to a reduced kinetic barrier and hence decrease the overpotential. Tilley et al demonstrated that the surface treatment of nanostructured hematite photoanode with IrO_2 nanoparticles yielded an overpotential shift of

0.2 V and a photocurrent as high as 3.75 mA/cm^2 [92]. IrO_2, considered as one of the best co-catalysts to reduce overpotential, can transfer photogenerated holes to a lower overpotential and thus yield a higher photocurrent density due to low charge carrier recombination probability. Although IrO_2 is a good water oxidation catalyst, but expensive non-abundant element (Ir) in it limits its potential. Hence, recently, earth abundant Mn and Co based nanoclusters have been explored which could achieve high turnover frequency (TOF) and are stable inorganic based oxide catalysts to be used on a large scale [94]. It would be interesting to couple these nanoclusters with nanostructured photoanodes to design an efficient water oxidation system.

Nocera et al introduced the remarkable oxygen evolving catalyst, Co-Pi, which could be deposited and integrated with photoanodes using electrodeposition technique [37]. Because of a low overpotential of only 0.41 V required to oxidize water at pH=7 with a current density of 1 mA/cm^2, it has gained a lot of interest. Zhong et al reported 0.35V cathodic shift in overpotential for Co-Pi/α-Fe_2O_3 composite photoanodes [36]. 1D Co-Pi modified $BiVO_4$/ZnO junction was reported by Moniz et al [95] which yielded a dramatic negative shift in onset potential which was attributed to hole transfer to Co-Pi and efficient electron transport along 1D ZnO. McDonald et al fabricated Co-Pi OEC photochemically on electrodeposited Fe_2O_3 films and demonstrated an enhancement in photocurrent density as well as in oxygen evolution activity which implied an enhancement in hole transfer kinetics [35].

Graetzel et al reported surface treatment of cauliflower like nanostructures based hematite [30]. The cobalt treatment using 10 mM $Co(NO_3)_2$ solution, resulted in a negative shift in onset potential of 80 mV, and a slightly higher photocurrent density of 2.7 mA/cm^2 at 1.23 V versus RHE as compared to pristine hematite (2.2 mA/cm^2 at same potential). The enhancement observed in cobalt-modified hematite was attributed to the trapping of surface holes primarily by Co(II) sites to get converted to Co(III), and then further oxidization by a second hole to create Co(IV) ions which then drives the water oxidation reaction. This suggests that cobalt oxide behaves like a cocatalyst but other explanations have also been explored. Peter et al extracted the photogenerated charge transfer rate and recombination constants in pristine and Co(II) oxide treated hematite thin film using Intensity Modulated Photocurrent Spectroscopy (IMPS) [96]. They demonstrated that the charge transfer rate of Co(II) treated hematite was similar to the untreated hematite, indicating that the improvement in photocurrent density was not due to catalytic behaviour of Co. On the other hand, the recombination rate constant was reduced for treated hematite as compared to the pristine film which seem to suggest that the improvement in photocurrent in the former was due to inhibition of surface recombination and not due to the change in hole transfer kinetics as suggested previously [30]. Xi et al used a Co_3O_4 as water oxidation catalyst of iron oxide nanorods array [49]. They showed in situ and ex situ growth of Co_3O_4 nanoparticles with hematite nanorods. With 5% Co in situ incorporated in hematite nanorods showed higher photocurrent of 1.2 mA/cm^2 as compared to pristine photocurrent of 0.72 mA/cm^2 and also a shift in overpotential by ~40 mV. In situ processes were reported to be of better performance than ex situ because of large Co_3O_4/hematite interfacial area, surface roughness and smaller Co_3O_4 particle size.

Since study into ultrafast charge carrier dynamics is extremely important to get an insight into fast processes undergoing in nanostructures, in designing efficient light harvesting devices, various spectroscopic analysis have been extensively explored [47, 97]. Ultrafast studies on Fe_2O_3 phase was earliest demonstrated by Cherepy et al which yielded a short charge carrier lifetime of the order of 1 ps in hematite nanoparticles [98]. Joly et al probed charge carrier dynamics of α-Fe_2O_3 thin films using femtosecond transient absorption spectroscopy and found that the electrons recombined with holes/traps at the lifetime order of

3ps [99]. Carrier trapping by midgap Fe d-d states was claimed to be the dominant trapping mechanism. Transient Absorption Spectroscopy on subpicosecond to second time scale was used to investigate the charge dynamics in Si-doped Fe_2O_3 photoanodes by Pendlebury et al. It was illustrated that with application of anodic bias, ultrafast recombination dynamics inhibited and caused the electron trapping on ps-µs scale. Huang et al reported in-situ Transient Absorption (TA) studies for hematite thin film electrodes which concluded that the ultrafast electron-hole recombination is the limiting factor for efficient water oxidation and the minimum hole lifetime for hematite to be catalytically active is 6 µs [100]. Pendlebury et al reported a correlation between photocurrent density and the population of holes with longer lifetime under external bias [101]. Through TA and Transient Photocurrent (TPC) measurements, it was shown that the long-lived holes drive the single hole oxidation under voltage bias as opposed to four-hole oxidation process. The role of surface passivation overlayers or cocatalysts have also been investigated through transient spectroscopic measurements. To understand the role of Co-Pi in the enhancement of photocurrent for hematite, TA measurements were performed by Barroso et al on α-Fe_2O_3/CoO_x nanocomposite photo electrodes [91]. The improvement in photoelectrochemical activity was attributed to the reduction in recombination losses. Another report by the same group showed the reduction in electron-hole recombination probability is responsible for cathodic onset potential shift for surface treated hematite with overlayer (Ga_2O_3) and cocatalyst (CoO_x) [93]. These strategies of coupling a nanostructured photoanode with surface overlayers or co-catalysts allow better hole injection into the electrolyte through improved surface kinetics, as shown by spectroscopic measurements, and hence play a major role in achieving enhanced performance in PEC Cells.

2.4 Heterojunctions as photoanode with Improved Charge Separation

As reviewed above, bulk recombination and surface recombination could be tackled by using nanostructuring, doping or surface treatment approaches in photoanodes [26, 102]. One way to improve the charge separation/transport in the bulk of photoanode is by forming a staggered gap (type II) band alignment based heterojunction as shown in **Figure 2.4.1**. Offsets in conduction band (ΔE_C) and valence band (ΔE_V) present in these heterojunctions allow a facile transfer of electrons and holes and increased charge separation due to an inbuilt potential [38].

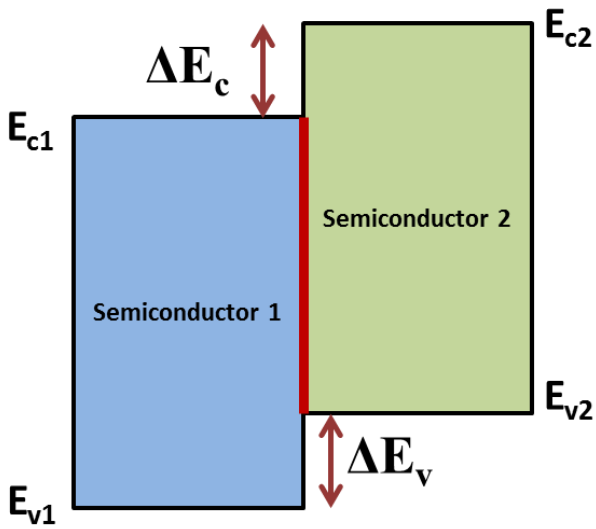

Figure 2.4.1 Schematic representation of Type II (Staggered) Band Alignment between two semiconductors (Red Line represents the heterojunction)

In context of heterojunction, the key is also to explore other stable and photo absorbing semiconductors which could couple with hematite, are crystalline in nature to avoid charge trapping on lattice disordering and share favourable band alignment and high interface quality with hematite. Diverse heterojunction thin film electrodes with enhanced performance have been reported earlier by various groups. Yang et al demonstrated branched heterojunction array of Co-doped Fe_2O_3 nanorods with $MgFe_2O_4$ for efficient photoelectrochemical water oxidation [103]. Fe_2O_3:Ti/$ZnFe_2O_4$

thin films [73] showed better charge separation owing to appropriate band alignment of semiconductor layers. $TiSi_2$ nanonet arrays used as a charge transporter integrated with hematite film yielded large improvement in photocurrent density [104]. Recently, Wang et al demonstrated Fe_2O_3/TiO_2 core-shell photoelectrodes for solar water splitting with improved photocurrent density than pristine Fe_2O_3 and TiO_2 films [105]. Peng et al reported WO_3/Fe_2O_3 composite photoanodes with one of the lowest onset voltages using hematite based PEC systems [106]. Another core-shell ZnO/Fe_2O_3 nanowires based photoanode has been presented by Hsu et al where a shift in onset potential was attributed to n/n heterojunction structure which also improved charge separation owing to favourable band alignment [107]. Recently, unassisted water splitting using hematite photoanode and Si photocathode has been demonstrated by Jang et al [108]. Through a facile re-growth strategy, an overall efficiency of 0.91% was demonstrated with a low turn-on voltage. Apart from hematite based heterojunctions, there have been other reports of nanostructured $WO_3/BiVO_4$ heterojunction with improved photoelectrochemical performance [109]. Leonard et al showed an improved charge separation by fabricating $ZnWO_4/WO_3$ composite, with a type II band alignment, in a single annealing step [110]. Recently, $BiVO_4$/ZnO Junction Cascade was demonstrated as a photoelectrode which resulted in a photocurrent density as high as 3 mA/cm^2 using CoPi as a cocatalyst [95]. The enhanced performance was attributed to increased light absorption and efficient electron transfer from $BiVO_4$ to ZnO 1D nanorods.

As mentioned in **Section 2.2,** Fe_2TiO_5, an abundant mineral with a band gap of 2.1 eV and stable in aqueous solutions, has favourable band levels with respect to water redox levels as compared to widely used hematite. This alignment could create a built-in potential, due to the conduction and valence band offsets, for electrons and holes to transfer towards their respective electrodes. There is also a structural coherency between pseudobrookite and hematite which allows the overgrowth of former on hematite [111]. It also possesses the physical and chemical properties that are highly demanded for photoanodes. A schematic representation of heterojunction with hematite (Fe_2O_3) and pseudobrookite (Fe_2TiO_5) on FTO substrate is as shown in **Figure 2.4.2**. It shows easy electron injection owing to the conduction band alignment and hole transport to electrolyte due to valence band alignment between both materials. Fe_2TiO_5 is hypothesized to possess better charge separation/transport properties than hematite which would be discussed in **Section 4.2** .

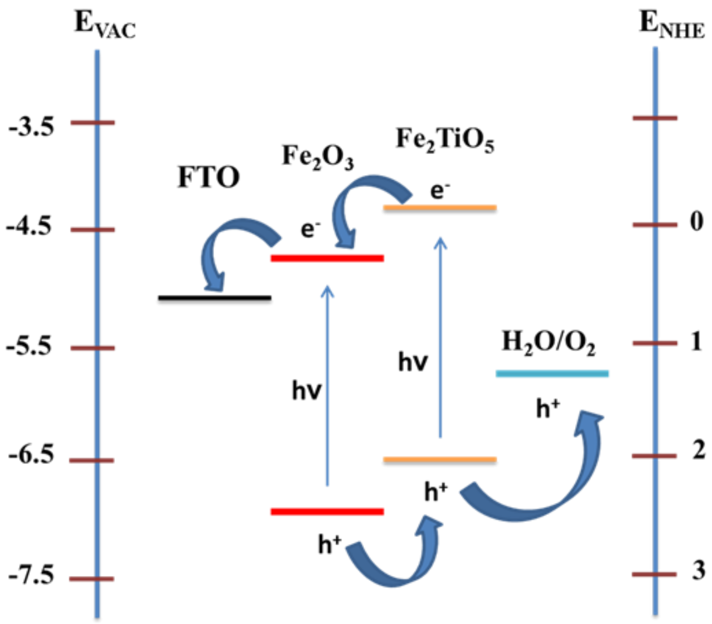

Figure 2.4.2 Schematic representation of Fe_2O_3/Fe_2TiO_5 heterojunction showing photogenerated electron/hole transport

The limitation for the synthesized iron titanate thin films is their low absorption coefficient and hence the total visible light absorption. On the other hand, Fe_2O_3 performance is limited due to its charge separation properties in spite of its high absorbance. Hence, both constituent oxides being complementary to each other with a similar band gap, it is hypothesized that the performance could be enhanced by coupling them together as a heterojunction.

There has been a report of coupling thin amorphous Fe_2TiO_5 overlayer acting as a visible light absorber with TiO_2 [112] which resulted in high performance and low onset potential. The amorphous layer had to be ultrathin for high performance since it blocks charge carriers after a certain thickness. Very recently, Deng et al demonstrated surface treatment of Fe_2O_3 with Fe_2TiO_5 for a surface passivating effect which enhanced photocurrent [113]. The structure formation was limited due to the treatment of hematite at longer durations resulted in TiO_2 overlayer and hence limited the performance. Hence, it opens up an opportunity to improve charge carrier separation in pristine Fe_2O_3 by integrating it with a nanoporous crystalline layer of Fe_2TiO_5, both of which could be fabricated using simple low cost hydrothermal technique. By this technique, heterojunction electrodes of two crystalline thin films could be attained to get an insight to the band alignment and to study bulk and surface charge recombination. This proposed methodology would be flexible in tuning its reaction conditions, in turn thickness of constituent oxides, to realize an optimum configuration for heterojunction thin film.

2.5 Theoretical Background for photoelectrochemical characterizations in PECs

2.5.1 Photocurrent Linear Sweep and Chopped

Linear Sweep Voltammetry under standard solar simulated light is a standard performance measurement for determining the amount of charge carriers created per unit time (photocurrent density) under the application of external bias between working electrode (anode) and counter electrode (cathode). Semiconductors that display higher photocurrent will yield higher water oxidation efficiency required for efficient solar water splitting. The typical curve for hematite based photoanodes and the desired performance for an ideal high efficiency photoanode was earlier shown in **Figure 2.1.1** .

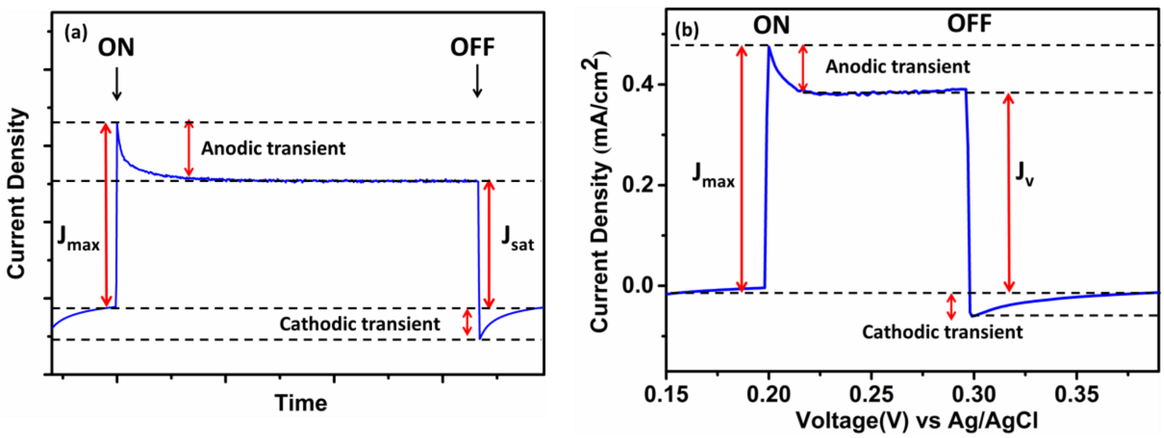

Figure 2.5.1 Photocurrent Anodic and Cathodic Transient under a chopped solar simulated Light with (a) varying time and a fixed voltage bias and (b) with varying applied bias

Photocurrent density under regularly chopped light provides basic insight into the recombination mechanism (bulk or surface) occurring in the photoanode. Typical photocurrent transients with varying time and bias are shown in **Figure 2.5.1 (a)** and **(b)** respectively. Photocurrent transients occur due to holes accumulation on the surface, electrons accumulation in bulk or due to electron-hole recombination via surface states [114].

Hence, if anodic transient and cathodic transient show similar transient, it shows the photogenerated holes getting accumulated on the surface while the light is on (anodic transient), are recombining with electrons after the light is off (cathodic transient) which facilitate back flow of electrons into the photoanode [115]. Hence, linear sweep voltammetry or Amperometric (I-T) curve under chopped light yields crucial information about the role of semiconductor-electrolyte interface in allowing transport of holes for water oxidation.

2.5.2 Photoconversion efficiency calculation

Photoconversion efficiency of conversion of solar energy to chemical energy under a voltage bias [31] is calculated as shown in Equation (2) below:

Photoconversion efficiency = $(J * (E_{rev0} - E_{app}) / I_o) \times 100$ (2)

Where J is the photocurrent density (mA/cm^2) at a certain potential (V), E_{rev0} is the standard reversible potential equal to 1.23 V for the water splitting reaction at pH = 0, $E_{app} = (V - V_{ocp})$ where V is the potential applied and V_{ocp} is the applied potential at open circuit condition under the standard illumination. V and V_{ocp} are with respect to Ag/AgCl. I_o is the measured intensity of the irradiated solar spectrum in mW/cm^2 which is $100 mW/cm^2$ corresponding to 1 sun (AM 1.5G).

2.5.3 Efficiency - IPCE

IPCE characteristics were characterized using a xenon light source (MAX-303, Asahi Spectra Co. Ltd.) coupled with a monochromator (CMS-100, Asahi Spectra Co. Ltd.). The wavelength was scanned from 300 to 700 nm keeping the voltage fixed at 1.23 V vs RHE i.e. 0.23 V vs Ag/AgCl. To calculate IPCE, the following relation was used [34]:

$IPCE(\%) = (1240/\lambda) * (I/J_{light}) * 100$

where I is the photocurrent density (mA/cm^2) obtained using a potentiostat (mentioned earlier) recording the I-T curve at 1.23V vs RHE, λ is the incident light wavelength (nm) from monochromator, and J_{light} (mW/cm^2) is the power density of monochromatic light at a specific wavelength. A source meter (Keithley Instruments Inc., model no. 2400) was used to measure the photocurrent of the standard Si diode (Bentham, DH-Si).

2.5.4 Electrochemical Impedance Spectroscopy

Electrochemical Impedance Spectroscopy yields information about charge dynamics occurring in semiconductor and across a double charged layer at semiconductor/electrolyte interface which is essential to estimate the band diagram of PEC system [38]. In PEC cells, semiconductor electrolyte interface plays a key role in hole transport to the electrolyte. A study into the band bending at the interface, due to Fermi level mismatch, and the space charge layer formation is of great importance in understanding charge dynamics of the system. Impedance Spectroscopy, especially, Mott Schottky plots provide details of the flat band potential of the semiconductor and donor charge concentration density in bulk photoanode. It is a plot of reverse of square of capacitance vs. external voltage bias applied. The intercept gives the flat band potential and the slope gives the donor concentration based on relation (3) shown below:

$$\left(\frac{A_S}{C_{SC}}\right)^2 = \frac{2}{q\varepsilon_0\,\kappa N_D}\left(V - E_{FB} - \frac{K_B T}{q}\right) \qquad (3)$$

Where C_{sc} is the space charge capacitance, A_s is the active area of device, E_{FB} is the flat band potential, N_D is the donor density, V is applied bias, K_B is Boltzmann constant, T is the absolute temperature, q is charge, κ is dielectric constant of active material and ε_0 is the vacuum permittivity.

Much research work has been done by Bisquert and coworkers for understanding role of surface states in water oxidation process through impedance spectroscopy. Klahr et al demonstrated a physical model for inclusion of surface states in PEC model which plays huge role in influencing water oxidation kinetics [41]. It showed the charging of surface states and hence accumulation of holes on semiconductor/electrolyte interface affects onset potential. It also showed the shift in flat band potential due to trapping of charges by surface states under illumination. Hence, the transfer of holes takes place predominantly from surface trapped sites, not through valence band, to electrolyte. Klahr et al demonstrated a study of interfaces between Fe_2O_3 and water/fast redox couples which give an insight into rate limiting processes of water oxidation [116]. It showed that an additional overpotential was needed for water oxidation as compared to fast redox couple of $[Fe(CN)_6]^{3-/4-}$. It was because of first step being the trapping of photogenerated holes by surface states and oxidizing the electrode surface. At higher bias, both water and fast redox couple showed similar performance due to release of these trapped holes into the electrolyte. These studies show how important surface passivation is for increasing O_2 evolution efficiency and minimizing overpotential.

2.5.5 Surface and Bulk Charge Separation Efficiency: Using a Hole Scavenger to determine Bulk and Surface recombination

Photooxidation of H_2O_2 allows the swift transport of photogenerated holes to the electrolyte and hence eliminates the surface recombination [117]. This could lead to evaluation of extent of bulk and surface recombination in the semiconductor. Bulk charge separation efficiency, denoted as η(separation), is the fraction of holes that do not recombine in bulk and reach semiconductor-electrolyte interface. Surface charge separation efficiency, denoted as η(catalysis), is the fraction of those holes which have reached the semiconductor-electrolyte interface and oxidize water without recombining with surface traps. Photocurrent density obtained from water oxidation is termed as J_{H_2O} and from H_2O_2 oxidation as $J_{H_2O_2}$.

Photocurrent density measured for water oxidation, J_{H_2O} is represented in equation (4) below:

$$\mathbf{J_{H_2O} = J_{abs} \times \eta(catalysis) \times \eta(separation)} \qquad \mathbf{(4)}$$

Due to absence of any hole injection barrier, η(catalysis) =1 for H_2O_2 oxidation.

Hence, $\boldsymbol{\eta}$**(separation) =** $\mathbf{J_{H_2O}/J_{abs}}$ **(5)**

and, $\boldsymbol{\eta}$**(catalysis) =** $\mathbf{J_{H_2O}/J_{H_2O_2}}$ **(6)**

where $\boldsymbol{J_{H_2O_2}}$ is the photocurrent density measured with H_2O_2 photo-oxidation.

$\boldsymbol{J_{abs}}$ is the photocurrent density obtained when all the absorbed photons are completely converted into current density. It is calculated by integrating the absorbance spectra with standard AM 1.5G spectrum. **Figure C1(b) (**Appendix) shows the absorbed photons for heterojunction and pristine thin films under frontside illumination for optimized condition of 120°C, 12 hours.

Chapter 3.

Experimental Procedures and Characterization

3.1 Preparation of clean FTO Substrates

Most of the chemicals, from Sigma Aldrich (unless specified), were used without any modification. Transparent Fluorine Doped Tin Oxide (FTO) substrates, bought from NSG group (400 nm thick FTO on 2.2 mm glass substrate with 14 Ohm/square), were used as the base electrode for thin film fabrication. Before depositing thin films, the FTO substrates were ultrasonically cleaned thoroughly with soap solution, DI water, ethanol and eventually with isopropanol. They were subsequently dried using a stream of N_2.

3.2 Hydrothermal Synthesis of pristine hematite nanorods and Atomic Layer Deposition of TiO_x overlayer

Pristine hematite nanorods were fabricated on FTO substrates using hydrothermal technique incorporated by Hemant et al [48]. 1.95 mmol $FeCl_3.6H_2O$ and 1.95 mmol Urea was dissolved in 13 mL DI water. Autoclaves of volume 25 mL were filled with 12.5 mL of solution and the cleaned FTO substrates were put in liner standing with FTO side facing towards the wall. Substrates were cleaned for DI water based solution as discussed in **Section 3.1**. To make a contact, small part of the FTO film was masked with a thermal tape which could withstand high temperature. Autoclaves were kept in oven and were heated at around 5°C/min to 100°C and were dwelled for 8 hrs before cooling it down naturally to room temperature. Substrates were taken out of liners and were rinsed with DI water to remove any precipitates from the film surface. Eventually the films were annealed with different annealing profiles: “550°C, 2hrs”, “550°C, 5hrs”, “650°C, 1 hr”, “650°C, 5hrs” and “750°C, 20 mins”, all ramped @ 2C/min, before cooling it down to room temperature naturally.

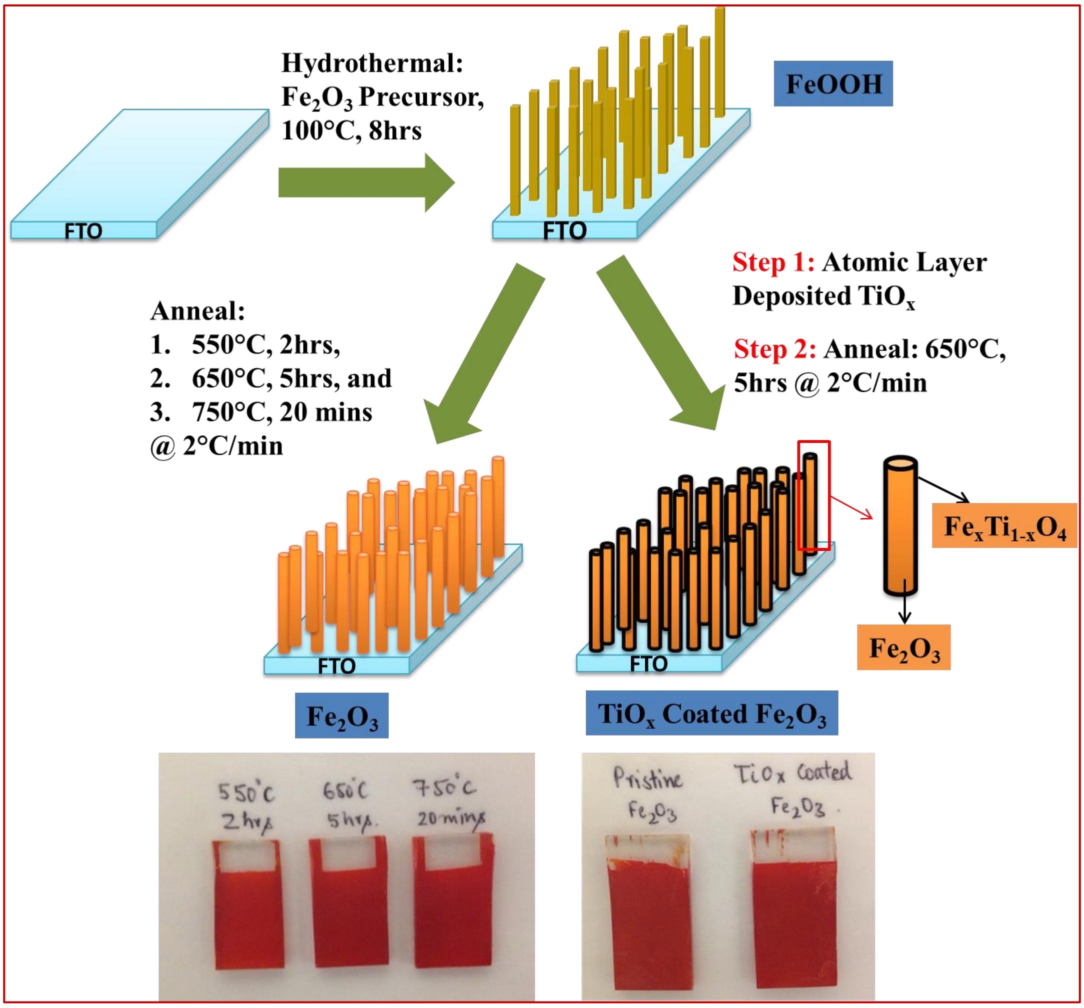

Figure 3.2.1 Process methodology for fabrication of Pristine Fe_2O_3 nanorods and ALD TiO_x coated nanorods using hydrothermal technique

Surface treatment of hematite nanorods with TiO_x overlayer was performed using methodology shown in **Figure 3.2.1** above. Atomic Layer Deposition of TiO_x overlayer was performed on a Fiji 200 system using Tetrakis (Di Methyl Amido) Titanium (TDMATi) and H_2O as precursors. The substrate temperature was kept at 120°C. The TDMATi source was maintained at 70 °C to achieve a suitable vapor pressure. The precursors were pulsed in the reactor with constant Ar flow at 40 sccm, with the base pressure for deposition of 0.8 torr.

The pulse time for TDMATi and H_2O were 0.6 and 0.1 sec, respectively. The purge time was 10 sec for both precursors. The growth rate per cycle of TiO_2 was 0.06 nm, which is consistent with previous report [118] from which the procedure for ALD has been adopted. After coating TiO_2 with 80 cycles, substrates were annealed in similar conditions of 650 °C, 5 hours.

3.3 Hydrothermal Technique and Surface modification of Fe_2TiO_5 Thin Films

Fe_2TiO_5 nanoporous thin films were prepared by solvothermal technique on the FTO substrates. The precursor solution (Iron(III) acetylacetonate [Fe(acac)$_3$] and Ti (isopropoxide) [2:1] in isopropanol) and two FTO substrates were placed inside the autoclave and heated at 150°C for 18 hrs. The resulting thin films were then washed with isopropanol and annealed in air at rate of 4°C/min up to 750°C and left for 20 min before natural cooling back to room temperature. The pure phase of Fe_2TiO_5 is achieved at firing temperature above 500°C as reported earlier [119]. The high temperature of 750°C was necessary to enhance crystallinity and the photocurrent response due to introduction of Sn (IV) element into the film from FTO [18].

The resulting pristine films were then surface treated using $SnCl_4{\cdot}5H_2O$. 20μl of 20mM $SnCl_2$ solution in isopropanol was drop casted and was left for 5 mins at room temperature to allow the adsorption of the solution into the thin films. Eventually, the coated films were annealed with same ramping temperature profile as for the fabrication of pristine films.

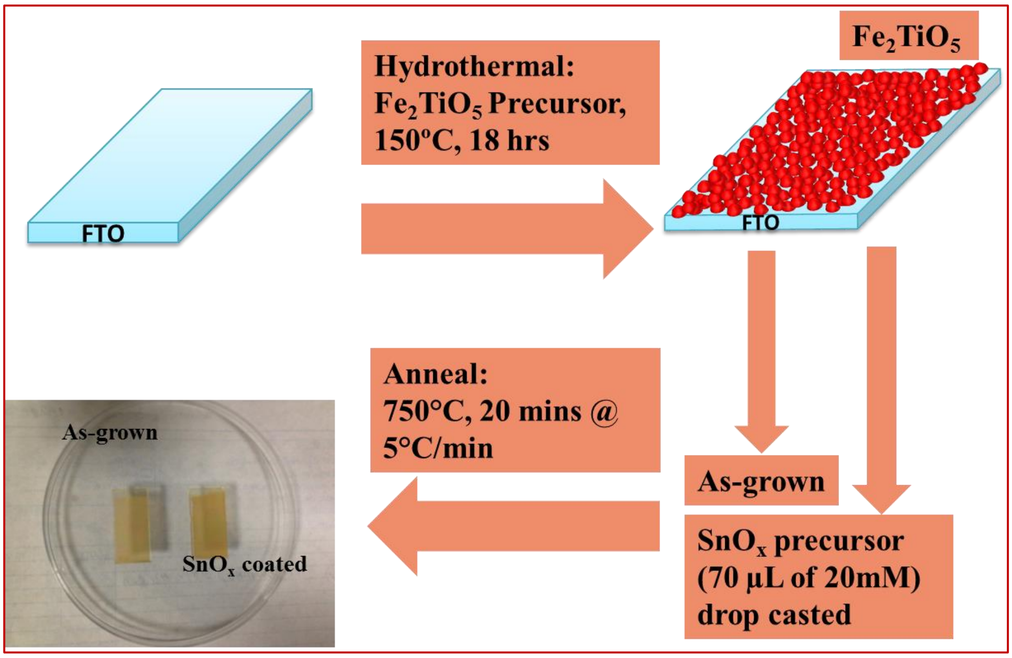

Figure 3.3.1 Process methodology of fabrication of Pristine Fe_2TiO_5 thin films using hydrothermal technique

3.4 Spray Deposition of Iron Titanate (Fe_2TiO_5) thin films on Glass Slides

For spray deposition of Fe_2TiO_5 thin films on microscopic glass slides, precursor solution (as mentioned in **Section 3.3)** similar to hydrothermal technique was used. 50 mL of solution was sprayed on cleaned glass slides, kept on hot plate with a set temperature of 250°C to evaporate any solvent from the substrate. Spray gun (Porshe) with compressed air supply was used for spray and was tuned for a flow rate of approximately 1 mL/min. Spraying of solution was kept "on" for 20 seconds and "off" for 10 seconds subsequently throughout the process. After spray, substrates were annealed to 650°C @ 2°C /min in air and were dwelled for 2 hours before cooling it naturally in furnace.

3.5 Fabrication of Fe_2O_3/Fe_2TiO_5 Heterojunction thin films

Step 1: Fabrication of Pristine FeOOH and Fe_2O_3 Thin Films

Cleaned substrates were kept with a precursor solution of $FeCl_3.5H_2O$ (1.5mmol) and Urea (1.5mmol) in 10 mL water inside an autoclave liner. The autoclave was heated at 100°C for 8 hrs at natural ramping for oven of around 5°C/min. After naturally cooling it down to room temperature, substrates were rinsed with DI water thoroughly to remove thermal tape mask and other unwanted precipitates from the film and were dried naturally in atmosphere. This step formed yellow coloured FeOOH phase. For pristine hematite thin films, these substrates were annealed in air at ramping rate of 2°C/min up to 650°C and dwelled for 5 hours before natural cooling back to room temperature. For heterojunction films, these FeOOH phase substrates were kept in the autoclaves with Fe-Ti precursor solution discussed in next session to deposit Fe_2TiO_5 phase on top of FeOOH phase.

Step 2: Deposition of Fe_2TiO_5 nanoporous thin films on hematite nanorods

Pristine pseudobrookite and heterojunction thin films were prepared by solvothermal technique on the clean FTO and FeOOH nanorods coated substrates respectively. The precursor solution ($Fe(acac)_3$ and Ti (isopropoxide) [2:1] in isopropanol) and substrates were placed inside the autoclave and heated at varied temperatures of 120°C, 135°C and 150°C for 12 hrs. As shown in methodology in Figure 3.5.1, FeOOH thin film substrates were used to fabrication heterojunction and cleaned FTO substrates were also used in same autoclave to fabricate pristine Fe_2TiO_5 thin film. The substrates after the reaction were then washed with isopropanol and naturally dried before annealing with same profile as pristine hematite films mentioned in previous subsection (Step 1).

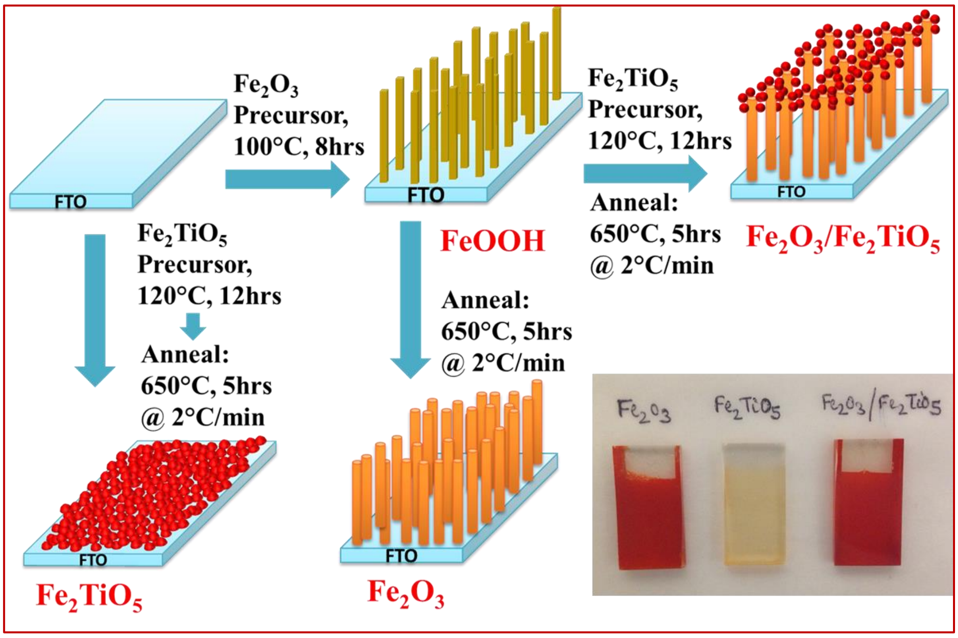

Figure 3.5.1 Process methodology of fabrication of optimized heterojunction and pristine thin films using hydrothermal technique

3.6 Morphological and Structural Characterization of Thin Films

The morphology of thin film samples was observed with Field Emission Scanning Electron Microscopy (FESEM, JEOL, JSM-7600F, 6kV). Films were coated with Au/Pt to avoid charging problems. For further Structural Characterization, HRTEM Analysis (JEOL 2010) was done by using thin film samples scratched from FTO substrates, dispersed in methanol and eventually loaded onto the copper grip. The phase for pristine films was determined from thin film X-ray diffraction (XRD) using a Shimadzu LabX-XRD-6000 equipment. Measurements were done using Cu Kα radiation (λ= 1.5418Å) on grazing incidence geometry with incident angle fixed at 1° and 2theta scanned from 20° to 60° at a scanning rate of 1°/min. Ultraviolet-visible (UV-Vis) measurements were performed using Perkin Elmer UV-Vis spectrophotometer. Samples were kept in the integrating sphere to evaluate diffuse reflectance using the reference as $BaSO_4$ pellet. This yielded normalized absorption spectra which were directly used in the plots. X-ray Photoelectron Spectroscopy (XPS) measurements were carried with VG Escalab 220i

XL. The binding energies were calibrated with respect to the residual C (1s) peak at 285.0 eV. Hall measurements were performed using temperature variable Hall measurement system (MMR technologies) with four probe configuration. Four aluminum square electrodes (1.6 X 1.6 mm^2) were thermally evaporated on pristine films deposited on glass substrates. The measurements were carried out in vacuum (50 mTorr) at room temperature (302 K).

3.7 Photoelectrochemical Characterization of Thin Film Photoanodes

PEC measurements were performed with a CHI 660D working station (CH Instruments, Inc.) using a three-electrode electrochemical system comprising of Platinum coil and Ag/AgCl as counter and reference electrode respectively with 1M NaOH (pH=13.6) electrolyte. The image of the setup used for PEC measurements in shown in **Figure A1 (**Appendix) and the schematic representation of the setup is shown in **Figure 3.7.1** below. Photoactive surface area (using mask on the setup) was fixed at 0.125 cm^2. Simulated sunlight from a 150 W xenon solar simulator (96000, Newport Corp.) through a solar filter (KG3) with intensity equivalent to standard AM1.5 sunlight (100 mW/cm^2) was irradiated on the sample (front or backside). The electrolyte i.e. the aqueous solution of 1 M NaOH (pH 13.6) was degassed by purging N_2 gas for 10 min. The hematite electrode was scanned at 50 mV/s between – 0.4 V and 1.0 V vs. Ag/AgCl. For measurements under the influence of hole scavenger H_2O_2, 1M NaOH +0.5M H_2O_2 was used as an electrolyte with other conditions kept same as mentioned above.

To calculate applied bias with respect to Reversible Hydrogen Electrode, V_{RHE} potential, Nernst equation was used as follows:

$$V_{RHE} = V_{Ag/AgCl} + 0.059 * pH + V^0_{Ag/AgCl} ,$$

where $V_{Ag/AgCl}$ is the voltage bias with respect to Ag/AgCl reference electrode, and $V^0_{Ag/AgCl}$ is the standard potential of Ag/AgCl at 25°C equal to 0.197 V.

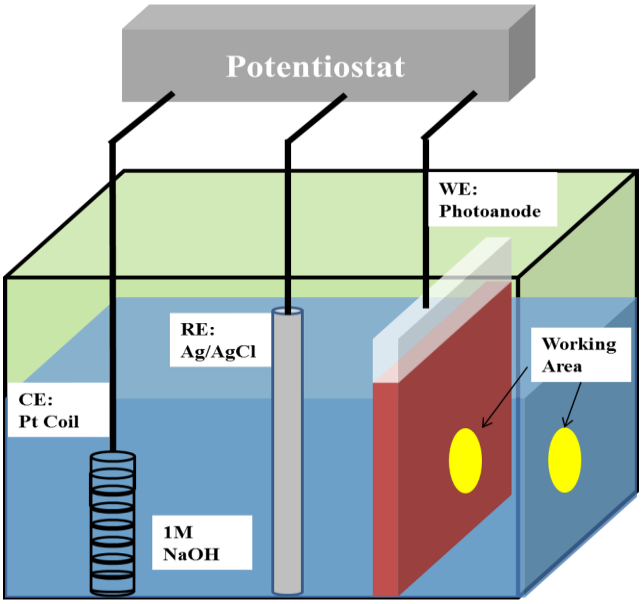

Figure 3.7.1 Schematic Diagram of a Standard Photoelectrochemical Cell Set-up

Incident Photon to Current Efficiency (IPCE) was measured using a xenon light source (MAX5303, Asahi Spectra Co. Ltd.) and a monochromator (CMS5100, Asahi Spectra Co. Ltd.). Electrochemical impedance spectroscopy (EIS) measurements were carried out using an automated potentiostat (Metrohm Autolab) in a three-electrode electrochemical system. Counter electrode, reference electrode and electrolyte were same as that used for PEC measurements. Measurements for Nyquist plots were performed both in dark and light conditions at 1.23V vs. RHE from 75000 to 0.1 Hz. For Mott Schottky plots, frequencies were scanned from 1 to 100000 Hz on the logarithmic scale for potentials ranging from 0V to 2V vs RHE under dark conditions. Curves were then extracted for frequency of 1KHz.

Chapter 4.

Results and Discussion

4.1 Charge Transport in Pristine Hematite (Fe_2O_3) Nanorods under Frontside and Backside Illumination

Introduction

Hematite as mentioned in **Section 2.1** has been used profoundly as a photoanode for solar water splitting and has developed immensely by employing strategies to improve its performance. It is known that hematite (Fe_2O_3) photoanodes need a thermal activation via high temperature annealing to yield a significant photocurrent density [120-122]. It has been shown by Ling et al [27] that high temperature annealing of hematite films on FTO substrates allow Sn diffusion from FTO into the semiconductor bulk which influences its electrical properties. Hence, there is a correlation between photocurrent and Sn concentration in hematite and photocurrent density increases due to increased electrical conductivity with higher Sn dopant diffused from the FTO. It was also shown that 650°C was the starting activation temperature when photocurrent started increasing due to Sn diffusion and was highest for 800°C after which it was lowered due to damage of morphology and hence loss in conductivity of FTO [120]. Morrish et al [123] reported that activation of hematite nanorods could be achieved using a longer time annealing process at a lower temperature. Higher temperature annealing affects the substrate texture and reduces the electrical conductivity of FTO substrate. For a long term and sustainable use it is advisable to use lower temperature annealed hematite photoanodes in PEC Cells. Considering the activation through high annealing of photoanodes an important factor in fabrication of high crystallinity and high conductivity optimized photoanodes, pristine FeOOH nanorods were annealed for 5 profiles: "550°C, 2hrs", "550°C, 5hrs", "650°C, 1 hr", "650°C, 5hrs" and "750°C, 20 mins". The 550°C, 2hrs profile is the standard procedure to fully crystallize FeOOH into α-Fe_2O_3 phase [27]. Annealing of hematite nanorods at 750°C for short duration (here 20mins) has been reported earlier as the optimized annealing profile for high photocurrent yielding Sn-doped Fe_2O_3 based photoanodes. Another profile was heating Fe_2O_3 nanorods for 1 hr at 650°C which is hypothesized to allow Sn diffusion from FTO [27] while maintaining crystallinity and conductivity of FTO. As reported by Morrish et al about the longer time increasing the activation for a lower temperature, both 550°C and 650°C type samples were also annealed for 5 hrs to observe the difference in photoactivity as compared to shorter time annealed samples [123]. It is to be noted that all these profiles were annealed directly to the respective temperatures at a ramping rate of 2°C/min and not through a profile of 550°C, 2 hours since such low ramp rate ensured complete crystallization of FeOOH to Fe_2O_3 phase during annealing.

This **Section 4.1** reports pristine Fe_2O_3 nanorods synthesized through hydrothermal technique and annealed for different profiles. Photoelectrochemical characterization of these pristine films under frontside and backside illumination would be presented to investigate how charge transport affects the photoelectrochemical performance. Pristine nanorods were then coated with ALD grown TiO_x overlayer to reduce surface recombination and improve charge transfer to the electrolyte. Characterizations like photocurrent transients, electrochemical impedance spectroscopic analysis and bulk/surface charge separation efficiency evaluation are also performed to get an insight into the charge transport in pristine and coated films.

Results and Discussion

Pristine Fe_2O_3 nanorods with different annealing profiles were fabricated with the methodology as mentioned in **Section 3.2**. Structural/Morphological characterization and photoelectrochemical characterizations under front and back illumination were performed for pristine hematite nanorods. The charge transport in different sides of illumination is illustrated in **Figure 4.1.1** below. Frontside illumination is when light falls on the semiconductor side resulting in charge generation near the semiconductor/electrolyte interface. Whereas backside illumination is the case where light is directed from the FTO side and hence the photon absorption takes place near the FTO/semiconductor junction.

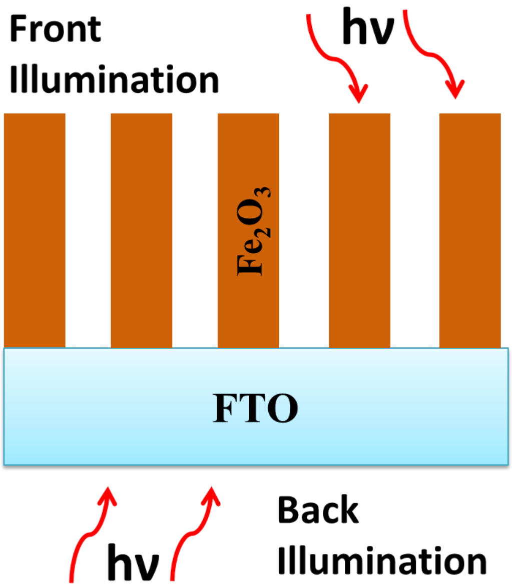

Figure 4.1.1 Schematic representation of hematite nanorods under front and backside illumination

XRD patterns for all the samples are presented in **Figure 4.1.2(a)** below. The peaks corresponding to 2theta value of 35.7° were considered for Gaussian fit. Peak intensity and FWHM values for different samples were: [550°C, 2hrs]: (200, 0.43), [550°C, 5hrs]: (219, 0.40), [650°C, 1hr]: (235, 0.39), [650°C, 5hrs]: (245, 0.38) and [750°C, 20 mins]: (89, 0.43). The peak intensity increases with annealing temperature till 650°C but decreases significantly at 750°C probably due to deformation of FTO as reported earlier by Annamalai et al [120]. FWHM is minimum and intensity is maximum for 650°C, 5 hrs which shows that the crystallinity of 650°C, 5 hrs samples was highest as compared to other samples. Photoelectrochemical characterization of these samples (as shown in **Figure 4.1.2(b)**) under frontside and backside illumination shows that the performance for 550°C, 5hrs is very low (<0.1 mA/cm^2) which indicates that annealing temperature was not enough for hematite thermal activation. The photocurrent for 650°C, 1 hr is also lower than 650°C, 5 hrs samples under back illumination.

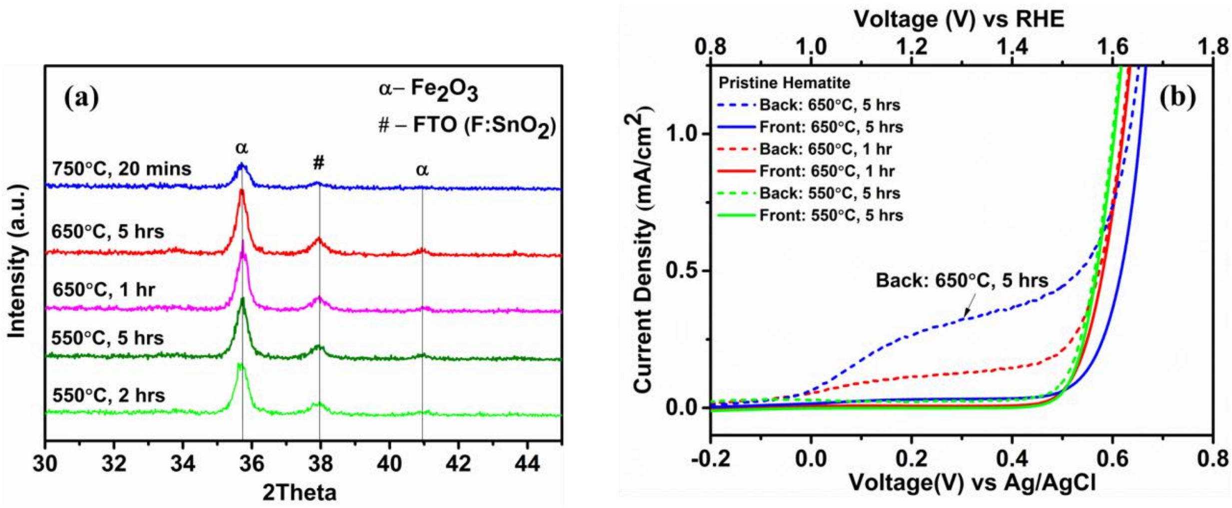

Figure 4.1.2 (a) XRD Spectra of pristine hematite nanorods prepared with different annealing profiles and (b) J-V Plots for different annealing profiles measured under standard conditions

This motivated us to work on sample annealed at 650°C, 5 hours which performs better than the 550°C sample. To compare samples diverse in their photocurrent and crystallinity trends and doping profile; only 550°C, 2 hrs, 650°C, 5hrs and 750°C, 20 mins samples were compared and studied in-detail as discussed further in this section.

After the hydrothermal reaction, FeOOH nanorods were formed (Cross-section Image is shown in **Figure A2,** Appendix) with a square cross-section, sharp edges and average rod length of around 700nm. After annealing them with different profiles mentioned above, these yellow colored nanorods changed to orange red colored films indicating the change of phase to α-Fe_2O_3 (Shown in **Figure 3.2.1**). FESEM images for these hematite films (as shown in **Figure A3,** Appendix) confirmed the circular cross section of Fe_2O_3 nanorods with diameter of around 70 nm for 550°C, 2 hours films. With higher temperature annealing, diameter of nanorods increased to about 100 nm probably due to aggregation of nanorods in compliance with earlier report by Ling et al [27]. EDS Spectra was also obtained for 650°C, 5 hours and 750°C, 20 mins annealed film (shown in **Figure A4,** Appendix) which confirmed the presence of Sn in the latter only due to Sn diffused from FTO.

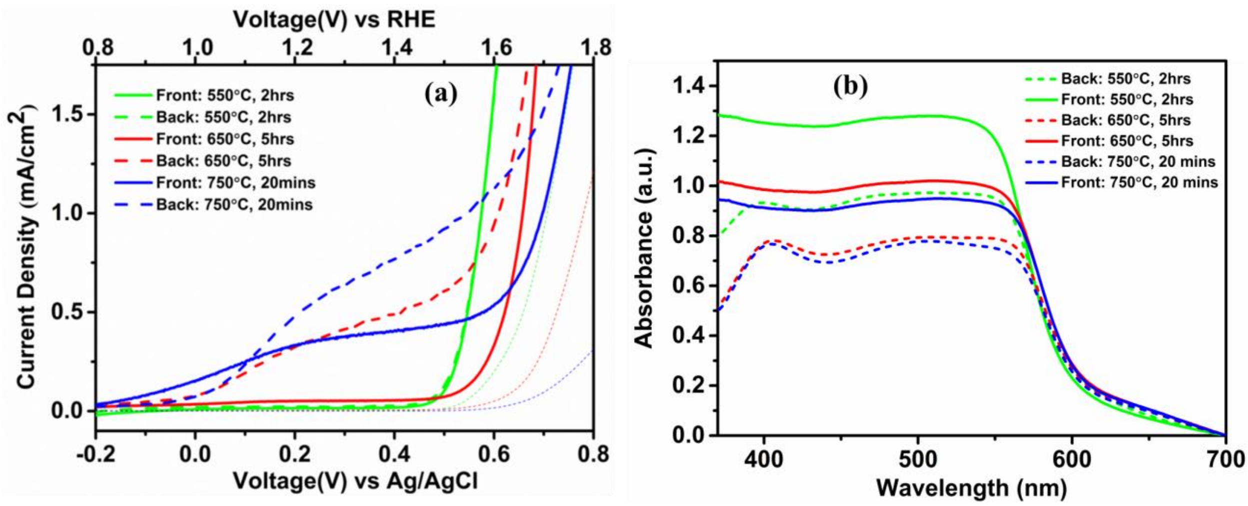

Figure 4.1.3 (a) Photocurrent Density-Potential (J-V) plots and, (b) Absorption Spectra for hematite nanorods fabricated using different annealing temperatures under back and front illumination

Photocurrent vs voltage bias curve for pristine hematite nanorods prepared with different annealing temperatures are shown in **Figure 4.1.3(a).** The measurements were performed under backside and frontside illumination for all samples, schematic for which is shown in **Figure 4.1.1.** It was observed that for 550°C, 2hrs profile, the pristine electrodes yielded very low photocurrent for both frontside and backside illumination indicating that carrier generation and their separation was limited because of poor charge transport properties of crystalline hematite [27]. In general, the samples show improved photocurrent when the annealing temperature increases to 650°C and 750°C for both frontside and backside illuminations. This can be attributed to the effect of improved crystallinity and Sn diffusion from FTO leading to doping of Sn^{+4} ions into the hematite semiconducting layer as reported earlier [27] which induces majority charge carriers - electrons in hematite nanorods. The absorption spectra of pristine nanorods under backside and frontside illumination are shown in **Figure 4.1.3(b)**. It is observed that the absorption decreases with increasing annealing temperature because of the agglomeration of nanorods which leads to less surface area and hence lesser light trapping. For all the films, backside showed a lower absorption as compared to the frontside measurement due to higher nanorods density near FTO/hematite which acts as a planar film resulting in lower light trapping as compared to more porous semiconductor/electrolyte surface exposed in frontside measurement.

To further investigate into the trends the photocurrent density-potential plots show, IPCE Spectra was performed for all the samples as shown in **Figure 4.1.4(a).** With increasing annealing temperature, the IPCE increased as in the case of photocurrent density due to increasing conductivity and crystallinity. Under backside and frontside illumination for respective samples, the plots showed a similar trend as the photocurrent density. IPCE for frontside illumination for all samples was lower than for backside which was is in contrast with the absorption spectra as shown in **Figure 4.1.3(b)**, where frontside absorption for all the samples was higher than backside. Hence, even though there are less photons being absorbed, backside illumination yield higher photocurrent and IPCE than frontside which is hypothesized to be due to the better charge transport driven by fast electron extraction to the back contact. This shows the reason behind photocurrent density trends is not due to the change in absorption but due to charge dynamics of the system.

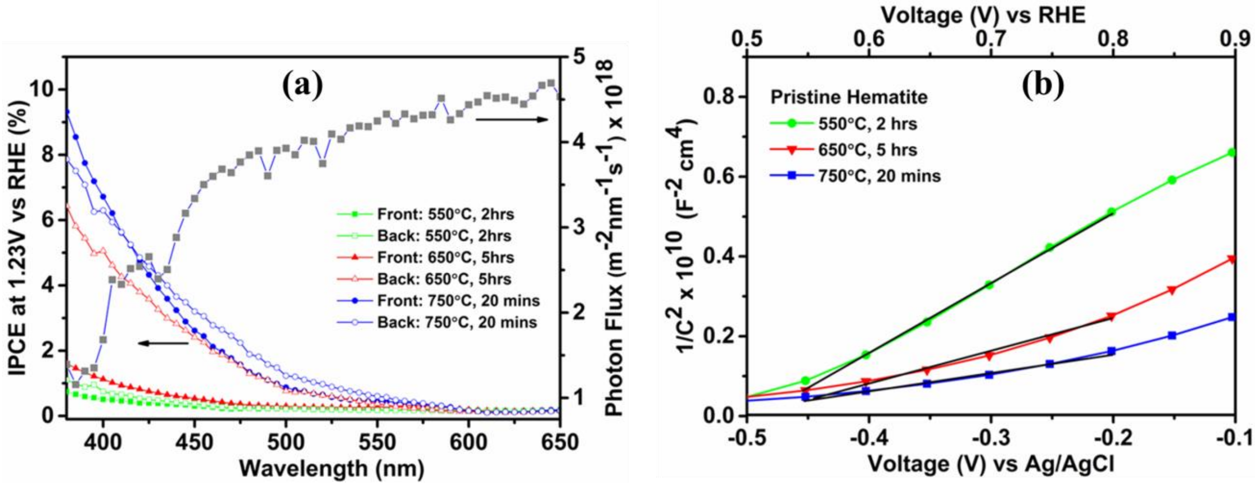

Figure 4.1.4 (a) IPCE Spectra for hematite films fabricated with varied annealing temperatures under back and frontside illumination. Grey Curve represents solar photon flux with varying wavelength, (b) Mott Schottky Plots for pristine Fe_2O_3 nanorods prepared with different annealing profiles

Mott Schottky analysis was performed for these films, as shown in **Figure 4.1.4(b)** which yielded a trend of decreasing slope of curves with increasing annealing temperature. As mentioned in **Section 2.5.4**, donor density increases with decreasing slope. Hence, with higher annealing, the donor density increased probably due to increase in Sn diffusion from FTO into the bulk semiconductor layer which explains the general trend in photocurrent density and IPCE Spectra with increasing annealing temperature.

The trends of J-V and IPCE curves under front and backside illumination could be explained using the schematic representation of charge transport in pristine nanorods shown in **Figure 4.1.5.** The yellow region represents the absorption depth of around 120nm for lowest energy photons (~550nm) with the total nanorods length of 700nm (represented as red region). As reported by Liang et al earlier for sprayed Fe_2O_3 films, the limiting factor in undoped Fe_2O_3 is the electron transport whereas for doped Fe_2O_3, it is hole transport [124].

In case of frontside illumination, electrons have to traverse a longer distance to FTO as compared to that in backside illumination where the collection of electron is higher due to the close proximity of photogenerated electrons with FTO back contact. Since the electrons are the majority carriers in an n-type semiconductor photoanode, their movement is driven by the conductivity of charge carriers in the bulk. This conductivity depends on the carrier concentration largely, since hematite possesses low electron mobility of around 10^{-2} $cm^{-2}V^{-1}s^{-1}$, which can be improved by adding electronic dopants to assist n-type doping [26]. On the other hand, the minority carriers- holes could move under electrical drift if they are generated in the depletion region or by diffusion if generated outside the space charge layer. Due to the low minority carrier diffusion length in hematite (2-4 nm) [26], the transport of these holes into the electrolyte before undergoing recombination is the key to efficiency. As mentioned earlier in context with influence of nanostructuring in **Section 2.1**, space charge region present in nanorods is formed along the edges of nanorods due to which hole transport occur radially outwards from their edges (semiconductor/electrolyte interface) into the electrolyte. Since it is known that undoped and un-passivated hematite nanorods exhibit poor surface properties and slow water oxidation kinetics, the holes are trapped and accumulated at the semiconductor/electrolyte interface in both frontside and backside illumination. Hence, electron transport becomes the limiting factor for photocurrent density which defines the photocurrent in undoped/un-passivated hematite.

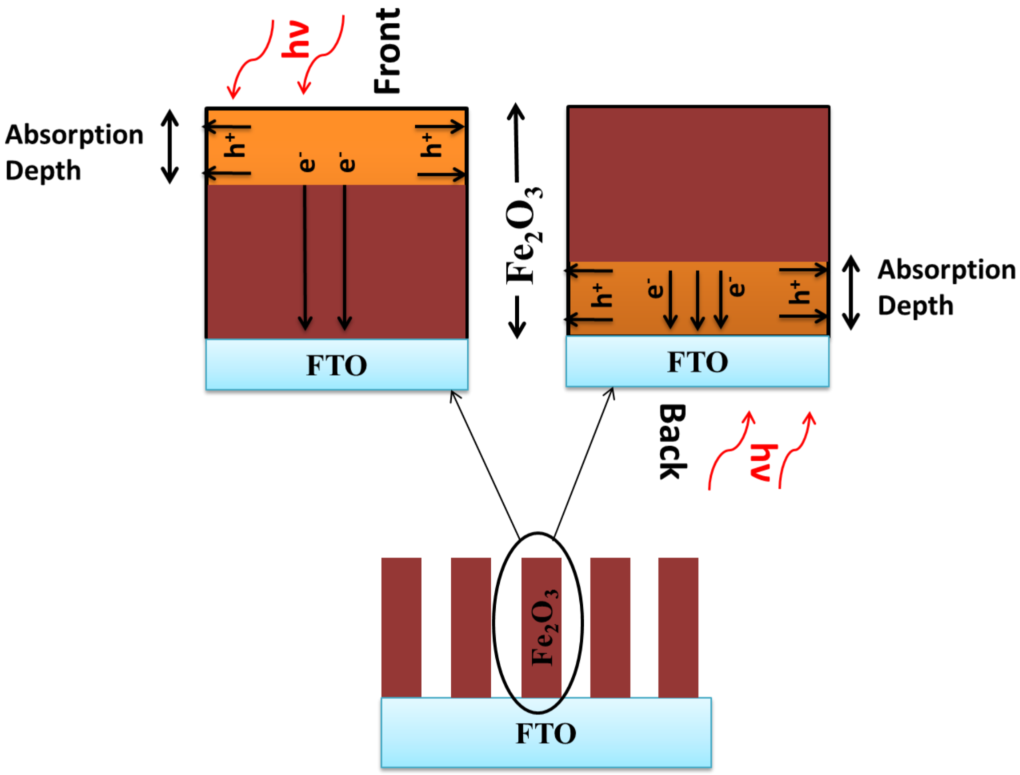

Figure 4.1.5 Schematic Representation of electron/hole transport in hematite nanorods under front and backside illumination

For 550°C, the conductivity in the bulk is very poor resulting in slow electron transport and hence in low photocurrent for both frontside and backside illumination as shown in **Figure 4.1.3(a)**. Interestingly, for 650°C hematite, frontside photocurrent is minimal due to poor electron transfer to the back contact but under backside illumination, the electron collection on the back contact is higher and hence shows significant photocurrent density. This trend for back and frontside photocurrent is similar to hematite annealed at 750°C as well. Backside photocurrent is relatively higher than frontside due to proximity of photogenerated electrons with back contact. For 750°C samples, the electron transport is easier even in case of frontside illumination where the electrons have to traverse to back contact possibly due to increased conductivity due to doping of Sn^{+4} ions in bulk. Hence, the photocurrent density under frontside illumination was higher for 750°C as compared to that for 650°C samples.

It has been shown through spectral evidence that photocurrent ascends with increased applied bias due to decreasing electron density in the bulk which in turn inhibits back electron-hole recombination in the semiconductor layer [97, 125]. This is in compliance with the photocurrent trend observed for the samples where apparently back electron-hole recombination mechanism is being suppressed through efficient collection of electrons at the back contact in backside illumination.

This trend of back and front side photocurrent was different for hematite nanorods annealed at higher temperature (800°C, 20 mins) i.e. frontside photocurrent was observed to be higher than the backside photocurrent as shown in **Figure A5** (Appendix). This could be due to the dependence of photocurrent trend on the extent of Sn doping in hematite nanorods which is higher for samples annealed at 800°C resulting in higher conductivity of electrons in bulk and hence efficient separation of electrons and holes. Since for doped films, the hole transport is the limiting factor for photocurrent [124]. In such highly doped films, holes can easily inject into the electrolyte due to their generation near the semiconductor/electrolyte interface under frontside illumination. The results of 750°C and 800°C annealed samples suggest that there is a competing mechanism where electrons and holes define the photocurrent trends under backside and frontside illumination depending on the extent of doping in hematite nanorods.

To get an insight into hole accumulation on the semiconductor/electrolyte interface, photocurrent density was evaluated under chopped light for both front and backside illumination as shown in **Figure 4.1.6**. Anodic transient for frontside illumination was observed to be smaller than the backside illumination. This could be due to the fact that photogenerated holes are being produced closer to the semiconductor/electrolyte surface and hence the hole accumulation on the surface is low. Whereas under backside illumination, holes accumulate on the surface of nanorods, which are densely concentrated near FTO and hence the recombination of holes is much higher than in the case of frontside illumination.

These results are also in agreement with the Amperometric curves extracted for these films under frontside and backside illumination at 1.23 V vs RHE (shown in **Figure A6,** Appendix). The trends of anodic and cathodic transients with time are similar to the transients with voltage bias as mentioned above.

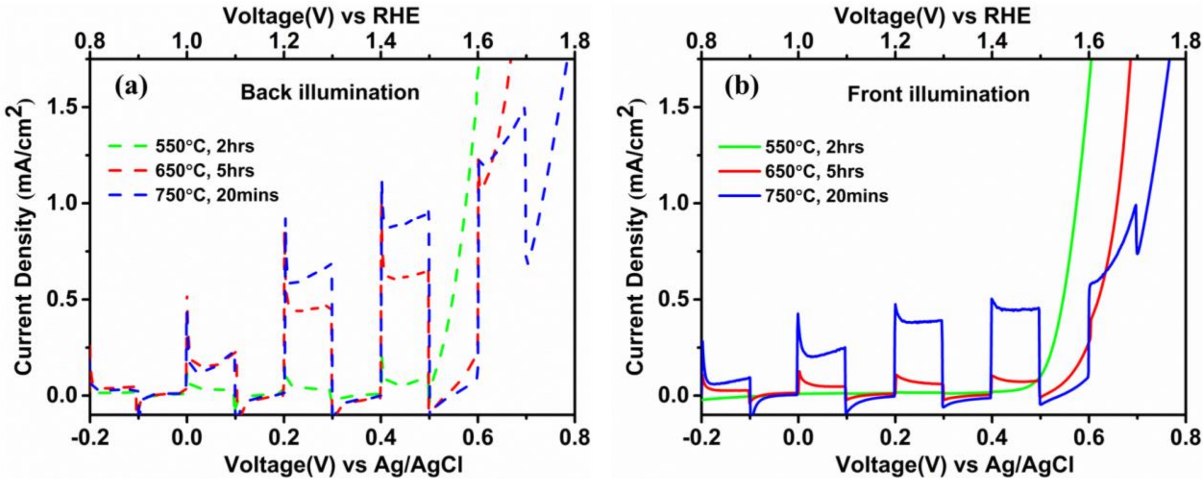

Figure 4.1.6 J-V plot for hematite thin films fabricated with different annealing temperatures under (a) backside and (b) frontside illumination of chopped solar simulated light

As discussed earlier, the charge transport in the pristine films under different annealing was preferentially limited to electron transport to the back contact. Hence, to explore the charge dynamics of the bulk, Electrochemical Impedance Spectroscopy (EIS) was performed for all the samples under frontside and backside illumination at 1.23V vs RHE. Nyquist plots for these measurements and the fitted data are shown in **Figure 4.1.7**. The circuit fitted for the measurements is shown in inset of **Figure 4.1.7(b).** R_s is the series resistance which depends on the contact of external circuit with FTO, C_{bulk} is the capacitance of bulk semiconducting layer, R_{trap} is the resistance of the trapping of photogenerated charge carriers at the surface states, $R_{ct,ss}$ is the resistance to injection of holes into the electrolyte through those surface states and C_{ss} is the capacitance attributed from the surface states.

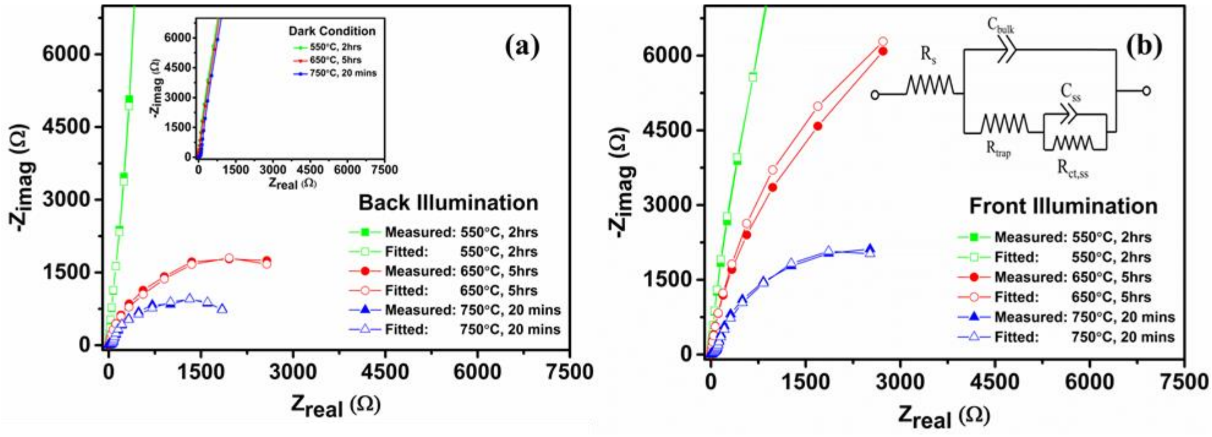

Figure 4.1.7 Measured and Fitted Nyquist plots for pristine hematite thin films under (a) back and (b) frontside illumination (inset: Nyquist plot for films under dark conditions for comparison)

Under dark conditions, R_{CT} values were very high of the order of 6 MΩ for all the films understandably due to absence of minority carriers (as shown in inset of **Figure 4.1.7(a)**). Under both backside and frontside illumination, R_{trap} and $R_{ct,ss}$ decreased with higher temperature annealing and was lowest for 750°C samples which implies holes from valence band were more likely to inject into electrolyte through surface states rather than undergoing bulk recombination with electrons. This symbolize the importance of Sn^{+4} ions doping from FTO which increased the electron transport in bulk by increasing the carrier concentration and hence conductivity.

For 650°C samples, R_{trap} under front illumination was high at 14KΩ whereas that under back side was 1400Ω which denotes increased conductivity and hence low bulk recombination. This trend was similar to 750°C samples, implying the electron transport under backside was higher than the frontside which followed the earlier trends shown by photocurrent density and IPCE Spectra. $R_{ct,ss}$ under backside illumination was lower as compared to frontside illumination for all different annealing profiles. This could be due to lower surface recombination with photogenerated electrons at the semiconductor-electrolyte interface in case of backside illumination where electron extraction to back contact is efficient.

To account for the bulk and surface charge separation efficiency for above samples, photoelectrochemical characterizations, under the presence of hole scavenger, H_2O_2 in the electrolyte, were performed. Hole scavenger allows the fast injection of holes into the electrolyte and hence the surface charge separation efficiency, denoted as η(catalysis), with H_2O_2 becomes unity.[117] Further details about the measurement are discussed in **Section 2.5.5**. J-V plots for all samples with 1M NaOH + 0.5M H_2O_2 as electrolyte are shown in **Figure 4.1.8(a)** below. For all the samples, the backside photocurrent (J_{H2O2}) was higher than the frontside probably due to better electron collection in backside while the hole transport for both sides is efficient owing to hole scavenging property of H_2O_2. Difference in front and back was small for the 750°C anneal samples which is due to better electron transport even for the frontside owing to higher conductivity of the sample as compared to the case for other two samples.

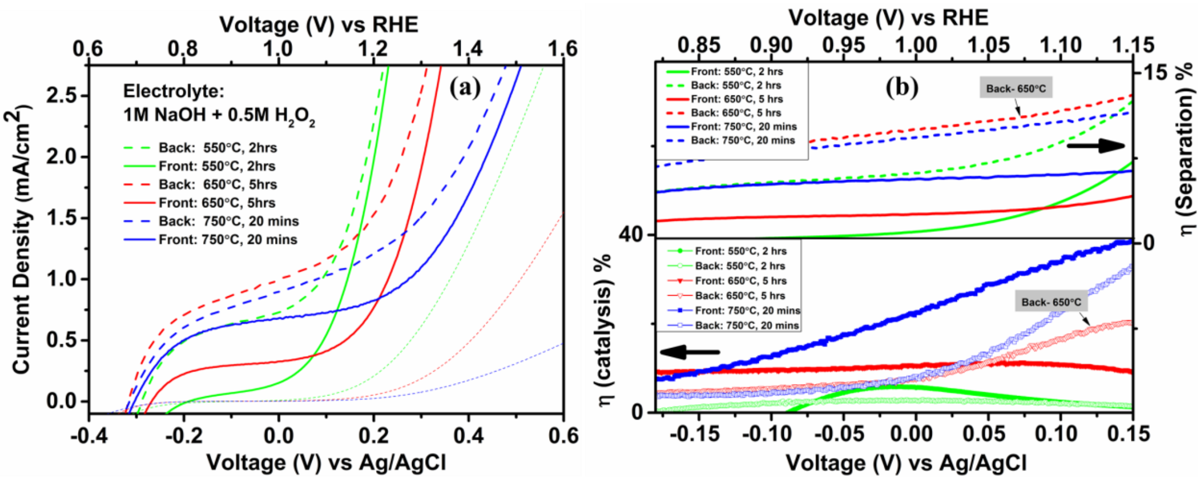

Figure 4.1.8 (a) J-V plots and (b) Bulk/Surface Charge efficiency curves for all the samples measured under back and frontside illumination in the presence of Hole Scavenger H_2O_2

Figure 4.1.8(b) shows the bulk [η(separation)] and surface [η(catalysis)] charge separation efficiency for these samples in the voltage region occurring before their dark current onset. Bulk charge separation efficiency for backside illumination is higher for all the samples presumably due to higher electron transport. This efficiency for 650°C is higher than doped samples (750°C) as well in spite of J_{abs} of 750°C being higher which motivated us to work on this temperature to effectively tackle the problem of bulk recombination.

While bulk charge separation efficiency is highest for 650°C samples, surface charge separation efficiency for 750°C was highest under both front and backside illumination as compared to 650°C. This suggests the surface properties of 750°C samples are much better than 650°C samples. Hence, to improve the surface kinetics of 650°C samples, for which surface recombination is the limiting factor, surface passivation of hematite nanorods was performed which will be discussed in following section.

Surface Passivation of Fe_2O_3 Nanorods using ALD Grown TiO_x overlayer

As discussed in the above section, η(separation) was highest for 650°C samples, even higher than 750°C doped samples which means bulk recombination among all the samples prepared was minimum for these 650°C samples under backside illumination. To tackle bulk recombination there have been methods of nanostructuring or forming heterojunctions as mentioned in **Section 2.1** and **Section 2.4** respectively, but this is all dependent on the process methodology used in preparation of electrodes. For the upcoming work in the present dissertation, the hematite (Fe_2O_3) nanorod samples prepared by the similar methodology as 650°C electrodes were used due to minimum bulk recombination exhibited by them and were then utilized to further improve charge separation and transport as mentioned in subsequent chapters in this thesis.

For 650°C samples, the challenge was to increase the surface charge efficiency represented as η(catalysis) which reflects on the surface recombination of photogenerated holes with surface defects or traps present on the semiconductor/electrolyte interface. As mentioned in **Section 2.3**, surface overlayers or coupling with a cocatalyst on the top of semiconductor layers is effective in enhancing hole injection into the electrolyte by passivating surface defects or changing hole transfer kinetics. It has been shown that oxide overlayers like Ga_2O_3, Al_2O_3, SnO_2 etc. on top of hematite resulted in a cathodic shift in onset potential and enhanced the photocurrent density. TiO_2 being an abundant oxide with a wide band gap semiconductor does not absorb much visible light spectrum and hence when coupled with hematite could act as the surface passivating layer without hindering the absorption exhibited by hematite. Hence, here we employed TiO_x overlayer on top of hematite nanorods using Atomic Layer Deposition technique which could fabricate a defined layer on top of diverse nanostructures with precise control.

FeOOH nanorods (intermediate of Fe_2O_3 nanorods before annealing in air) were coated with TiO_x overlayer using Atomic Layer Deposition (ALD) technique through alternate pulsing of TDMATi and H_2O precursors, before annealing it to similar conditions of 650°C for 5 hours. The back and frontside illumination photocurrent and efficiencies were analyzed for the pristine and TiO_x coated samples.

Atomic Layer Deposition Technique allows a precise control on fabrication of a thin overlayer with similar geometry as the base material, here nanorods. The precursors were pulsed through ALD on as-grown FeOOH nanorods prepared as mentioned in **Section 3.2**. This allowed a very thin overlayer of TiO_x, of around 5 nm, to form on FeOOH Nanorods. Due to high temperature annealing, Fe atoms diffused to the overlayer and Ti atoms diffused inside which resulted in a very thin overlayer of $Fe_xTi_yO_z$ (~8nm) on the top of Fe_2O_3 [126].

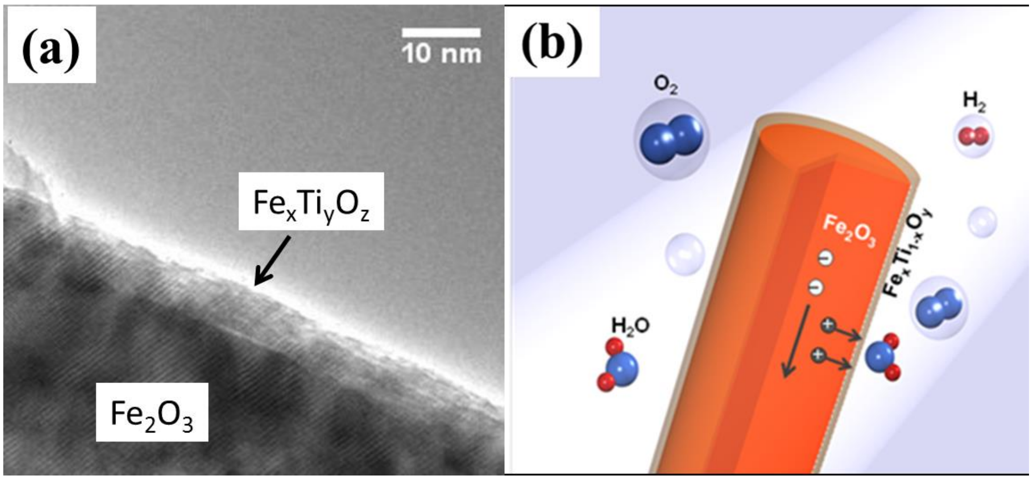

Figure 4.1.9 (a) TEM image and (b) Schematic representation of TiO_x coated Fe_2O_3 nanorods (Adapted from Li, X.; Bassi, P. S.; Boix, P.; Fang, Y.; Wong, L. H. Revealing the role of TiO_2 surface treatment of hematite nanorods photoanodes for solar water splitting. *ACS Appl. Mater. Interfaces, , 2015, 7 (31), 16960–16966* © 2015 American Chemical Society)

FESEM images of coated thin films showed no significant difference in the dimensions from the pristine thin films (**Figure A7**, Appendix). For both samples, nanorods of around 700 nm in length and a circular cross-section of diameter around 80-100 nm were observed. The coated films looked rough as compared to pristine films due to $Fe_xTi_yO_z$ overlayer. **Figure 4.1.9(a)** shows a crystalline Fe_2O_3 nanorod and contrasting amorphous layer of $Fe_xTi_{1-x}O_y$ (thickness around 8 nm) on top of nanorod. A schematic representation of TiO_x coated Fe_2O_3 nanorods system with photogenerated electron and hole transport is demonstrated in **Figure 4.1.9(b)**. It shows the electron transport is along the [110] direction of nanorods whereas the hole injection into the electrolyte is across radially. The thin TiO_x overlayer converted into $Fe_xTi_yO_z$ layer on the top after annealing. This could be realized through the Raman Spectra of pristine and TiO_x coated hematite nanorods as shown in **Figure A8,** Appendix. It can be observed that the peak corresponding to TiO_2 E_g (~130cm^{-1}) appeared for films annealed at 400ºC signifying formation of TiO_2 layer. The peak diminished after annealing at 650ºC which marked the formation of $Fe_xTi_yO_z$ layer which has a well-defined geometry along the periphery of Fe_2O_3 nanorods desirable for surface passivation.

Photoelectrochemical characterizations were performed to observe the effect of TiO_x coating on the photocurrent density under front and backside side illumination as shown in **Figure 4.1.10**. J-V plots in **Figure 4.1.10(a)** shows the pristine Fe_2O_3 nanorods showing a similar trend prepared with annealing condition of 650ºC, 5 hours as discussed in **Section 4.1**. Backside photocurrent is higher than the frontside photocurrent which is almost negligible. After coating with TiO_x overlayer, photoanode showed a manifold enhancement of around 1.2 mA/cm^2 for frontside and 0.8 mA/cm^2 for backside at 1.23 V vs RHE as compared to the pristine nanorods which showed 0.2 mA/cm^2 at same potential.

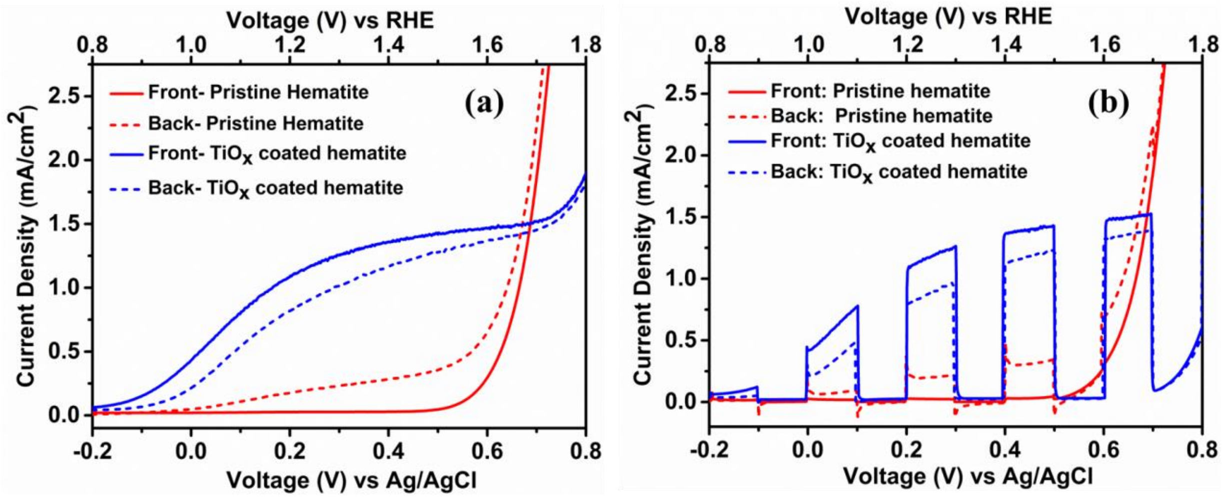

Figure 4.1.10 (a) Standard J-V plots and (b) J-V plots under chopped light, for pristine and TiO_x coated hematite films under front and backside illumination

J-V plots were also evaluated under chopped light as shown in **Figure 4.1.10(b)**. Anodic and cathodic transients for coated films diminished as compared to the pristine films which show that there is no accumulation at all and photogenerated holes and electrons are participating efficiently in photocurrent as compared to pristine nanorods. Absorption spectra shown in **Figure 4.1.11(a)** shows the frontside absorption is higher for both pristine and coated films which are probably due to the difference in light trapping on FTO/Fe_2O_3 or $Fe_2O_3/Fe_xTi_{1-x}O_y$ surface owing to the porosity of nanorods.

From JV plots shown in **Figure 4.1.10,** it could be observed that there is a reversal of trend for frontside and backside photocurrent for coated films as compared to pristine films which complies with the absorption spectra i.e. the frontside absorption of both coated and pristine nanorods is higher than that of backside. This suggests under frontside, there is more potential of higher photocurrent than backside for both kinds of samples.

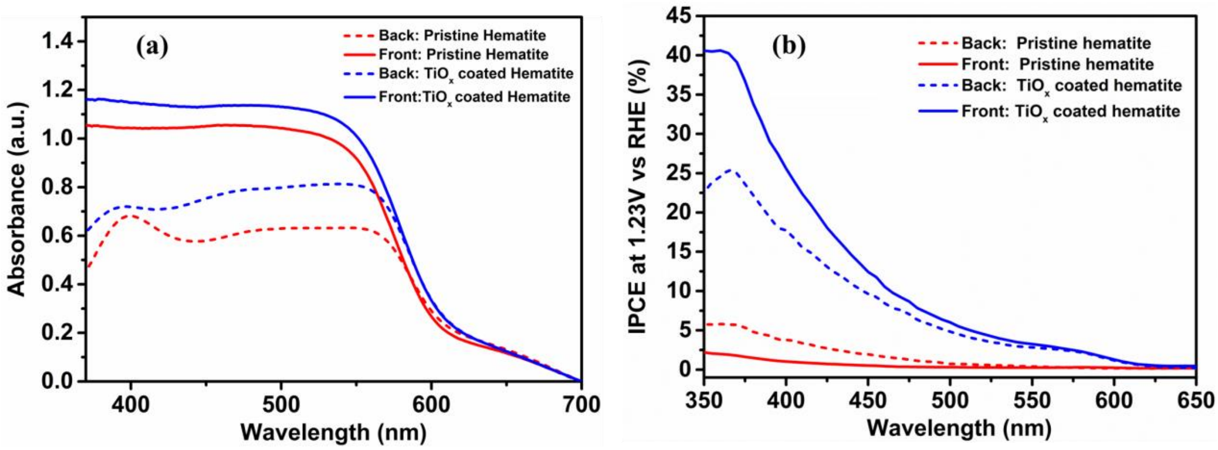

Figure 4.1.11 (a) Absorption and (b) IPCE Spectra for pristine and TiO_x coated hematite films under back and frontside illumination

For pristine samples, as mentioned earlier, higher backside photocurrent was observed due to better collection of electrons to the back contact which drives the overall reaction. But the holes undergo trapping or accumulation on the semiconductor/electrolyte interface leading to recombination with photogenerated electrons. Whereas for coated films, holes generated undergo lesser accumulation due to surface passivating effect exhibited by TiO_x overlayer and hence contribute to the overall photocurrent in coated samples apart from electron transport. Since for coated samples, higher absorption is on the frontside, more carriers are generated and hence more holes could participate to yield higher photocurrent in frontside as compared to backside.

The IPCE of coated and pristine thin films is shown in **Figure 4.1.11(b)**. It shows IPCE of coated films around 35% and 22% for 380nm photons under frontside and backside illumination respectively. Compared to the pristine nanorods which exhibit IPCE around 5% and 2% for backside and frontside respectively for 380 nm photons, coated films efficiency is improved immensely. This trend is consistent with the photocurrent trends shown earlier in **Figure 4.1.10**. For coated films, frontside IPCE is higher than backside IPCE consistent with the photocurrent density which could be due to higher absorption exhibited by the former. For pristine nanorods, the backside is higher because the mechanism of electron transport which is the driving force for photocurrent under poor hole injection into the electrolyte. For coated films, higher absorption in frontside yields higher IPCE probably due to the better hole injection into the electrolyte after surface passivation

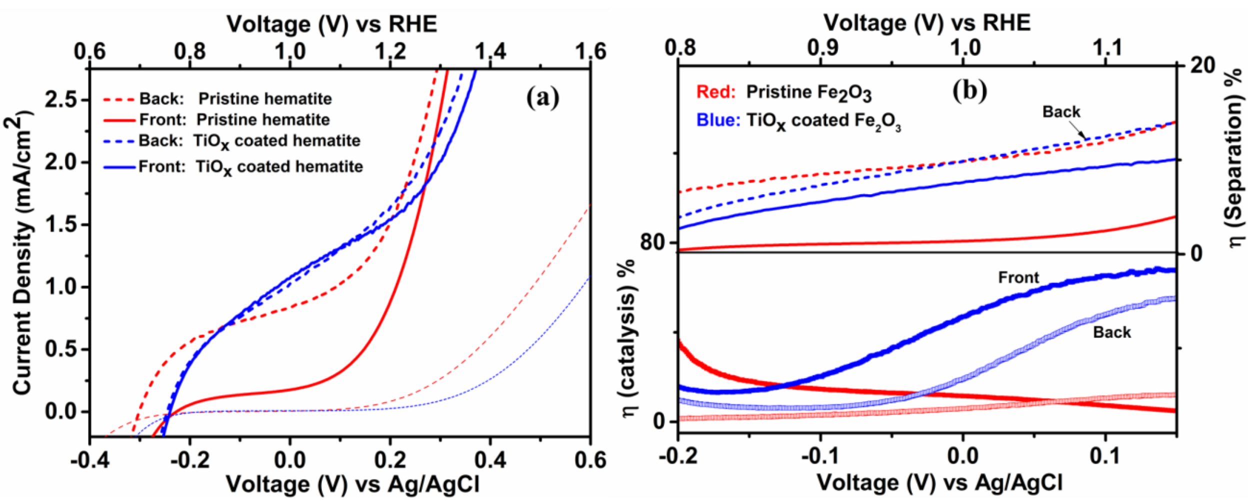

Figure 4.1.12 (a) Current-potential curves for pristine and TiO_x coated hematite thin films under the presence of hole scavenger (H_2O_2) , and (b) Charge carrier efficiency for surface [η(catalysis)] and bulk [η(separation)] for pristine and coated films extracted from (a)

Charge transport in coated nanorods was investigated by performing photoelectrochemical characterizations under the influence of hole scavenger (H_2O_2) as shown in **Figure 4.1.12(a).** Photocurrent density was higher for backside illuminated pristine Fe_2O_3 nanorods than its frontside with H_2O_2 in electrolyte which is similar to the photocurrent trend without H_2O_2. On the other hand, the coated nanorods yielded a similar photocurrent under backside and frontside illumination. This suggests after induction of hole scavenger, hole injection into the electrolyte is no longer limiting the photocurrent and hence the photons absorbed defines the photocurrent. This could be understood by observing the bulk and surface charge separation efficiency as shown in **Figure 4.1.12(b).** Bulk Charge separation efficiency, η(separation), which determines the amount of bulk recombination of charge carriers, suggests that for coated films, back efficiency is higher than the frontside which could be due to the J_{abs} which is lower under backside since $J_{H_2O_2}$is similar for both sides. This means the photogenerated holes are transported to the electrode surface more effectively under backside illumination possibly due to inhibition of back electron-hole recombination mechanism owing to better electron collection at the back contact. Whereas the surface charge separation efficiency is lower for backside suggesting that the hole injection into the electrolyte is limiting the photocurrent. Another interesting observation is about the bulk charge separation efficiency exhibited by the pristine and coated films under backside illumination. Both shows similar efficiency which suggests for both pristine and coated films, holes are reaching the surface efficiently but the limiting factor is the hole injection into the electrolyte due to which the difference in surface charge separation efficiency, η(catalysis), is observed under backside illumination. After coating with TiO_x overlayer, η(catalysis) increased manifold and reached as high as 70% at 1.15 V vs RHE for frontside illumination as compared to very low efficiency, of the order of 10%, displayed by pristine nanorods. This suggests that the performance of pristine nanorods was limited by hole injection into the electrolyte which improved after coating TiO_x on top of hematite which substantiates its role as a surface passivating layer. It is to be noted that the region chosen for the efficiency curve is upper bounded by the dark current onset potential and lower bounded by the region where positive photocurrent is observed.

Conclusion

Pristine hematite nanorods were synthesized under different annealing profiles for application as photoanode in PEC Cell and were then characterized under front and back illumination. An optimized annealing condition that yield thermally activated and crystalline hematite nanorods based electrode without damaging the morphology or conductivity of FTO substrates, was obtained. These nanorods displayed different photocurrent trends under front and back illumination which was claimed to be due to the better electron transport in back illumination which yielded higher photocurrent for all samples as compared to their front counterparts. Bulk and surface charge efficiency measurements with hole scavenger (H_2O_2) yielded information that back illumination of 650ºC samples displayed least bulk recombination. Hence, this annealing profile of 650ºC, 5 hours was used for further optimization to reduce surface recombination which was still higher as compared to 750ºC Sn-doped samples. ALD grown TiO_x overlayer on top of hematite nanorods resulted in an overlayer of $Fe_xTi_{1-x}O_y$ (~5 nm) after solid state reaction at high temperature. A manifold enhancement in performance was observed, after TiO_x coating, with photocurrent reaching around 1.2 mA/cm^2 at 1.23V vs RHE under frontside illumination. It was observed that after coating, the frontside photocurrent exceeded the backside which was in contrast to the trend in pristine nanorods where significant backside photocurrent was mainly driven by electron transport. Through evaluation of IPCE and charge separation efficiency, it was illustrated that the hole injection into the electrolyte was enhanced due to the overlayer and hence photons absorbed were efficiently converted to photocurrent due to inhibition of electron-hole recombination. This strategy of surface passivating Fe_2O_3 nanorods using ALD grown TiO_x overlayer was helpful in dealing with the challenge of low performing hematite nanorods whose performance is limited by the hole accumulation on the semiconductor/electrolyte interface.

4.2 Introducing Crystalline Fe_2TiO_5, with Better Band Energetics than Fe_2O_3, as Photoanode

Introduction

For solar water splitting, hematite is one of the strongest candidates and has achieved appreciable performance in terms of photocurrent but still has intrinsic limitations of poor charge transport properties and unfavorable band level positions for efficient overall water splitting. Hence, there is a need to explore new photoanodes and as discussed in **Section 2.2**, iron titanates could possess fascinating properties that could be confluent of diverse complementary characteristics exhibited by iron and titanium compounds. We investigated $FeTiO_3$ as a photoanode for solar driven water oxidation. But owing to the band gap of $FeTiO_3$ (~2.5-2.9 eV), using it by itself as a photoanode results in an incomplete light absorption in the visible range [127]. Also, Fe^{2+} oxidation state present in the material was difficult to process as it may result in mixed phases with Fe^{3+} ions after high temperature annealing. Due to these difficulties we switched to a more stable phase Fe_2TiO_5 which is a hybrid of Fe_2O_3 and TiO_2. The idea behind using hybrid of Fe_2O_3 and TiO_2 is to utilize good charge transport properties of TiO_2 and the better band gap of Fe_2O_3 for absorption of solar spectrum to be used as a photoanode in PEC. Fe_2TiO_5 is a promising candidate with stability in aqueous solution and an optimum band gap.

In this **Section 4.2**, synthesis of Fe_2TiO_5 thin films grown on FTO substrates through hydrothermal technique has been reported. Surface passivation of as-grown films using thin SnO_x overlayer was performed to enhance the performance of pristine films. Structural/Morphological characterization of thin films have been shown here which confirms pure phase of Fe_2TiO_5 nanoporous network based thin films with a feature size of 30-50 nm.

Photoelectrochemical characterizations of pristine and SnO_x coated Fe_2TiO_5 thin films were performed to present its potential as a photoanode for PEC Cells. Further measurements like UPS/XPS and Hall measurements are reported to evaluate its band level positions and intrinsic electronic properties which are influential in determining its development as a viable candidate for application in solar water splitting.

* Reprinted this section with permission from: "Bassi P.S.; Chiam S. Y.; Gurudayal; Barber J.; Wong L. H.; "Hydrothermal Grown Nanoporous Iron Based Titanate, Fe_2TiO_5 for Light Driven Water Splitting"; *ACS Appl. Mater. Interfaces, 2014, 6 (24), pp 22490–22495"*, Copyright 2014, American Chemical Society

Results and Discussion

Figure 4.2.1(a) shows top-view FESEM image of pristine Fe_2TiO_5 sample annealed in air ambience at 750°C. A nanoporous network of particles size around 30-50 nm could be observed. In the inset of **Figure 4.2.1(a),** FESEM Image of SnO_x coated sample with a very thin layer of SnO_x nanoparticles on the surface is shown. XRD pattern of as-grown and annealed films at 750°C (with earlier mentioned annealing profile) are as shown in **Figure 4.2.1(b)**. The as-grown films were amorphous and only the peaks corresponding to the FTO substrates (JCPDS no. 001-0625) were observed.

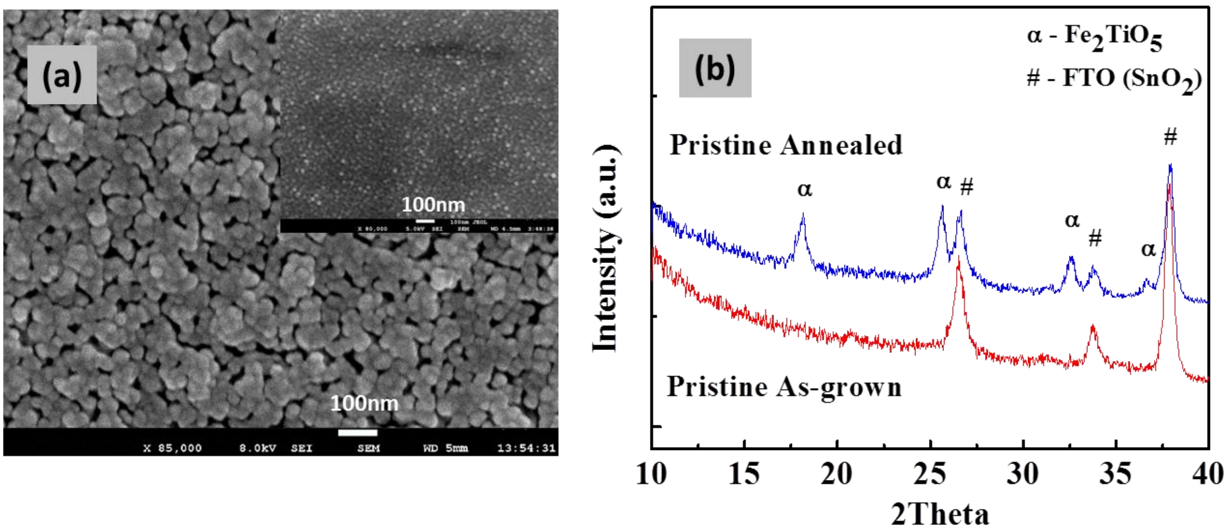

Figure 4.2.1 FESEM top-view image of (a) Fe_2TiO_5 thin film (inset: SnOx coated thin film) (b) XRD for pristine as-grown and annealed films; Adapted from Bassi, P.S.; Chiam S. Y.; Gurudayal; Barber J.; Wong L. H.; *"*Hydrothermal Grown Nanoporous Iron Based Titanate, Fe_2TiO_5 for Light Driven Water Splitting"; *ACS Appl. Mater. Interfaces, 2014, 6 (24), pp 22490–22495".* © 2014, American Chemical Society

For pristine annealed film, apart from FTO, characteristic peaks from Fe_2TiO_5 (JCPDS no. 009-0182) were observed which shows formation of pseudobrookite, Fe_2TiO_5 in orthorhombic phase. The crystallite size was calculated from the full-width half maximum of

Fe_2TiO_5 (230) peak and was found to be about 40 nm. This confirms fabrication of a single phase Fe_2TiO_5 which is desirable for photoactivity applications since the mixed phases could act as the recombination centres. The thickness of the film was found to be around 100 nm, measured using Surface Profilometer. HRTEM image was also analyzed and is presented in **Figure 4.2.2** below:

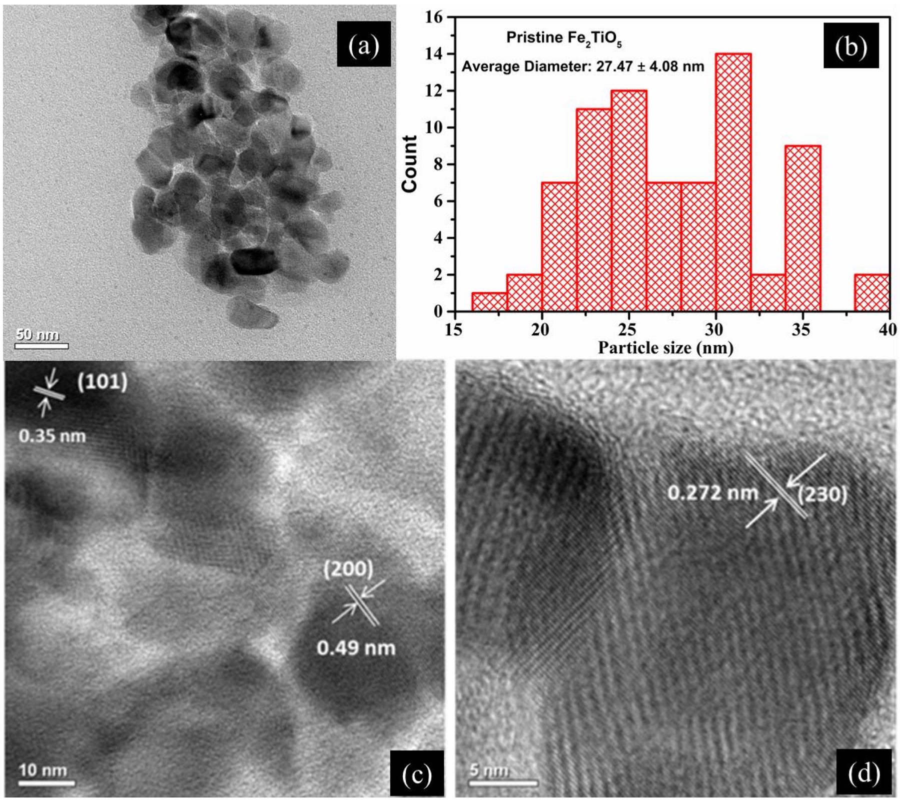

Figure 4.2.2 (a) HRTEM Image of pristine Fe_2TiO_5 nanoporous film, (b) Size distribution diagram for Fe_2TiO_5 nanoparticles, (c) and (d) showing lattice planes (101), (200) and (230) corresponding to Fe_2TiO_5

It shows the TEM image of Fe_2TiO_5 nanoparticles in which the average size of the Fe_2TiO_5 nanoparticles are 27.47 ± 4.08 nm and the particle size distribution is shown in **Figure 4.2.2(b)**. The d spacing calculated from the selected area, as shown in the HRTEM image ((c) and (d)), were 0.27, 0.35 and 0.49 nm corresponding to the (230), (101) and (200) planes respectively for orthorhombic Fe_2TiO_5 (pseudobrookite) crystal.

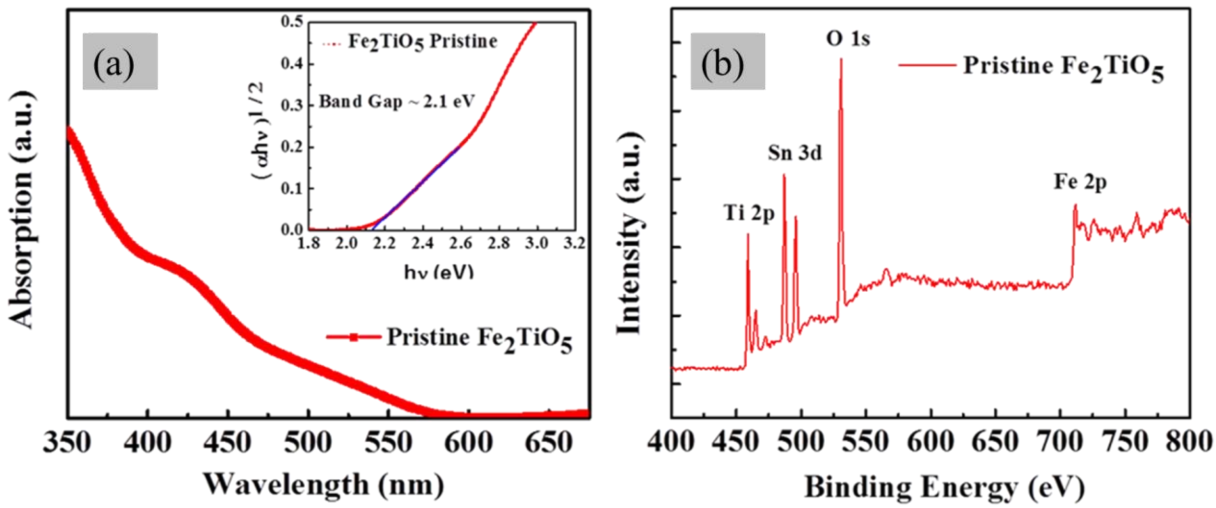

Figure 4.2.3 (a) Absorption Spectra (inset: Tauc plot) and (b) XPS Scan, for Fe_2TiO_5 thin film. Adapted from Bassi, P.S.; Chiam S. Y.; Gurudayal; Barber J.; Wong L. H.; *"Hydrothermal Grown Nanoporous Iron Based Titanate, Fe_2TiO_5 for Light Driven Water Splitting"; ACS Appl. Mater. Interfaces, 2014, 6 (24), pp 22490–22495".* © 2014, American Chemical Society

UV-Vis spectrum for pristine Fe_2TiO_5 thin film is shown in **Figure 4.2.3(a).** It shows absorption in visible region of solar light spectrum with absorption band edge around 570 nm. Absorption coefficient evaluated from the diffuse reflectance measurement is shown in **Figure B1**, Appendix. It showed a low absorption coefficient which is one of the limitations of pristine Fe_2TiO_5 which can be tackled by fabrication of thicker films. To evaluate the band gap, tauc plot analysis was performed for Fe_2TiO_5 thin film. Being an indirect band gap semiconductor, it yielded a band gap of around 2.1 eV which is in compliance with the earlier reported value [84]. The effect of SnO_x overlayer on nanoporous thin film did not show much effect on absorbance in visible range of solar spectrum due to wide band gap (~3.2 eV) of SnO_2, To identify the presence and oxidation state of Fe, Ti in pristine Fe_2TiO_5 thin films, XPS scan was performed and is as shown in **Figure 4.2.3(b)**. Peaks corresponding to valence states of Fe^{+3}, Ti^{+4} were observed in the survey scan. The high resolution scans for Fe^{+3}, Ti^{+4}, O^{-2} and Sn^{+4+} are shown in **Figure B2** (Appendix) for more detailed peak assessment. It should also be noted that the peak corresponding to Sn^{+4} also appears which may be the consequence of the high temperature annealing of thin films at 750°C which allows the diffusion of Sn from FTO substrates in the semiconducting film [27].

Photoelectrochemical characterizations of Fe_2TiO_5 thin films as photoanodes for solar water oxidation were performed under dark and standard illumination condition. A photocurrent density of 0.1 mA/cm^2 at 1.23 V vs. RHE and 0.28 mA/cm^2 at 1.75 V near the dark current onset was observed for pristine films as shown in **Figure 4.2.4(a)**. As presented in the inset of the mentioned figure, transparent films with a brownish colour could be observed. The low photocurrent density could therefore be due to an insufficient absorption of solar light spectrum. Photocurrent density was also evaluated for pristine films annealed at 550°C and 650°C which yielded 0.04 mA/cm^2 and 0.07 mA/cm^2 at 1.23V vs RHE respectively (**Figure B3**, Appendix). Since the performance for these films were lower than that for samples annealed at 750°C (0.1 mA/cm^2), the latter was used for in-detail characterization. As mentioned earlier, due to low absorption coefficient of Fe_2TiO_5 films, the films are required to be thick to allow complete solar spectrum absorption. To increase the thickness of the films, efforts were made by changing the hydrothermal conditions through optimization of hydrothermal reaction time, reaction temperature and concentration of precursor solution which resulted in either a non-uniform powder like film with poor adhesion to the substrate or did not have much effect on the thickness of the films. Other efforts resulted in formation of mixed phases with presence of a hematite phase which was not desirable.

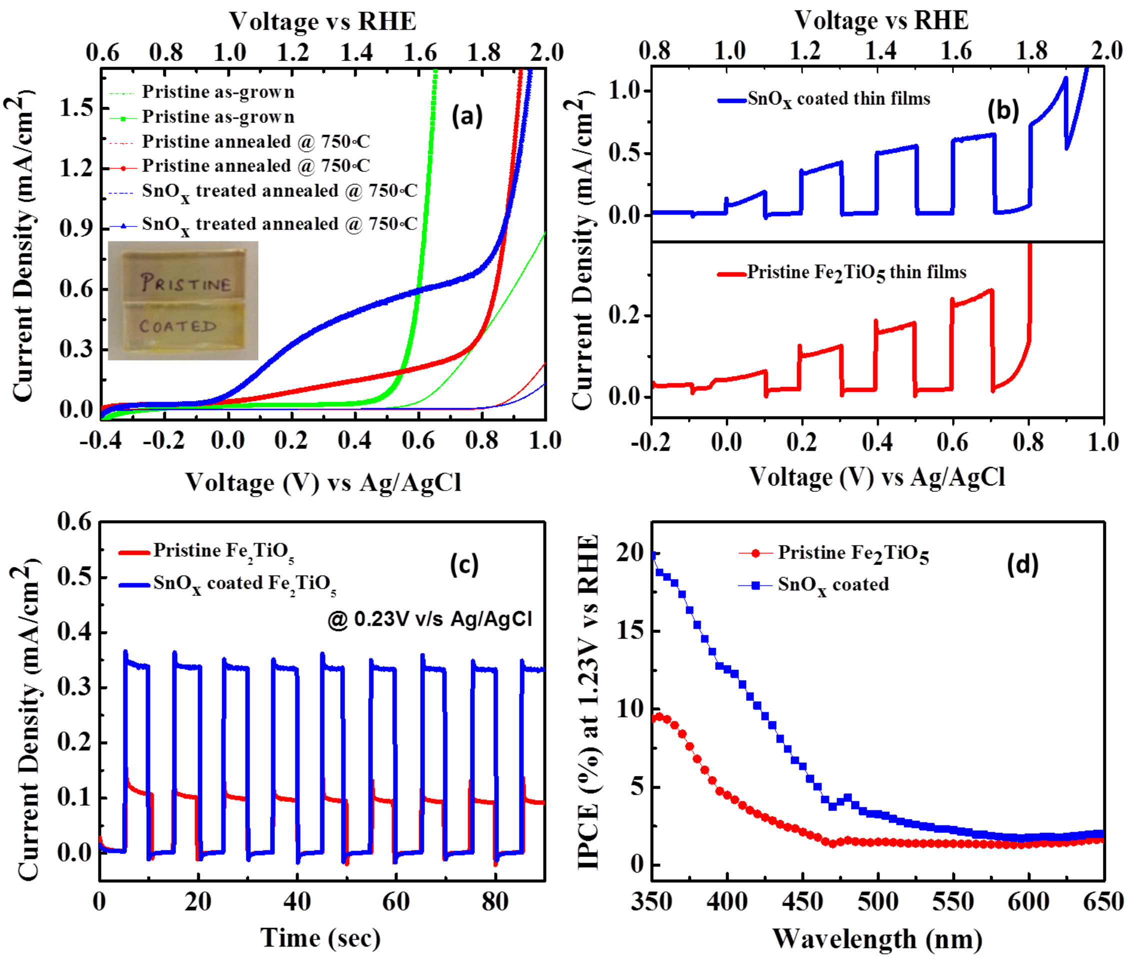

Figure 4.2.4 (a) JV curves for as-grown, pristine annealed and SnOx coated annealed thin films (inset: pictures of thin films) under standard illumination (thin/dashed curves under dark conditions); (b) JV curves under chopped light (c) Amperometric (i-t) curves and (d) IPCE curves for pristine and SnO_x coated films. Adapted from Bassi, P.S.; Chiam S. Y.; Gurudayal; Barber J.; Wong L. H.; "Hydrothermal Grown Nanoporous Iron Based Titanate, Fe_2TiO_5 for Light Driven Water Splitting"; ACS Appl. Mater. Interfaces, 2014, 6 (24), pp 22490–22495". © 2014, American Chemical Society

Surface treatment with SnO_x coating resulted in enhancement of photocurrent to 0.36 mA/cm^2 at 1.23V vs. RHE and 0.64 mA/cm^2 at 1.8V before onset of dark current as shown in **Figure 4.2.4(a)**. The improvement in photocurrent could be due to the inhibition in recombination of charge carriers at semiconductor/electrolyte interface through surface passivation. **Figure 4.2.4(b)** illustrates the J-V plots under chopped simulated light for pristine and SnO_x coated samples. Anodic photocurrent transient is symbolic of the holes accumulation at semiconductor-electrolyte interface whereas the cathodic transient signifies electrons recombining with accumulated holes [117]. A very small transient anodic photocurrent was observed when the light was on which diminished with increasing potential for coated samples which demonstrated the lower recombination in SnO_x coated thin films.

Figure 4.2.4(c) shows Amperometric (I-T) curve under voltage bias of 1.23 V vs. RHE. It could be observed from the plots that there is very little difference in anodic/cathodic transient behaviour for coated and pristine samples. This indicates that the voltage of 1.23V vs. RHE was not enough to provide driving force for both pristine and coated samples to facilitate water oxidation through surface trapped photogenerated holes. But as demonstrated in **Figure 4.2.4(b),** with increasing potential bias, both anodic and cathodic transients decreased after SnO_x coating which is in compliance with passivation of surface defects. In this way, the thin overlayer on the Fe_2TiO_5 film improved hole transport across the interface and enhanced oxygen evolution of pristine Fe_2TiO_5 thin films.

To further measure the performance of pristine and coated films, Incident Photon to Current Efficiency (IPCE) curves were extracted as shown in **Figure 4.2.4(d)**. SnO_x coated thin films showed higher efficiency than pristine thin films which corroborate the higher photocurrent density trend exhibited by treated samples. However, IPCE for both samples were found to be relatively low which could be due to inherent recombination of charges in bulk or at the semiconductor/electrolyte interface which is needed to be further investigated.

To get an insight into the charge dynamics in the bulk/surface of pristine or coated films, electrochemical impedance spectroscopic analysis was performed under dark and standard illumination. Nyquist plots recorded at 1.23V vs. RHE under standard illumination are shown in **Figure 4.2.5(a)**. R_s is the series resistance of the external circuit and depends on the contact with the substrates, C_{SC} is the space charge capacitance of semiconducting layer. The charge transfer resistance (R_{CT}) for hole injection across the semiconductor-electrolyte interface into the electrolyte was calculated by fitting simple Randle's circuit as shown in inset of **Figure 4.2.5(a)**. R_{CT}, under dark conditions, was very high of the order of 500 kΩ for pristine films and 800 kΩ for SnO_x coated films due to the absence of charge carriers. Under standard illumination, pristine films yielded R_{CT} around 12.17 kΩ and 5.12 kΩ after coating. The reduction in R_{CT} after SnO_x coating indicated an increase in hole transfer rate across the semiconductor-electrolyte interface. These results were in compliance with the surface charge passivation observed with chopped light photocurrent measurement. Hence, it further strengthens our suggestion that the SnO_x overlayer is providing a surface passivation layer.

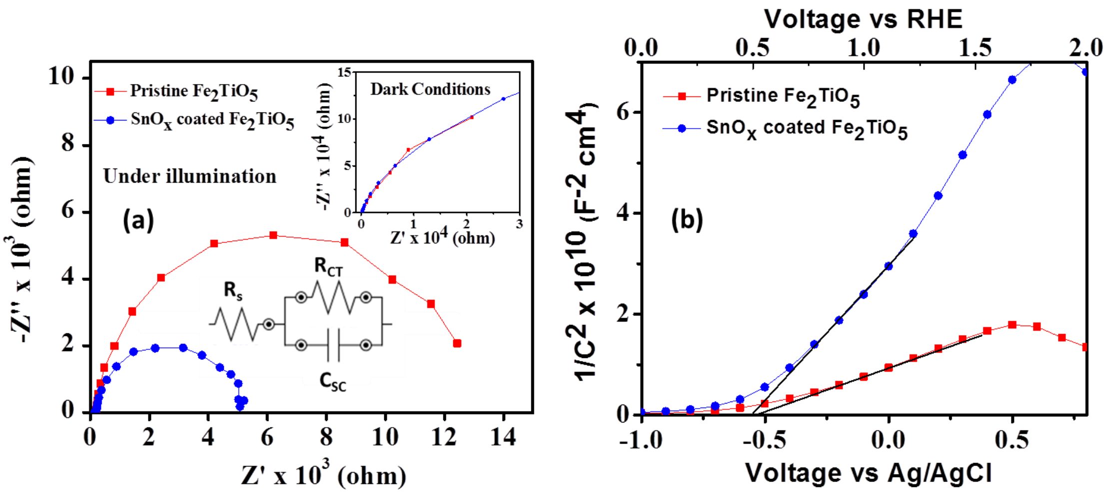

Figure 4.2.5 (a) Nyquist curves under illumination (inset: under dark conditions) and (b) Mott Schottky plots; for pristine Fe_2TiO_5 and coated thin films. Adapted from Bassi, P.S.; Chiam S. Y.; Gurudayal; Barber J.; Wong L. H.; "Hydrothermal Grown Nanoporous Iron Based Titanate, Fe_2TiO_5 for Light Driven Water Splitting"; *ACS Appl. Mater. Interfaces, 2014, 6 (24), pp 22490–22495.* © 2014, American Chemical Society

Mott Schottky plots under dark conditions for pristine Fe_2TiO_5 and SnO_x coated Fe_2TiO_5 photoanodes extracted at 1 KHz are shown in **Figure 4.2.5(b)**. To calculate the flat band potential (V_{FB}), following formula shown as equation (7) was used:

$$\mathbf{1/C_{sc}^{2} = (2/\varepsilon_0\varepsilon_r eA^2N_D)\,[V - V_{FB} - KT/e]} \qquad \mathbf{(7)}$$

where ε_0 is the permittivity of vacuum, ε_r is the dielectric constant for Fe_2TiO_5(100), V_{FB} is the flat band potential, V is the applied voltage bias, e is the elemental charge, KT/e is a temperature–dependent correction term (0.026 V at 25 °C) and N_D is the dopant density (cm^{-3}). V_{FB} i.e. flat band potential values, for pristine and SnO_x coated films extracted from the above equation were 0.47 V and 0.41 V vs. RHE respectively. A negative shift in flat band potential of around 60 mV was observed for coated samples due to the thin surface passivating SnO_2 overlayer. It should be noted that there is an increase in slope after the treatment of pristine films which could be attributed to the decrease in effective surface area of electrode due to the coating of thin SnO_x overlayer on porous Fe_2TiO_5 thin films.

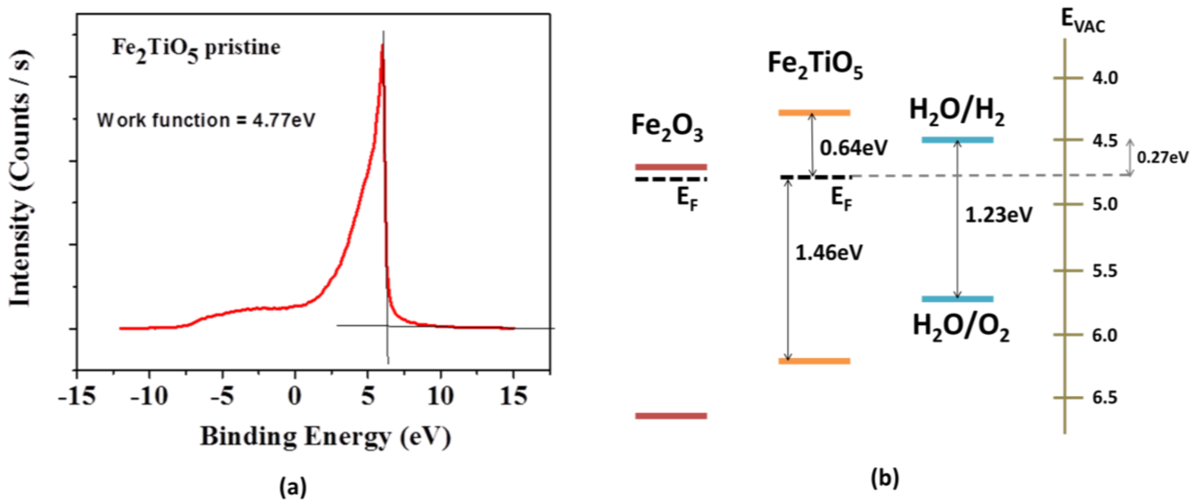

Figure 4.2.6 (a) UPS scan for pristine annealed films demonstrating evaluation of Work Function Adapted from Bassi, P.S.; Chiam S. Y.; Gurudayal; Barber J.; Wong L. H.; “Hydrothermal Grown Nanoporous Iron Based Titanate, Fe_2TiO_5 for Light Driven Water Splitting”; *ACS Appl. Mater.*

Interfaces, 2014, 6 (24), pp 22490–22495". © 2014, American Chemical Society, and (b) Schematic representation of band and fermi level positions for Fe_2TiO_5 and Fe_2O_3 with respect to Water Redox levels

To investigate the conduction band positions with respect to vacuum level (E_{VAC}), UPS spectra for pseudobrookite pristine Fe_2TiO_5 thin films were evaluated. It is to be noted that the thin films used for UPS study were annealed at 550ºC for around 4 hrs to avoid any doping effect of Sn from FTO which could impact the analysis. **Figure 4.2.6(a)** shows the extraction of work function (E_F) to be around 4.77 eV from vacuum level. For UPS measurement, Photon energy – (Secondary cut off – Fermi energy) = work function. The excitation source was He I, with photon energy of 21.2 eV, generated from high purity He gas. The secondary cut off is the electrons essentially with 0eV kinetic energy (KE). Considering the rigid shift of -10eV in case with respect to fermi level of 0eV, the work function (= 4.77eV) is calculated as: 21.2- (6.43-0) -10eV for secondary cutoff of 6.43 eV.

From the information extracted from XPS measurement, (E_F – E_{VB}) was around 1.46 eV. Through tauc plot analysis, the band gap was evaluated to be around 2.1 eV. Since, water reduction level (E_{H2}) is 4.5 eV with respect to E_{VAC}; it shows the conduction band (E_{CB}) lies in the region of hydrogen generation (see **Figure 4.2.6(b)**). Hence, the band levels of Fe_2TiO_5 straddle the oxidation/reduction levels of H_2O. This conclusion is in compliance with the recent reports on Fe_2TiO_5 where the authors deduced its band level positions. [112-113, 128] In context with this, the flat band potential as observed from Mott Schottky plots in **Figure 4.2.5(b)** turned out to be similar to reported pristine Fe_2O_3 films.[33] Since there is a difference between their band levels, this matter deserves an in-detail insight into it and can be understood through **Figure 4.2.6(b).** Flat band potential signifies the difference in the fermi level of semiconductor and the redox potential of electrolyte. The work function of Fe_2TiO_5 which is also its quasi fermi level is calculated to be 4.77 eV as compared to its conduction band level estimated to be above H^+/H_2 level. Conduction band and fermi levels are close in the order of KT (0.026eV) for mostly n-type semiconductors, which is around 4.7- 4.8 eV for Fe_2O_3. Hence, the flat band potential is possibly similar for both of them due to similarity in their work function. Hall measurements were also performed on the Fe_2TiO_5 films sprayed on Glass slides using the methodology as mentioned in **Section 3.4**. The pristine n-type films showed an electron mobility of 6.32 cm^{-2} V^{-1} s^{-1} with a majority carrier concentration of around 10^{14} cm^{-3} (shown in **Figure B4,** Appendix) which was higher as compared to the reported values of Fe_2O_3. The difference between conduction band and work function/fermi level of Fe_2TiO_5 is around 0.5 V which is possible considering the low intrinsic carrier concentration of the order of 10^{14} measured from Hall measurements reported in **Figure B3**, Appendix. To the best of our knowledge, this is the first report of direct measurements of Fe_2TiO_5 electronic band positions using UPS and electronic properties through Hall Measurement.

Conclusion

In summary, we report the fabrication of Fe_2TiO_5 thin films through a simple low cost hydrothermal technique for application in solar water splitting. Films obtained were crystalline and nanoporous with pure phase of orthorhombic Fe_2TiO_5. Pristine films were characterized as the photoanode in PEC Cell which yielded a photocurrent of around 0.1 mA/cm^2 at 1.23V vs RHE. The photocurrent improvement was then facilitated by surface treating pristine thin films with SnOx thin overlayer. The improvement in treated samples was attributed to passivation of surface defects which inhibited surface recombination mechanisms. This was corroborated by Impedance Spectroscopy which showed a clear change in surface charge resistance after the coating. Gas Chromatography measurements yielded the amount of oxygen evolution for both pristine and coated films. XPS/UPS measurements of pristine film yielded its work function and indicated that the Fe_2TiO_5 films had band level positions more favourable for water splitting as compared to hematite. The synthesis of nanoporous Fe_2TiO_5 films and their characterization shows great promise for the application of Fe_2TiO_5 as a photoanode in solar water splitting.

4.3 Crystalline Fe_2O_3/Fe_2TiO_5 Heterojunction for Solar Water Oxidation: Controllable Synthesis and Efficient Hole Injection into Electrolyte

Introduction

It has been discussed earlier that the bulk recombination could be inhibited by using heterojunction of two photoanodes with complementary properties. On the other hand, problem of surface recombination of holes is solved by using a thin overlayer of oxide to minimize surface defects like lattice disordering or absorbed ions on the semiconductor-electrolyte interface. Here, we present a strategy to address both these challenges by integrating low performance Fe_2O_3 nanorods with nanoporous Fe_2TiO_5 thin films using simple low-cost hydrothermal technique. This would allow the formation of a type II band alignment due to their conduction and valence band offsets as mentioned earlier in **Section 2.4** (As shown in **Figure 2.4.2**) and also could enhance the performance of Fe_2O_3 nanorods by lowering its surface defects or improving the catalytic activity on the semiconductor/electrolyte interface.

In this **Section 4.3**, we report Fe_2O_3/Fe_2TiO_5 heterostructures based photoanodes deposited on FTO substrates by initially fabricating hematite (Fe_2O_3) nanorods and subsequently pseudobrookite (Fe_2TiO_5) nanoporous thin film on top of it before annealing. Crystalline heterojunction showed enhanced photocurrent density of 1.4mA/cm^2 as compared to hematite (0.01mA/cm^2) at 1.23V vs RHE. Higher photoconversion efficiency as compared to pristine Fe_2O_3 and Fe_2TiO_5 films is also observed and discussed here. This is claimed to be firstly due to good band level positioning of hematite and pseudobrookite films which improves photogenerated charge carrier separation in bulk and secondly due to appreciable catalytic effect of Fe_2TiO_5 on

Fe_2O_3 films. Impedance Spectroscopic measurements have also been reported to highlight significant reduction in surface charge transfer resistances and increased hole transfer into the electrolyte. Bulk/surface charge separation efficiency are also evaluated for heterojunction and pristine films which supported the impedance analysis results. These results combined corroborate the catalytic effect of Fe_2TiO_5 on Fe_2O_3 in attaining facile charge-transfer kinetics on semiconductor/electrolyte interface.

* Reprinted this section with permission from: “Prince Saurabh Bassi, Rajini Antony, Pablo P Boix, Yanan Fang, James Barber, Lydia Helena Wong; “Crystalline Fe_2O_3/Fe_2TiO_5 Heterojunction Nanorods with efficient charge separation and hole injection for Solar Water Oxidation”; Nano Energy, 2016, DOI:10.1016/j.nanoen.2016.02.013, Copyright 2016, Elsevier

Results and Discussion

Pristine Fe_2O_3 nanorods were fabricated with the same reaction conditions as earlier reported methodology [49] with a fixed hydrothermal reaction temperature and time whereas Fe_2TiO_5 thin films were deposited under different reaction temperature conditions for hydrothermal method as mentioned in **Section 3.5**. Reaction temperatures for Fe_2TiO_5 hydrothermal were varied as 120°C, 135°C and 150°C with a fixed reaction time of 12 hours**. Figure 4.3.1(a)** shows the XRD pattern of heterojunction thin films prepared with different reaction temperatures of 120°C, 135°C and 150°C. Characteristic peaks from Fe_2O_3 (JCPDS no. 006-0502), Fe_2TiO_5 (JCPDS no. 009-0182) apart from FTO (JCPDS no. 003-1114) can be observed which shows crystalline hematite and pseudobrookite (Fe_2TiO_5) phase formation in heterojunction films.

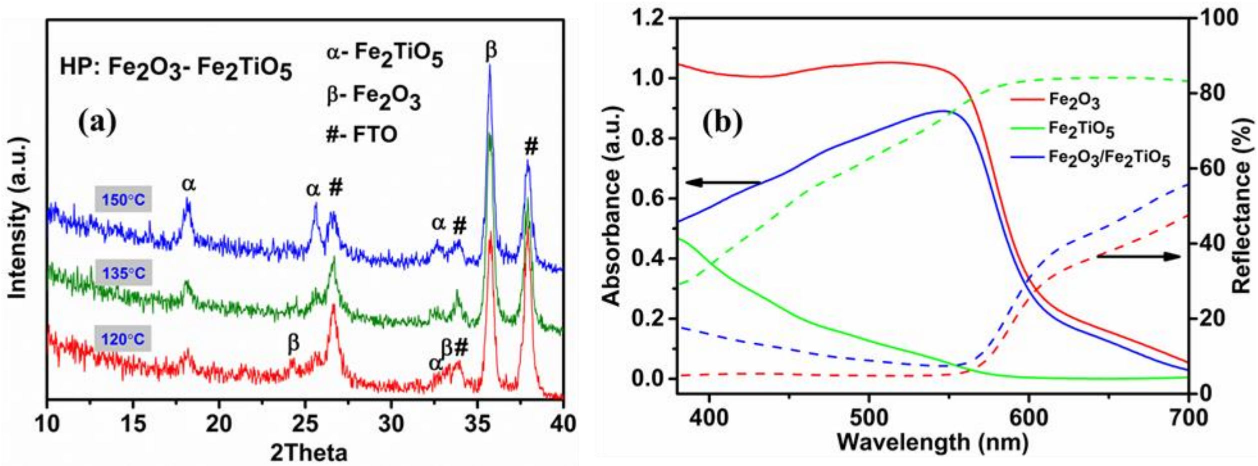

Figure 4.3.1 (a) XRD spectra for heterojunction thin films for three different reaction temperatures (b) Absorbance and Reflectance Spectra for optimized heterojunction and pristine thin films deposited at 120°C, 12 hrs

With increasing temperature, the peak corresponding to both Fe_2TiO_5 and Fe_2O_3 phase increased in intensity preferably due to thicker and higher crystalline films owing to rigorous hydrothermal reaction. Apart from peak corresponding to Fe_2O_3 at 35.7°

(anisotropic growth in [110] direction), two peaks at 24.1° and 33.3° were also observed for 120°C samples. XRD pattern shows that hydrothermal synthesis route to fabricate heterojunction films provide a good control on forming a pure crystalline phase of Fe_2TiO_5 on crystalline Fe_2O_3 nanorods which is beneficial for reproducibility and in-depth study of Fe_2O_3/Fe_2TiO_5 heterojunction.

To account for the photoactivity of thin films as photoanodes, it is imperative to observe the solar light absorption exhibited by semiconductor thin films. **Figure 4.3.1(b)** shows the UV Vis Absorption and Reflectance Spectra for pristine and heterostructure thin films with frontside illumination. Pristine Fe_2O_3 nanorods showed much better absorption than pristine Fe_2TiO_5 thin film with a similar band edge due to the thickness difference between them. The thickness of Fe_2O_3 nanorods is 500 nm while that of Fe_2TiO_5 thin film is around 80 nm. Pristine Fe_2TiO_5 films showed relatively high reflectance in visible light region than Fe_2O_3. Due to this reflectance, heterojunction films showed overall lower absorption than pristine Fe_2O_3 nanorods. This could be further understood by observing absorption spectra under frontside and backside orientation (shown in **Figure C1(a),** Appendix). Backside absorption for heterojunction films yielded similar absorption profile as the pristine Fe_2O_3 since the high reflectance exhibited by Fe_2TiO_5 films do not play a role in this case. The number of photons absorbed by heterojunction and pristine thin films calculated by multiplication of standard photon flux from solar spectrum, with individual absorption values is shown in **Figure C1(b),** Appendix. This would be used to determine J_{abs} as already mentioned in **Section 2.5.5.** Through Tauc Plot analysis, it was already established in **Figure 4.2.1** that Fe_2TiO_5 possess a band gap of around 2.1 eV.

The Scanning and Transmission electron microscopic studies were used to confirm the morphology and structure of the Fe_2O_3, Fe_2TiO_5 and Fe_2O_3/Fe_2TiO_5 heterojunction thin films as shown in **Figure 4.3.2.** In case of pristine Fe_2O_3, well aligned nanorods are formed with average diameter of 60 nm and length of 500 nm length whereas for pristine Fe_2TiO_5, nanoporous thin film of thickness around ~80-100 nm is observed (shown in Figure C2, Appendix). Cross-section image of Fe_2O_3-Fe_2TiO_5 heterojunctions, formed at optimized condition of 120°C for 12 hrs, with vertical hematite nanorods coated with Fe_2TiO_5 nanoporous thin film (thickness ~ 80nm) on top is shown in **Figure 4.3.2(a)**. Top view image (**Figure 4.3.2(b)**) shows coating of crystalline Fe_2TiO_5 particles on hematite nanorods. At higher temperature, 150°C (Shown in **Figure C3,** Appendix), the more rigorous reaction results in a thicker coating of pseudobrookite particles on nanorods. The higher reaction rate also results in rupturing the nanorods and filling more particles between the gaps of the nanorods.

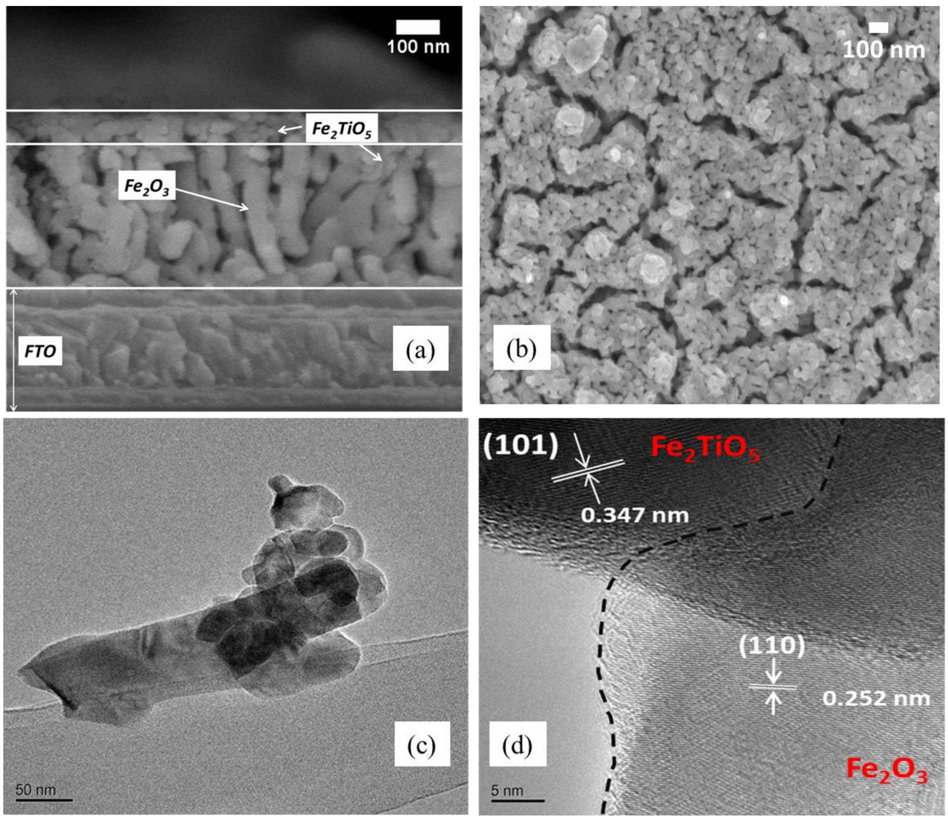

Figure 4.3.2 (a) Cross-section FESEM Image, (b) Top-view FESEM Image, (c) HRTEM Image and (d) d-spacing corresponding to constituent oxides; for Fe_2O_3/Fe_2TiO_5 Heterojunction deposited under optimized conditions of 120°C, 12 hours

High Resolution Transmission Electron Microscopic image (HRTEM) shown in **Figure 4.3.2(c)** reveals the formation of crystalline Fe_2TiO_5 nanoparticles attached to Fe_2O_3 nanorods. The d spacing calculated from the HRTEM image shown in **Figure 4.3.2(d)** are 0.347 nm and 0.252 nm which are (101) and (110) planes of orthorhombic Fe_2TiO_5 and Fe_2O_3 respectively. This indicates that the crystallinity of the heterojunctions were similar to that of the individual components. This was earlier confirmed by XRD analysis (in **Figure 4.3.1(a)**) where existence of (230) and (101) planes of Fe_2TiO_5 was evident in the XRD pattern of heterojunctions. To confirm the presence of Ti, elemental mapping and Energy Dispersive X-ray analysis (EDAX) was carried out. **Figure 4.3.3** shows the elemental distribution of Fe, O and Ti in single Fe_2O_3 nanorod where distribution of Ti is revealed (**Figure 4.3.3(d)**). The amount of Ti was comparatively lesser as evident from the mapping and EDAX studies. It is also noted that no Sn content in heterojunction was found in EDAX which is in compliance with report by Ling et al stating that annealing at 650°C induce negligible amount of Sn from FTO [27].

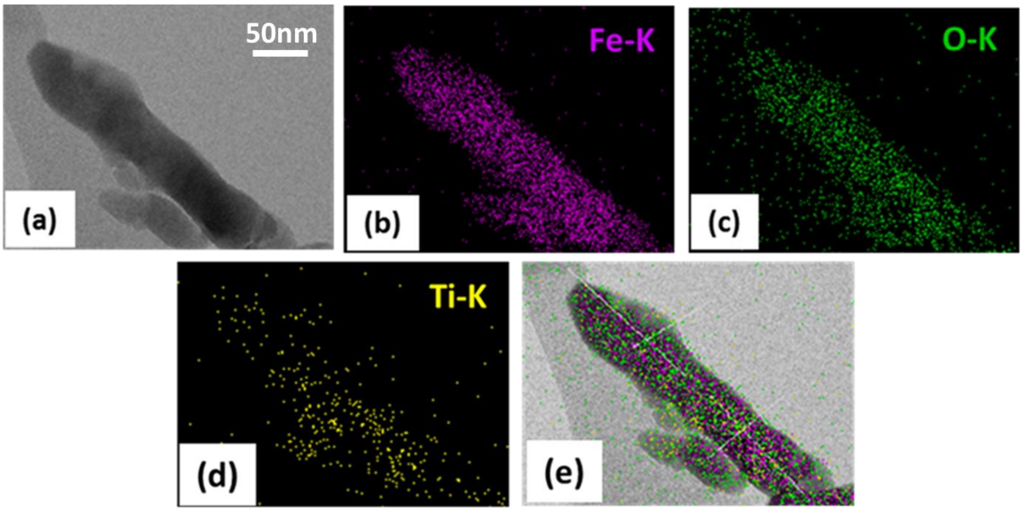

Figure 4.3.3 (a-e): Elemental Mapping of Fe_2O_3-Fe_2TiO_5 Heterojunction in which presence of Ti element is revealed

Photoelectrochemical Characterizations of Heterojunction and Pristine films

Linear sweep voltammetry in a 3 electrode configuration with heterojunction thin films, fabricated with different reaction temperatures, as working photoanodes yielded significant changes in photocurrent under both frontside and backside illumination (as shown in **Figure C4,** Appendix). Trends show the maximum current density for 120°C under frontside illumination and the lowest for 150°C for heterojunction thin films. This is in contrast with the current density exhibited by pristine Fe_2TiO_5 films which reaches maximum value for the samples deposited under 150°C, 12 hours condition, possibly due to thicker films and hence higher absorption. Since 120°C yielded highest performance under frontside illumination, we have studied these heterojunction films for further investigation. All the results that are presented from here-on corresponds to optimized heterojunction and pristine films with 120°C, 12 hours profile under frontside illumination, unless stated otherwise. **Figure 4.3.4(a)** shows photocurrent density-applied bias (J-V) plot under frontside illumination for optimized Fe_2O_3/Fe_2TiO_5 heterojunction, Fe_2O_3 and Fe_2TiO_5 thin films on FTO substrates with Fe_2TiO_5 reacted at 120°C, 12hrs. Heterojunction films show large enhancement in the photocurrent to 1.4mA/cm^2 at 0.23V vs Ag/AgCl equivalent to 1.23 V vs RHE for pH=13.6 electrolyte (1M NaOH) as compared to pristine films. Pristine Fe_2O_3 shows a very low photocurrent of the order of 0.01 mA/cm^2 at 1.23V vs RHE which is similar to the earlier reported performance of pristine hematite nanorods annealed at 650°C [27]. Pristine Fe_2TiO_5 thin films are observed to yield better photocurrent, of around 0.2 mA/cm^2, as compared to Fe_2O_3 nanorods at 1.23V vs RHE. This is believed to be due to better charge transport properties that Fe_2TiO_5 possess as compared to Fe_2O_3.

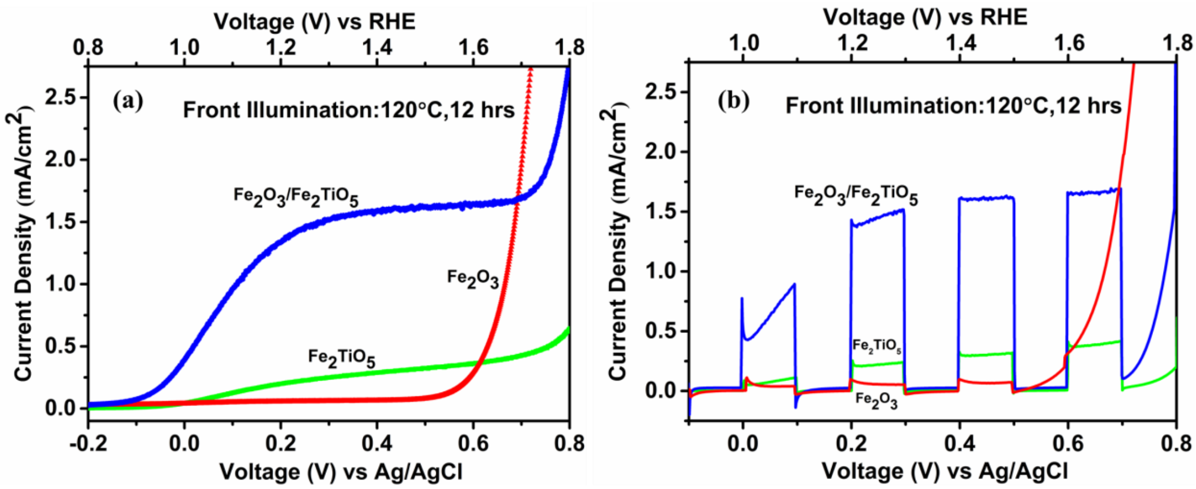

Figure 4.3.4 (a) Linear Sweep Voltammetry and (b) Chopped photocurrent-potential curves for Fe_2O_3, Fe_2TiO_5 and Fe_2O_3/Fe_2TiO_5 heterojunction for 120°C, 12 hours sample

One method to determine if there is any recombination in a system is through chopped photocurrent-potential curves. Higher anodic/cathodic transient signifies the high recombination of photogenerated holes with electrons or other surface defects present in the semiconductor leading to accumulation of holes. **Figure 4.3.4(b)** shows chopped photocurrent density vs voltage bias curve for heterojunction and pristine electrodes. Photocurrent transient in the pristine Fe_2O_3 electrodes was high due to its poor charge transport properties and slow water oxidation kinetics. On the other hand, Fe_2TiO_5 electrodes showed a significant photocurrent with lower transient due to significantly better charge dynamics in the system. For heterojunction electrodes, the transient is appreciably lower, for lower potentials (< 0.2 V vs Ag/AgCl) which diminish with higher potentials, apparently due to improved charge separation owing to the favourable band alignment between Fe_2O_3 and Fe_2TiO_5 films. It could also be due to improvement in hole transfer through surface states, the process which has been claimed by Klahr et al as the primary step for water oxidation [41, 116]. This would be further investigated in the following section.

Performance of Optimized Heterojunction Films under Frontside and Backside Illumination:

To find out the effect of light absorption with the proximity of heterojunction on photocurrent, J-V measurements were performed under frontside and the absorption backside illumination on all the samples. **Figure 4.3.5(a)** shows the current-potential curves for both back and frontside illumination of optimized heterojunction samples (120°C, 12 hrs). It was observed that the front illumination yielded a negative shift in the onset potential (~ 40mV) and a higher photocurrent as compared to the back illumination. Although the photocurrent under frontside and backside illumination was competing around 1.23V vs RHE, a clear trend for onset potential difference was observed for all the heterojunction batches fabricated. **Figure C5** (appendix) shows the box chart for the varied onset potential difference for 15 samples. It shows the onset potential difference (= Back - Front) to be positive throughout with most of the samples having a difference of 30-50mV suggesting the cathodic shift in onset potential under frontside illumination was reproducible. The shift suggests that the kinetics of hole transport is better in front as compared to backside illumination. For frontside, the photocurrent reaches a plateau current suggesting that the holes transport is limited due to electron transport to the back contact. In backside illumination, current keeps rising with increasing potential bias implying the removal of electrons to the back contact is very fast and hence the electron-hole recombination is reduced [20].

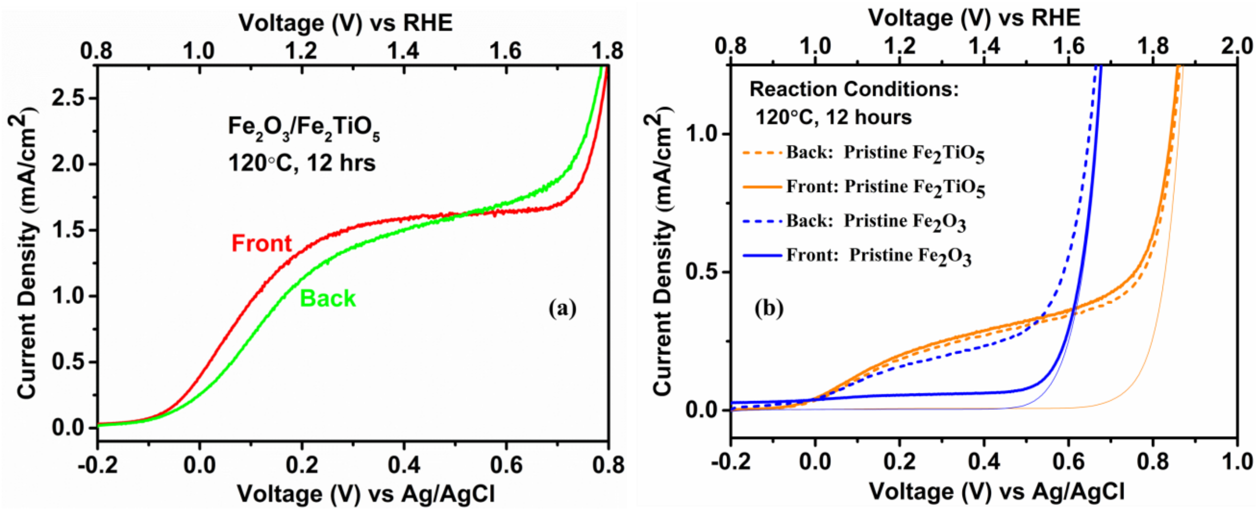

Figure 4.3.5 (a) Current Density-Potential curve under frontside and backside illumination for (a) Optimized Heterojunction sample and (b) pristine Fe_2O_3 and Fe_2TiO_5 films.

For a comparison, the back and frontside photocurrent for pristine films is shown in **Figure 4.3.5(b)**. There is no visible difference in the onset potential for Fe_2TiO_5 thin film. Whereas for Fe_2O_3 nanorods, the onset potential is observed for backside illumination and due to very low photocurrent, onset potential is not clear corresponding to frontside illumination which was already discussed in **Section 4.1.**

To get an insight into the charge transport for heterojunction films under frontside and backside illumination, **Figure 4.3.6** shows the schematic representation of transport of charge carriers under both conditions for the mentioned sample. It is to be noted that due to low absorption coefficient of Fe_2TiO_5 (shown in **Figure B2**, Appendix), most of the solar spectrum is absorbed by Fe_2O_3 nanorods. Red line represents the approximate absorption depth. Green region is Fe_2TiO_5 nanoparticles and orange is Fe_2O_3 nanorod. Their interface represents heterojunction. Since photons are absorbed in the absorption depth for a specific material, the frontside and backside illumination changes the absorption depth a photon witnesses.

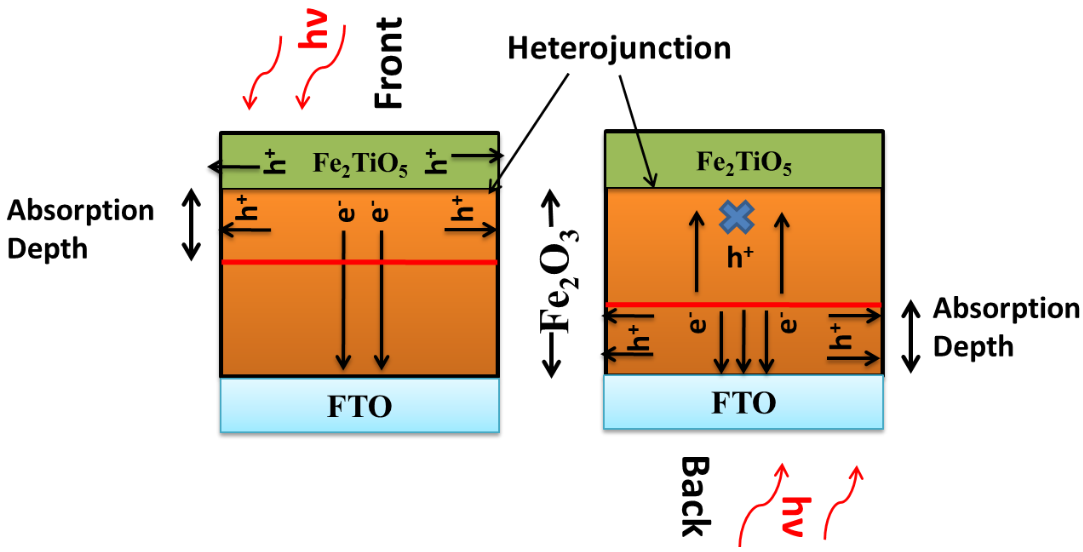

Figure 4.3.6 Schematic representation of charge transport under Backside and Frontside illumination in heterojunction sample

During frontside illumination, majority of photons are absorbed in the proximity of heterojunction formed between Fe_2O_3 nanorods and Fe_2TiO_5 film. This allows more efficient charge separation and hence the higher photocurrent is achieved for frontside illuminated samples. Also, due to the presence of a better charge transporting thin film on top of hematite, the photogenerated holes could easily reach the semiconductor/electrolyte interface. For backside illumination, the photogenerated holes have to travel across the densely concentrated nanorods present near the FTO/Fe_2O_3 junction which has low electrolyte presence. Due to low minority carrier diffusion length, higher bias is needed to increase depletion layer width and hence the onset potential is shifted to higher potentials for backside photocurrent as compared to frontside illuminated samples. This is supported by the fact that for 150°C sample, the backside illumination photocurrent is higher as compared to frontside illumination because of the presence of a more homogeneous heterojunction (Shown in **Figure C4,** Appendix). Fe_2TiO_5 particles, due to extensive reaction at higher temperature, penetrates into the space between the nanorods and form more heterojunction points. This makes the distance of photons and heterojunction closer. Whereas the overall photocurrent (both backside and frontside) observed for 150°C is significantly lower than that for 120°C because of the incoherent transport of electrons along [110] axis of the ruptured nanorods (FESEM Image shown in **Figure C3,** Appendix).

To evaluate the performance of photoelectrodes, Incident Photon to Current Efficiency (IPCE) for optimized Fe_2O_3/Fe_2TiO_5 heterojunction and pristine electrodes was evaluated at 1.23V vs RHE using the formula stated in **Section 2.5.3**. IPCE spectra shown in **Figure 4.3.7(a)** has a similar trend as the photocurrent measurements suggesting that more carriers were generated for heterojunction thin films for the similar amount of photons as compared to pristine electrodes. **Figure C6** (Shown in Appendix**)** shows the IPCE Spectra for heterojunction and pristine Fe_2TiO_5 films for different temperatures. The trend of efficiency at 1.23V vs RHE with varying temperatures is similar to that shown by the photocurrent density. To determine the stability of the heterojunction, the amperometric curve at 1.23V vs RHE was recorded for 2 hours continuously under standard illumination conditions. The stability of the photocurrent density of around 1.4mA/cm^2 ± 0.1mA/cm^2 throughout the measurement period of 2 hours (as shown in **Figure 4.3.7(b))** demonstrates the potential of Fe_2O_3/Fe_2TiO_5 heterojunction as a photoanode for practical applications.

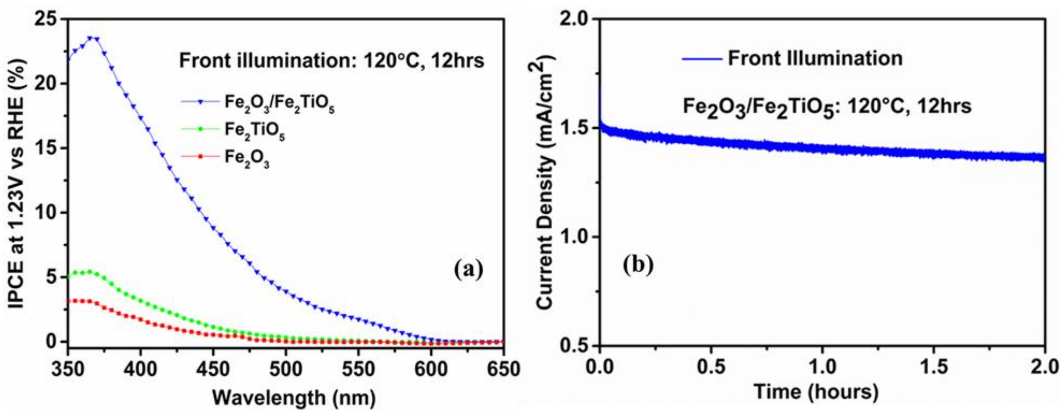

Figure 4.3.7 (a) IPCE Spectra, for optimized heterojunction and pristine Fe_2O_3 and Fe_2TiO_5 photoelectrodes (b) Stability Test for Fe_2O_3/Fe_2TiO_5 Heterojunction prepared at 120°C, 12 hours. Signals recorded under applied bias of 1.23V vs RHE

Investigation into Charge Dynamics using Electrochemical Impedance Spectroscopy

Heterojunction thin films showed an appreciable enhancement in the photocurrent as compared to pristine films. IPCE spectra in the previous section showed higher charge carrier generation with photons absorbed. While carrier generation is important, charge separation has to be efficient to allow the transport of the charge carriers to back contact. Once carriers are generated, they can recombine either in bulk or on surface. The role of Fe_2TiO_5 overlayer in heterojunction films could be as a surface passivation layer, i.e. minimizing the dangling bonds present on hematite or as a catalytic overlayer allowing an efficient hole injection into the electrolyte by improving surface charge kinetics. To investigate into this, electrochemical impedance spectroscopy was performed to unveil information about the transport of charge carriers across the semiconductor/electrolyte interface. The details about the measurements performed are presented in **Section 3.7**. The resulting Nyquist plots followed the behaviour previously reported in these systems, and they were fitted with the corresponding equivalent circuit model (as shown in **Figure 4.3.8** below) [41, 129].

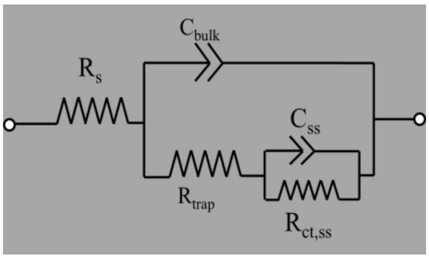

Figure 4.3.8 Model of Circuit fitted with the Nyquist plots for Heterojunction and Pristine films

In this model, R_{trap} accounts for the resistance of the trapping of both photogenerated charge carriers at the surface states, whereas $R_{ct,ss}$ is the resistance to transfer of holes to the electrolyte through those surface states. The measured capacitance in the system is distributed in C_{bulk} (from the bulk material) and C_{ss} (from the surface states). **Figure 4.3.9(a)** shows the photocurrent density – potential curve for optimized heterojunction film (grey curve) along with the values of $R_{ct,ss}$ and C_{ss} obtained from fitting, where the coincidence of the peak of C_{ss} and the valley of $R_{ct,ss}$ with the increase of the current supports the viability of the employed model. This is also compatible with the theory reported by Pendlebury et al that long lived photogenerated holes were responsible for better water oxidation kinetics in hematite [101]. It was claimed by Cowan et al that in nanostructured Fe_2O_3 and TiO_2, the rate-limiting step of water oxidation was the hole transfer from metal oxide to a surface-bound water species [130]. This seems to be similar for our case where the hole transfer is relatively easier for heterojunction films as compared to the pristine films as shown in **Figure 4.3.9**.

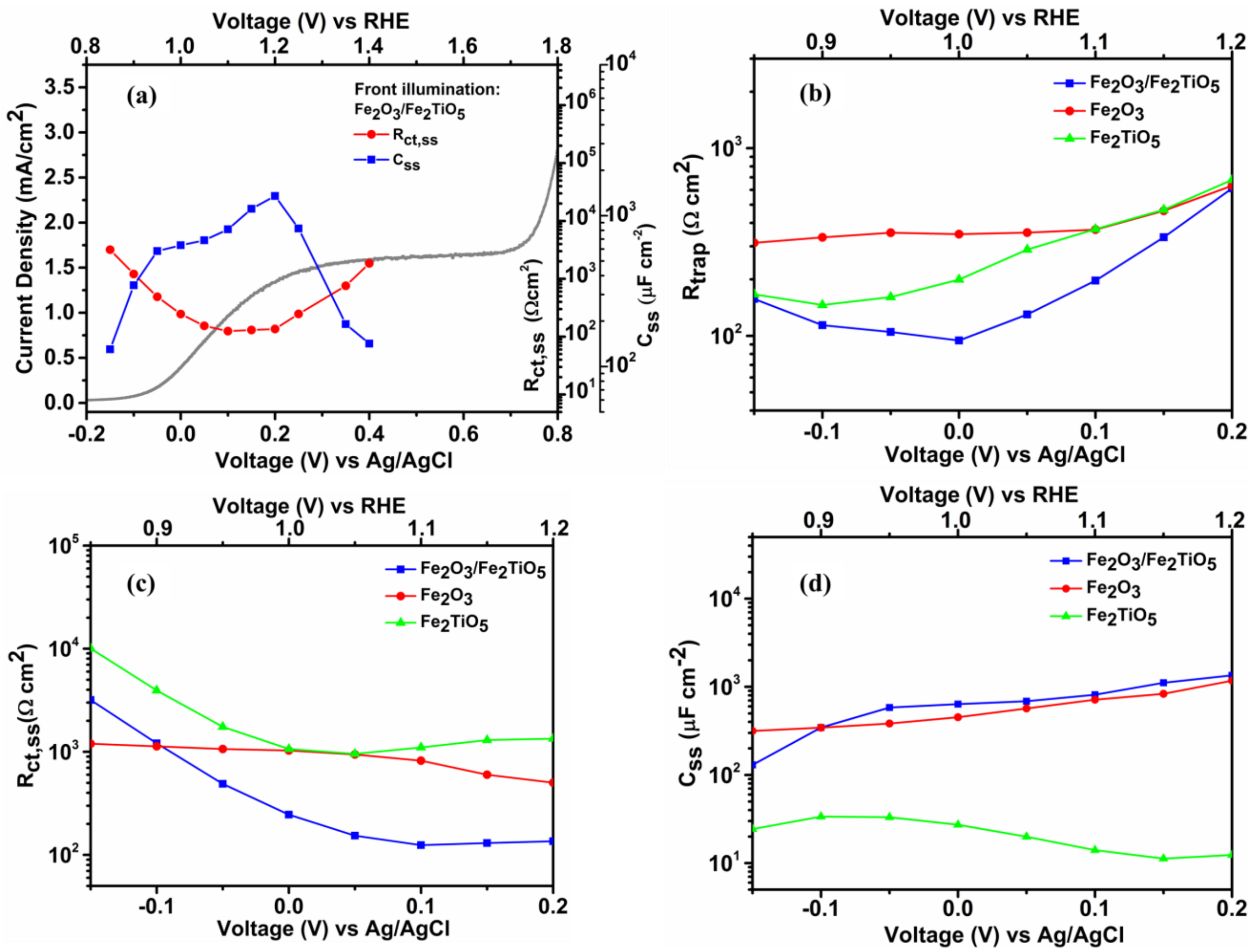

Figure 4.3.9 (a) Current Density-Potential curve (grey), Surface state capacitance (Css) and resistance through surface states (Rct,ss) with potential applied for optimized heterojunction (b) Charge trapping resistance (R_{trap}), (c) Resistance through surface states (Rct,ss) and (d) Surface state

capacitance, for optimized heterojunction (blue square), pristine Fe_2O_3 nanorods (red circle) and pristine Fe_2TiO_5 nanoporous thin films (green triangle)

Figure 4.3.9(b) shows a lower value of resistance for the trapping (R_{trap}) for the heterojunction as compared to pristine Fe_2O_3 nanorods and Fe_2TiO_5 films which indicates the holes mediate via surface states for the former efficiently. This can contribute to a more efficient water oxidation in case of heterojunction, which is consistent with the correlation of dip in $R_{ct,ss}$ and peak in C_{ss} profile resulting in a more suitable charge transfer kinetics. **Figure 4.3.9(c),** shows the surface charge transfer resistance $R_{ct,ss}$ with potential bias for all the samples. It is observed that the resistance reduced significantly for heterojunction suggesting easier hole injection into the electrolyte through surface states than in pristine electrodes. Chopped photocurrent profile (in **Figure 4.3.4(b)**) corroborates the claim that surface traps in heterojunction film are efficiently transferring the holes to the electrolyte since around 0.2V vs Ag/AgCl, the anodic and cathodic transients are minimal and hence faradaic current sustains for higher potentials [116].

Figure 4.3.9(d) shows surface capacitance for pristine Fe_2TiO_5 films is low, with the peak slightly shifted, suggesting the modification of the surface energetic by Fe_2TiO_5. Very low value of C_{ss} suggests the lower surface defects density which is higher for Fe_2O_3. Very low value of C_{ss} suggests a low surface defects density. For heterojunction, C_{ss} is similar to that for Fe_2O_3 since the overall surface area and hence defects density is dominated by the nanorods surface area given that the location of Fe_2TiO_5 is only on the top of nanorods. The Mott-Schottky plots (Shown in **Figure 4.3.10**) indicate that the heterojunction films have the minimum slope of the curve, and in accordance heterojunction has the highest majority carrier density. This could be due to the passivation of surface defects by Fe_2TiO_5 overlayer."

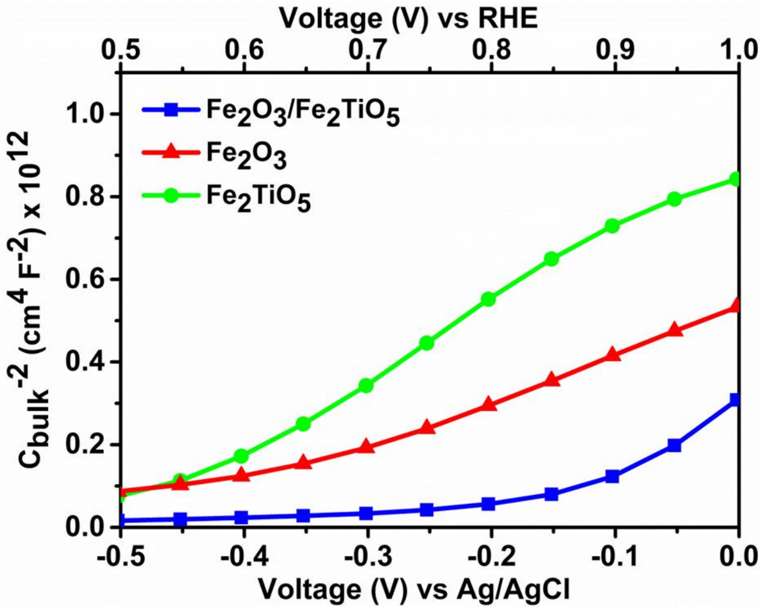

Figure 4.3.10 Mott Schottky Plots for Fe_2O_3/Fe_2TiO_5 Heterojunction and Pristine thin films prepared at 120°C, 12 hours

Bulk and Surface Charge Separation Efficiency for Heterojunction and Pristine films:

In the previous section, the role of surface states was highlighted using impedance spectroscopy. As suggested by Klahr et al, the surface states charging and discharging appears to be a process common to porous materials having large amount of surface defects. The hole transfer for water oxidation takes place significantly from surface trapped holes [116]. The role of surface defects as a recombination centre limits the photocurrent at lower potential whereas with higher potential, the developed oxidized intermediates enhance the water oxidation kinetics. In the heterojunction devices, the higher photocurrent could be attributed to an improvement of the surface kinetics by these intermediates even at lower potentials, which is probably due to catalytic effect by Fe_2TiO_5 overlayer in enhancing indirect charge transfer from surface states. Very recently, Bisquert and group showed, through drift-diffusion simulations, that surface states could be beneficial for solar fuel production in providing good charge transfer kinetics and hence lower onset voltage with higher photocurrent [131].

Since both bulk and surface recombination play a part in enhancement of photocurrent, photoelectrochemical characterization was performed for all samples in the presence of a hole scavenger, H_2O_2. As discussed earlier in **Section 2.5.5**, photooxidation of H_2O_2 allows the swift transport of photogenerated holes into the electrolyte and hence eliminates the surface recombination which could lead to evaluation of the extent of bulk recombination in the semiconductor [117]. Photocurrent potential curves for optimized heterojunction with (blue curve) and without hole scavenger (red curve) are shown in **Figure 4.3.11(a)**. There is an obvious enhancement in the photocurrent and cathodic shift in onset potential (~150mV) owing to fast water oxidation kinetics with presence of H_2O_2. **Figure C7, (**Appendix) can be referred for the J-V plots of heterojunction and pristine films under the influence of H_2O_2 in electrolyte.

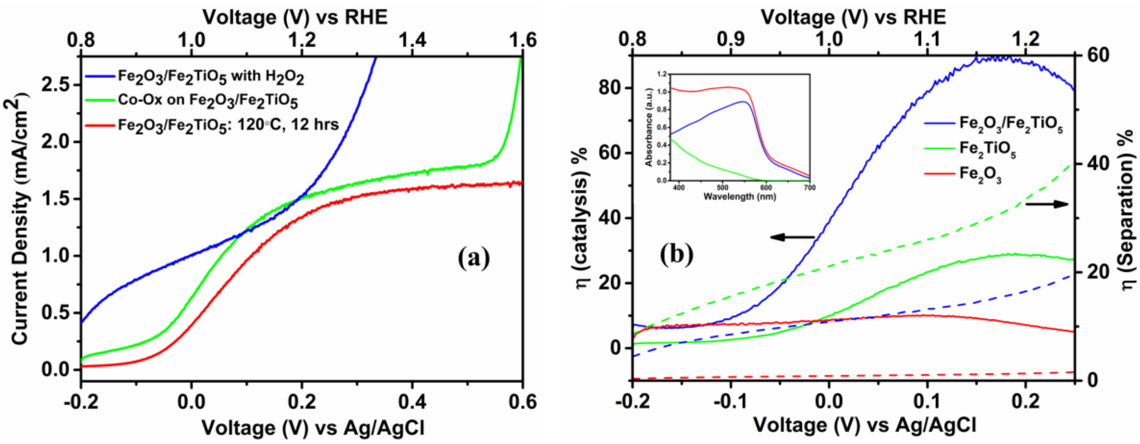

Figure 4.3.11 (a) Current-potential curves for heterojunction thin films coupled with co-catalyst or under the presence of hole scavenger (H_2O_2), (b) Charge Separation efficiency for surface [η(catalysis)] and bulk [η(separation)] in heterojunction films

Figure 4.3.11(b) shows surface charge separation as η(catalysis) and bulk as η(separation) for optimized samples i.e. 120°C, 12 hours. η(separation) is the fraction of holes that do not recombine in bulk and reach semiconductor-electrolyte interface. η(catalysis) is the fraction of those holes which have reached the semiconductor-electrolyte interface and oxidize water without recombining with surface traps. Photocurrent obtained from water oxidation is termed as J_{H_2O} and from H_2O_2 oxidation as $J_{H_2O_2}$. In **Section 2.5.5** further details of analysis are discussed.

Figure 4.3.11(b) shows η(catalysis) curve obtained as $J_{H_2O}/J_{H_2O_2}$ since η(catalysis) is equal to unity for H_2O_2 due to its facile photooxidation. For heterojunction sample, η(catalysis) reaches an appreciable value of 85% at 1.23 V vs RHE which indicates the overlayer of Fe_2TiO_5 is improving the surface charge carrier efficiency. Pristine Fe_2TiO_5 films show a significant efficiency of 25% whereas pristine Fe_2O_3 films attain a low efficiency of only 5% suggesting that hematite nanorods consists of high number of surface defects which limits its photocurrent. Thus, it is believed that the poor surface kinetics of hematite nanorods was appreciably affected by using Fe_2TiO_5 overlayer which enhances the catalytic activity on the surface as earlier suggested by impedance spectroscopy where dip in $R_{ct,ss}$ was found to be in compliance with peak of C_{ss} implying the process is surface state mediated water oxidation.

On the other hand, bulk charge recombination was observed by η(separation) which was obtained as $\mathbf{J_{H_2O_2}/J_{abs}}$ **w**here $\mathbf{J_{abs}}$ is the total absorbed photocurrent density for films depending on their visible light absorption. The absorbance spectra along with the standard AM 1.5G solar spectrum is shown in **Figure C1(b),** Appendix. Depending on the absorption of the respective films, $\mathbf{J_{abs}}$ was obtained for all the samples using the formula mentioned in **Section 2.5.5.** Pristine Fe_2O_3 electrodes showed the lowest bulk charge separation efficiency (~2% at 1.23V vs RHE) validating the fact that hematite has poor charge transport properties in the bulk as well. Highest bulk charge separation efficiency of around 35% at 1.23V vs RHE is shown by pristine Fe_2TiO_5 electrodes. Fe_2TiO_5 films were transparent and showed low absorption, but in spite of that, it showed an appreciable photocurrent under hole scavenging conditions and hence highest efficiency. Heterojunction thin films had intermediate efficiency significantly better than hematite due to its coupling with a good charge carrier separation efficiency material i.e. Fe_2TiO_5.

To further improve the performance of optimized heterojunction thin films, the system was coupled with Co_{ox} catalyst using methodology previously reported by Liu et al[112]. The oxidation activity of the holes was claimed to be enhanced by Co_{ox} catalyst which when coupled with Fe_2TiO_5 overcome the reaction barrier to effectively enhance hole transport across the semiconductor-electrolyte interface. Here, integrating the co-catalyst marginally enhances the photocurrent (~10%) at 1.23 V vs RHE which shows that heterojunction without co-catalyst had low recombination of charge carriers. Improvement in onset potential of around 30mV (as shown in **Figure 4.3.11(a)** indicates an improvement in surface kinetics for optimized heterojunction thin films. This could be due to the presence of an energy band corresponding to Co_{ox} catalyst which regulates the hole transfer across to the electrolyte via the surface states.

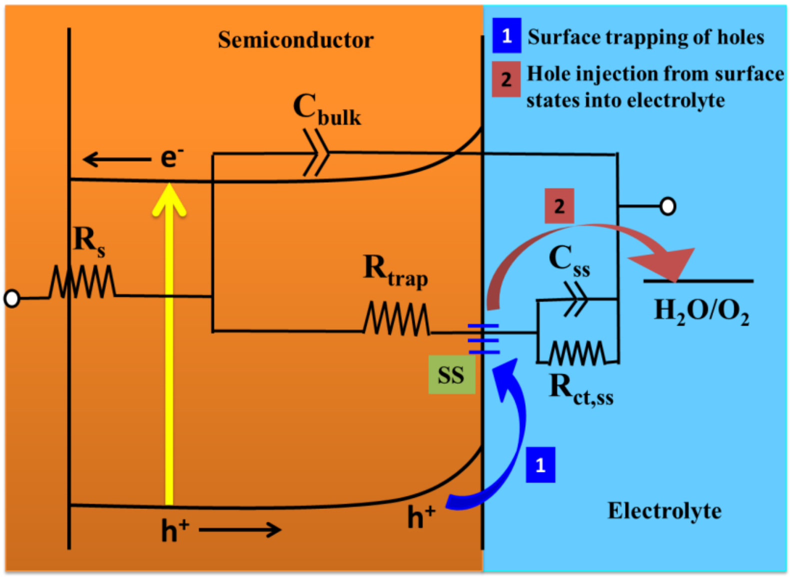

Figure 4.3.12 Schematic representation of proposed charge transport model in Fe_2O_3/Fe_2TiO_5 nanoheterojunction thin films

Conclusion

In summary, Fe_2O_3/Fe_2TiO_5 heterojunction consisting of crystalline hematite and pseudobrookite has been successfully fabricated. The heterojunction shows superior PEC performance compared to the pristine Fe_2O_3 nanorods. Photocurrent density at 1.23V vs RHE for heterojunction films witnessed manifold enhancement to 1.4mA/cm^2 without co-catalyst as compared to photocurrent of 0.01mA/cm^2 exhibited by pristine Fe_2O_3 nanorods. Heterojunction films also showed a low onset voltage of 0.9 V vs RHE which cathodically shifted further by around 30mV with the use of CoO_x as a cocatalyst. IPCE efficiency curves for Fe_2O_3/Fe_2TiO_5 films demonstrated photons converted to charge carriers easily indicating an inhibition of bulk electron-hole recombination as compared to pristine Fe_2O_3 and Fe_2TiO_5 films probably due to heterojunction/band level alignment. Highest η(separation) values for Fe_2TiO_5 film corroborated the hypothesis that it possesses better charge properties as compared to Fe_2O_3 since it efficiently converted photons to current even with low visible absorption. Through impedance spectroscopic analysis, a charge transfer model was proposed (as shown in **Figure 4.3.12**) which shows a surface charge mediated water oxidation process i.e. the photogenerated holes got trapped in surface states in step 1 followed by step 2 where these oxidized species enabled the water oxidation efficiently. High η(catalysis) confirmed the high surface charge separation efficiency in Fe_2O_3/Fe_2TiO_5 films as compared to pristine electrodes. These results proved the catalytic effect of Fe_2TiO_5 layer on the top of Fe_2O_3 apart from a favourable band alignment which improves the overall performance of heterojunction thin films.

Chapter 5.

Conclusions

Iron based semiconductors are attractive for developing cheap and robust photoanodes for PEC cells to split water and generate hydrogen as a solar fuel. Hematite is the suitable candidate with some limitations like non-optimal conduction band level, high electron-hole recombination probability, incomplete solar light absorption, poor hole diffusion length and low catalytic kinetics at the surface. Due to this, hematite photoanodes are used in the form of nanostructures to tackle bulk recombination and surface recombination is inhibited by using surface overlayers/cocatalysts. Generally, hematite nanorods fabricated on FTO substrates are activated to achieve a significant photocurrent by sintering it at very high temperature (>750°C) but this also limits the conductivity of FTO and lead to damage in its morphology which eventually limits the photocurrent. Hence, there is a trade-off between the crystallinity and conductivity (by Sn diffusion) of hematite nanorods and the conductivity of FTO substrate. To get an insight into this trade-off, pristine hematite nanorods were synthesized and annealed at different temperatures and were characterized under frontside and backside illumination. Their morphological characterization showed a temperature profile which achieves appreciable crystallinity of hematite. For this profile, i.e. 650°C, 5 hrs, a significant photocurrent was observed under backside illumination whereas under frontside, it was similarly poor as the 550°C samples. Photocurrent in backside was attributed to the good electron transport to the back contact which inhibits the back electron-hole recombination. Bulk and surface charge separation efficiency measurements with hole scavenger (H_2O_2) yielded information that back illumination of 650°C samples displayed least bulk recombination in compliance with better photocurrent density. But surface charge separation efficiency was still lower than samples annealed at 750°C. Hence, this annealing profile of

650°C, 5 hours was chosen to demonstrate reduction in surface recombination by employing the surface passivation technique of using a very thin oxide overlayer to cover hematite nanorods. ALD grown TiO_x overlayer deposited on hematite nanorods resulted in a uniform thin overlayer of $Fe_xTi_{1-x}O_y$ after solid state reaction at high temperature. A manifold enhancement in performance was observed, after TiO_x coating, with improvement in photocurrent under frontside illumination up to 1.2 mA/cm^2 at 1.23V vs RHE as compared to minimal photocurrent exhibited by pristine hematite nanorods. This was claimed to be due to the surface passivation by TiO_x layer (~5 nm) which also enhanced the surface charge efficiency and efficiently converted photons absorbed into photocurrent density. This strategy was helpful in dealing with the challenge of low performing hematite nanorods by using surface passivation technique.

In spite of good photocurrent achieved by hematite, the biggest drawback it possesses is the unfavourable band level positioning with respect to water redox levels. Based on earlier reports that Fe-Ti-O system may offer better band level positions, research on iron titanate was conducted. Being an air –stable abundant mineral with a band gap of 2.1 eV, Fe_2TiO_5 was synthesized by low cost hydrothermal technique for the first time which yielded a nanoporous pure-phase thin film on FTO. Photocurrent achieved by these films was not high possibly due to incomplete solar light absorption exhibited by the transparent films with thickness of the order of 100 nm and due to high surface recombination owing to their porous nature. A very thin SnO_x overlayer was deposited on these films before annealing the as-grown films and resulted in a double photocurrent due to the surface passivation of Fe_2TiO_5 films. UPS measurements were performed on these films to extract information about their band levels. Work function of around 4.77 eV was exhibited by them and through Tauc plot and information extracted from XPS measurement about (E_f – E_v); the conduction band levels were determined to be above the water reduction level. Hall measurement of sprayed Fe_2TiO_5

films on glass slide yielded mobility of around 6 $cm^2V^{-1}s^{-1}$ which was higher than reported Fe_2O_3 values. The synthesis of nanoporous Fe_2TiO_5 films showed great potential for the application of Fe_2TiO_5 as a photoanode in solar water splitting.

To tackle bulk recombination and improve charge separation of photoanodes, Fe_2O_3/Fe_2TiO_5 heterojunction was demonstrated. Since Fe_2O_3 and Fe_2TiO_5 band levels were known and both in equilibrium could form a type II band alignment, a nanoheterojunction was synthesized with combination of FTO/Fe_2O_3/Fe_2TiO_5 with similar methodology as their pristine films. These heterojunctions were prepared by varying reaction temperature of Fe_2TiO_5 thin film deposition, while keeping methodology of preparation of Fe_2O_3 nanorods fixed, followed by characterization under frontside and backside illumination. The highest photocurrent density was achieved for 120°C samples under frontside illumination which decreased with increasing reaction temperatures (135°C, 150°C). A similar trend was observed for backside illumination as well. The increased photocurrent density was mainly attributed to the efficient charge separation and hole transport across the semiconductor-electrolyte interface owing to the band alignment and catalytic effect demonstrated by Fe_2TiO_5 thin film. This was confirmed using impedance spectroscopy which revealed that hole transfer occurred through surface states into the electrolyte for heterojunction films in contrast with that for pristine films. Both bulk and surface charge efficiencies were enhanced as well for heterojunction films as compared to the pristine Fe_2O_3 nanorods. The optimized heterojunction of Fe_2O_3 nanorods coated with nanoporous film of Fe_2TiO_5 on the top yielded highest photocurrent (1.4 mA/cm^2) at 1.23V vs RHE and significant photoconversion efficiency at same voltage as compared to pristine Fe_2O_3 and Fe_2TiO_5 thin films. From photocurrent transients, EIS analysis and bulk/charge separation efficiency evaluation, it was concluded that the catalytic activity exhibited by the Fe_2TiO_5 layer stimulates the hole transfer at the surface into the electrolyte which enhanced the performance of heterojunction thin films. These findings reported a novel method to improve the low photocurrent exhibited by pristine hematite nanorods by coating it with a good charge transporting material i.e. Fe_2TiO_5 which is also stable in wide pH ranges. Heterojunction of stable materials with appropriate band alignment and good visible light absorption is the way forward. Fe_2TiO_5 being inexpensive and possessing good charge transport properties could surely be fascinating for research on Fe_2O_3 based heterojunctions for efficient solar energy conversion. We believe that these hybrid iron based semiconducting photocatalysts are promising contender in artificial photosynthesis technology due to their cheapness, robustness, good light absorption and enhanced charge separation and transport properties.

Chapter 6.

Recommendations for Future Work

6.1 Performance Enhancement of Pristine Fe_2TiO_5 films and its Application as a Photocatalyst for Overall Water Splitting

Fe_2TiO_5 thin films as photoanodes studied in this thesis yielded the low photocurrent of the order of 0.5 mA/cm^2 at 1.23 V vs RHE. Owing to its low band gap of around 2.1 eV, according to the calculations, the maximum STH efficiency it can exhibit is around 16% and a maximum photocurrent of the order of 13 mA/cm^2 [132]. This suggests that there is a vast improvement possible in the photocurrent and efficiency of Fe_2TiO_5 films based photoelectrodes. In this study, hydrothermal technique was used to develop crystalline nanoporous thin films of thickness of the order of 100 nm. Thickness was found to be limited by the reaction conditions employed to fabricate these thin films with hydrothermal technique. This thickness, as observed in absorption spectra, was not enough to completely absorb the solar spectrum. Efforts were made to develop thicker films using tuning of precursor concentration, reaction temperature, reaction time and also changing the precursors. But the crystalline pure phase of Fe_2TiO_5 film was achieved by the reported methodology. Hence, there is a scope of improvement in photocurrent by using different organic or inorganic precursors or by employing a different technique that can yield thicker, crystalline and porous films. It is realized here that Fe_2TiO_5 possesses appreciable charge transporting properties which could yield higher performance. But it is also important to invest some time on fabricating nanostructures with 1D dimensions which can assist a good electron transport along the axis similar to the hematite nanorods which witnessed a manifold enhancement owing to its [110] axis [30]. Nanostructuring also allows the easy hole transport into the electrolyte if the minority carrier diffusion length is not large enough. To further increase the conductivity, doping with Group V elements could also be employed which can significantly improve the photocurrent density.

Till now electrical properties like minority carrier diffusion length, carrier lifetime has not been explored in this system. To look into the charge dynamics inside the system, spectroscopic technique like Transient Absorption Spectroscopy (TAS) could be employed. TAS allows the tracking of energy transfer processes and formation of charge separated states in real time by monitoring their photoinduced absorption [133]. In context with solar water oxidation, it helps in understanding recombination pathways, trapping, charge carrier's lifetime after illumination and the effect of p-n junctions or overlayer or blocking layer on passivating the defects present in materials and hence inhibiting recombination. It can also yield information about minority carrier diffusion length which largely impacts the hole injection into the electrolyte and in turn design of the photoanode nanostructures.

Another important development possible in utilizing the favourable band positions exhibited by Fe_2TiO_5 is by using it as a photocatalyst for overall water splitting. It has been discussed earlier that conduction and valence band of semiconductor should straddle the water redox levels to allow both hydrogen and oxygen evolution. UPS measurements showed work function lying around 4.77 eV with respect to vacuum. After extracting the information about the difference of work function and valence band through XPS measurements, it is evident that the conduction band lies above the hydrogen evolution level (i.e. 4.5 eV with respect to vacuum level). This suggests this photocatalyst could be utilized for both water reduction and oxidation. There have been reports of using Fe_2O_3/TiO_2 composites as a photocatalyst [134] or using $FeTiO_3$ nanodiscs on TiO_2 nanoparticle as an efficient absorber for visible light photocatalysis [80]. Recently, synthesis and characterization of Fe_2TiO_5 nanoparticles has been reported as a photocatalyst for decolourisation of Rhodamine-B and

Methylenblue to demonstrate its photoactivity [135]. But as per our knowledge, pure phase of Fe_2TiO_5 as photocatalyst for hydrogen/oxygen evolution has not been reported yet. This promising aspect of using Fe_2TiO_5 as a photocatalyst for overall water splitting opens a new facet to solar fuel production research.

6.2 Morphological Improvement of Fe_2O_3/Fe_2TiO_5 Photoanodes by Fabricating Defined Heterojunction and Introducing Hole Blocking Layer

A stable heterojunction of Fe_2O_3/Fe_2TiO_5 was demonstrated as a photoanode for solar water splitting. Since it comprises of earth abundant and non-toxic elements like Fe, Ti already being used highly in PEC, it opens up a way which could lead to realization of a robust photoelectrode system which could be fine- tuned to yield impressive photocurrent density and efficiency. Currently, photocurrent density as high as 1.4 mA/cm^2 was achieved without using a cocatalyst which enhanced to 1.6 mA/cm^2 with CoO_x as a cocatalyst deposited on the thin film. These films are capable of good solar spectrum absorption and have a type II band alignment which suggests there is a lot of scope of improvement in the performance of these photoanodes. Morphological characterizations through FESEM and TEM showed that Fe_2TiO_5 thin film was coated on the top of Fe_2O_3 nanorods. Some Fe_2TiO_5 nanoparticles also were found inside the empty space of nanorods. But most of the nanorods surface was still without a defined heterojunction. There is a need to develop a strategy where a uniform and precise coverage of Fe_2TiO_5 film is achieved which would mean a heterojunction along the edge of nanorods. This would result in photons absorption in the proximity with the depletion region and hence would result in injection of holes into the electrolyte more efficiently. This could be either achieved by tuning the reaction conditions of hydrothermal methodology or by choosing a controlled growth technique like ALD or CVD.

In photoanode systems, another important component which could enhance charge separation and hence performance is Hole blocking layer (HBL). Generally, an HBL is a very thin layer of an air-stable oxide material with high band gap and a conduction band level position lying between the work function of the back contact (here FTO) and the conduction band of photoanode adjacent to the contact (here Fe_2O_3). Its role is to allow the transport of electrons across it but to block holes entering into the contact without involving into absorption due to its high optical transparency. HBL should also have a valence band lower than the photoanode to block photogenerated holes. An n-type semiconductor SnO_2 possesses high transparency, high permittivity and an electron mobility (~ 100-200 $cm^2V^{-1}s^{-1}$) which could assist a fast transport of electrons through the layer [136-137]. A very thin SnO_2 underlayer on FTO could be deposited using spin coating or spray pyrolysis technique. Due to similarity in the crystal structure between SnO_2 and Fluorine Doped SnO_2, the interfacial effects could be minimized and formation of Fe_2O_3 nanorods could also be similar as in this case. A study with SnO_2 present as an underlayer in the Fe_2O_3/Fe_2TiO_5 heterojunction based device could be investigated for higher performance.

List of References

[1] MacKay, D. J. C. Solar energy in the context of energy use, energy transportation and energy storage. *Phil Trans R Soc A* 2013**,** *371*.

[2] Kudo, A.; Miseki, Y. Heterogeneous Photocatalyst Materials for Water Splitting. *Chem. Soc. Rev.* 2009**,** *38*, 253-278.

[3] Tachibana, Y.; Vayssieres, L.; Durrant, J. R. Artificial Photosynthesis for Solar Water-Splitting. *Nature Photonics* 2012**,** *6*, 511-518.

[4] Liao, P.; Carter, E. A. Hole Transport in Pure and Doped Hematite. *Journal of Applied Physics* 2012**,** *112*.

[5] Butler, M. A.; Ginley, D. S. Principles of Photoelectrochemical, Solar Energy Conversion. *Journal of Materials Science* 1980**,** *15*, 1-19.

[6] Grätzel, M. Photoelectrochemical cells. *Nature* 2001**,** *414*, 338-344.

[7] Walter, M. G.; Warren, E. L.; McKone, J. R.; Boettcher, S. W.; Mi, Q.; Santori, E. A.; Lewis, N. S. Solar Water Splitting Cells. *Chem. Rev.* 2010**,** *110*, 6446-6473.

[8] Chen, X.; Shen, S.; Guo, L.; Mao, S. S. Semiconductor-Based Photocatalytic Hydrogen Generation. *Chem. Rev.* 2010**,** *110*, 6503-6570.

[9] Tong, H.; Ouyang, S.; Bi, Y.; Umezawa, N.; Oshikiri, M.; Ye, J. Nano-photocatalytic Materials: Possibilities and Challenges. *Adv. Mater.* 2012**,** *24*, 229-251.

[10] Kubacka, A.; Fernandez-Garcia, M.; Colon, G. Advanced Nanoarchitectures for Solar Photocatalytic Applications. *Chem Rev* 2012**,** *112*, 1555-1614.

[11] Maeda, K.; Domen, K. Oxynitride Materials for Solar Water Splitting. *MRS Bull.* 2011**,** *36*, 25-31.

[12] Fujishima, A.; Honda, K. Electrochemical Photolysis of Water at a Semiconductor Electrode. *Nature* 1972**,** *238*, 37-38.

[13] Ni, M.; Leung, M. K. H.; Leung, D. Y. C.; Sumathy, K. A Review and Recent Developments in Photocatalytic Water-Splitting using TiO_2 for Hydrogen Production. *Renewable and Sustainable Energy Reviews* 2007**,** *11*, 401-425.

[14] Murphy, A. B.; Barnes, P. R. F.; Randeniya, L. K.; Plumb, I. C.; Grey, I. E.; Horne, M. D.; Glasscock, J. A. Efficiency of Solar Water Splitting using Semiconductor Electrodes. *International Journal of Hydrogen Energy* 2006**,** *31*, 1999-2017.

[15] Alexander, B. D.; Kulesza, P. J.; Rutkowska, I.; Solarska, R.; Augustynski, J. Metal Oxide Photoanodes for Solar Hydrogen Production. *J. Mater. Chem.* 2008**,** *18*, 2298-2303.

[16] Lewis, N. S.; Nocera, D. G. Powering the Planet: Chemical Challenges in Solar Energy Utilization. *P Natl Acad Sci USA* 2007**,** *104*, 20142-20142.

[17] Zhang, H.; Chen, G.; Bahnemann, D. W. Photoelectrocatalytic Materials for Environmental Applications. *J. Mater. Chem.* 2009**,** *19*, 5089-5121.

[18] Lin, Y.; Yuan, G.; Liu, R.; Zhou, S.; Sheehan, S. W.; Wang, D. Semiconductor Nanostructure-based Photoelectrochemical Water Splitting: A brief Review. *Chemical Physics Letters* 2011**,** *507*, 209-215.

[19] Young, K. M. H.; Klahr, B. M.; Zandi, O.; Hamann, T. W. Photocatalytic Water Oxidation with Hematite Electrodes. *Catalysis Science and Technology* 2013**,** *3*, 1660-1671.

[20] Wheeler, D. A.; Wang, G.; Ling, Y.; Li, Y.; Zhang, J. Z. Nanostructured Hematite: Synthesis, Characterization, Charge Carrier Dynamics, and Photoelectrochemical Properties. *Energy Environ. Sci.* 2012**,** *5*, 6682-6702.

[21] Liu, X.; Wang, F.; Wang, Q. Nanostructure-based WO_3 Photoanodes for Photoelectrochemical Water Splitting. *Phys. Chem. Chem. Phys.* 2012**,** *14*, 7894-7911.

[22] Marsen, B.; Miller, E. L.; Paluselli, D.; Rocheleau, R. E. Progress in Sputtered Tungsten Trioxide for Photoelectrode Applications. *International Journal of Hydrogen Energy* 2007**,** *32*, 3110-3115.

[23] Sayama, K.; Nomura, A.; Arai, T.; Sugita, T.; Abe, R.; Yanagida, M.; Oi, T.; Iwasaki, Y.; Abe, Y.; Sugihara, H. Photoelectrochemical Decomposition of Water into H_2 and O_2 on Porous $BiVO_4$ Thin-Film Electrodes under Visible Light and Significant Effect of Ag Ion Treatment. *J. Phys. Chem. B* 2006**,** *110*, 11352-11360.

[24] Luo, W.; Yang, Z.; Li, Z.; Zhang, J.; Liu, J.; Zhao, Z.; Wang, Z.; Yan, S.; Yu, T.; Zou, Z. Solar Hydrogen Generation from Seawater with a Modified $BiVO_4$ Photoanode. *Energy Environ. Sci.* 2011**,** *4*, 4046-4051.

[25] Abdi, F. F.; Firet, N.; van de Krol, R. Efficient $BiVO_4$ Thin Film Photoanodes Modified with Cobalt Phosphate Catalyst and W-doping. *ChemCatChem* 2013**,** *5*, 490-496.

[26] Sivula, K.; Le Formal, F.; Grätzel, M. Solar Water Splitting: Progress Using Hematite (α-Fe_2O_3) Photoelectrodes. *ChemSusChem* 2011**,** *4*, 432-449.

[27] Ling, Y.; Wang, G.; Wheeler, D. A.; Zhang, J. Z.; Li, Y. Sn-doped Hematite Nanostructures for Photoelectrochemical Water Splitting. *Nano Lett.* 2011**,** *11*, 2119-2125.

[28] Sivula, K.; Zboril, R.; Le Formal, F.; Robert, R.; Weidenkaff, A.; Tucek, J.; Frydrych, J.; Gratzel, M. Photoelectrochemical Water Splitting with Mesoporous Hematite Prepared by a Solution-Based Colloidal Approach. *J. Am. Chem. Soc.* 2010**,** *132*, 7436-7444.

[29] Cherepy, N. J.; Liston, D. B.; Lovejoy, J. A.; Deng, H. M.; Zhang, J. Z. Ultrafast Studies of Photoexcited Electron Dynamics in Gamma- and Alpha-Fe_2O_3 Semiconductor Nanoparticles. *J. Phys. Chem. B* 1998**,** *102*, 770-776.

[30] Kay, A.; Cesar, I.; Grätzel, M. New Benchmark for Water Photooxidation by Nanostructured α-Fe_2O_3 Films. *J. Am. Chem. Soc.* 2006**,** *128*, 15714-15721.

[31] Gurudayal; Chiam, S. Y.; Kumar, M. H.; Bassi, P. S.; Seng, H. L.; Barber, J.; Wong, L. H. Improving the Efficiency of Hematite Nanorods for Photoelectrochemical Water Splitting by Doping with Manganese. *ACS Appl. Mater. Interfaces* 2014**,** *6*, 5852-5859.

[32] Le Formal, F.; Tétreault, N.; Cornuz, M.; Moehl, T.; Grätzel, M.; Sivula, K. Passivating Surface States on Water Splitting Hematite Photoanodes with Alumina Overlayers. *Chemical Science* 2011**,** *2*, 737-743.

[33] Xi, L.; Bassi, P. S.; Chiam, S. Y.; Mak, W. F.; Tran, P. D.; Barber, J.; Chye Loo, J. S.; Wong, L. H. Surface Treatment of Hematite Photoanodes with Zinc Acetate for Water Oxidation. *Nanoscale* 2012**,** *4*, 4430-4433.

[34] Xi, L. F.; Chiam, S. Y.; Mak, W. F.; Tran, P. D.; Barber, J.; Loo, S. C. J.; Wong, L. H. A Novel Strategy for Surface Treatment on Hematite Photoanode for Efficient Water Oxidation. *Chemical Science* 2013**,** *4*, 164-169.

[35] McDonald, K. J.; Choi, K. S. Photodeposition of Co-Based Oxygen Evolution Catalysts on alpha-Fe_2O_3 Photoanodes. *Chem. Mater.* 2011**,** *23*, 1686-1693.

[36] Zhong, D. K.; Cornuz, M.; Sivula, K.; Grätzel, M.; Gamelin, D. R. Photo-Assisted Electrodeposition of Cobalt-Phosphate (Co-Pi) Catalyst on Hematite Photoanodes for Solar Water Oxidation. *Energy and Environmental Science* 2011**,** *4*, 1759-1764.

[37] Kanan, M. W.; Nocera, D. G. In Situ Formation of an Oxygen-evolving Catalyst in Neutral Water containing Phosphate and Co^{2+}. *Science* 2008**,** *321*, 1072-1075.

[38] Mayer, M. T.; Lin, Y. J.; Yuan, G. B.; Wang, D. W. Forming Heterojunctions at the Nanoscale for Improved Photoelectrochemical Water Splitting by Semiconductor Materials: Case Studies on Hematite. *Acc. Chem. Res.* 2013**,** *46*, 1558-1566.

[39] Thimsen, E.; Biswas, S.; Lo, C. S.; Biswas, P. Predicting the Band Structure of Mixed Transition Metal Oxides: Theory and Experiment. *J. Phys. Chem. C* 2009**,** *113*, 2014-2021.

[40] Danzfuss, B.; Stimming, U. Iron(III)-Titanium(IV)-Oxide Electrodes: Their Structural, Electrochemical and Photoelectrochemical Properties. *Journal of Electroanalytical Chemistry and Interfacial Electrochemistry* 1984**,** *164*, 89-119.

[41] Klahr, B.; Gimenez, S.; Fabregat-Santiago, F.; Hamann, T.; Bisquert, J. Water Oxidation at Hematite Photoelectrodes: The Role of Surface States. *J. Am. Chem. Soc.* 2012**,** *134*, 4294-4302.

[42] Liu, R.; Zheng, Z.; Spurgeon, J.; Yang, X. Enhanced Photoelectrochemical Water-Splitting Performance of Semiconductors by Surface Passivation Layers. *Energy Environ. Sci.* 2014**,** *7*, 2504.

[43] Gurudayal; Sabba, D.; Kumar, M. H.; Wong, L. H.; Barber, J.; Gratzel, M.; Mathews, N. Perovskite-Hematite Tandem Cells for Efficient Overall Solar Driven Water Splitting. *Nano Lett* 2015**,** *15*, 3833-3839.

[44] Brillet, J.; Yum, J. H.; Cornuz, M.; Hisatomi, T.; Solarska, R.; Augustynski, J.; Graetzel, M.; Sivula, K. Highly Efficient Water Splitting by a Dual-Absorber Tandem Cell. *Nature Photonics* 2012**,** *6*, 823-827.

[45] Kennedy, J. H.; Frese, K. W. Photooxidation of Water at alpha-Fe_2O_3 Electrodes. *J Electrochem Soc* 1977**,** *124*, C130-C130.

[46] Cesar, I.; Sivula, K.; Kay, A.; Zboril, R.; Graetzel, M. Influence of Feature Size, Film Thickness, and Silicon Doping on the Performance of Nanostructured Hematite Photoanodes for Solar Water Splitting. *J. Phys. Chem. C* 2009**,** *113*, 772-782.

[47] Baxter, J. B.; Richter, C.; Schmuttenmaer, C. A. Ultrafast Carrier Dynamics in Nanostructures for Solar Fuels. *Annual review of physical chemistry* 2014**,** *65*, 423-447.

[48] Mulmudi, H. K.; Mathews, N.; Dou, X. C.; Xi, L. F.; Pramana, S. S.; Lam, Y. M.; Mhaisalkar, S. G. Controlled Growth of Hematite (α-Fe_2O_3) Nanorod Array on Fluorine

Doped Tin Oxide: Synthesis and Photoelectrochemical Properties. *Electrochemistry Communications* 2011**,** *13*, 951-954.

[49] Xi, L.; Tran, P. D.; Chiam, S. Y.; Bassi, P. S.; Mak, W. F.; Mulmudi, H. K.; Batabyal, S. K.; Barber, J.; Loo, J. S. C.; Wong, L. H. Co_3O_4-decorated Hematite Nanorods as an Effective Photoanode for Solar Water Oxidation. *J. Phys. Chem. C* 2012**,** *116*, 13884-13889.

[50] Boris, D. C.; Harry, B. R.; Uros, C.; Jacek, B. J.; Vivekanand, K.; Todd, D.; Mahendra, K. S. Photoelectrochemical Activity of As-grown, α-Fe_2O_3 Nanowire Array Electrodes for Water Splitting. *Nanotechnology* 2012**,** *23*, 194009.

[51] Grigorescu, S.; Lee, C.-Y.; Lee, K.; Albu, S.; Paramasivam, I.; Demetrescu, I.; Schmuki, P. Thermal Air Oxidation of Fe: Rapid Hematite Nanowire Growth and Photoelectrochemical Water Splitting Performance. *Electrochemistry Communications* 2012**,** *23*, 59-62.

[52] Li, L.; Yu, Y.; Meng, F.; Tan, Y.; Hamers, R. J.; Jin, S. Facile Solution Synthesis of α-$FeF_3 \cdot 3H_2O$ Nanowires and Their Conversion to α-Fe_2O_3 Nanowires for Photoelectrochemical Application. *Nano Lett.* 2012**,** *12*, 724-731.

[53] Zheng, J. Y.; Kang, M. J.; Song, G.; Son, S. I.; Suh, S. P.; Kim, C. W.; Kang, Y. S. Morphology Evolution of Dendritic Fe Wire Array by Electrodeposition, and Photoelectrochemical Properties of alpha-Fe_2O_3 Dendritic Wire Array. *Crystengcomm* 2012**,** *14*, 6957-6961.

[54] Yang, T.-Y.; Kang, H.-Y.; Jin, K.; Park, S.; Lee, J.-H.; Sim, U.; Jeong, H.-Y.; Joo, Y.-C.; Nam, K. T. Iron Oxide Photoanode with Hierarchical Nanostructure for Efficient Water Oxidation. *J. Mater. Chem. A* 2013.

[55] Deng, J.; Zhong, J.; Pu, A.; Zhang, D.; Li, M.; Sun, X.; Lee, S. T. Ti-doped Hematite Nanostructures for Solar Water Splitting with High Efficiency. *Journal of Applied Physics* 2012**,** *112*.

[56] Kim, J. Y.; Magesh, G.; Youn, D. H.; Jang, J.-W.; Kubota, J.; Domen, K.; Lee, J. S. Single-Crystalline, Wormlike Hematite Photoanodes for Efficient Solar Water Splitting. *Sci. Rep.* 2013**,** *3*.

[57] Morin, F. J. Electrical Properties of α-Fe_2O_3 and α-Fe_2O_3 Containing Titanium. *Physical Review* 1951**,** *83*, 1005-1010.

[58] Morin, F. J. Electrical Properties of alpha-Fe_2O_3. *Physical Review* 1954**,** *93*, 1195-1199.

[59] Lin, Y.; Xu, Y.; Mayer, M. T.; Simpson, Z. I.; McMahon, G.; Zhou, S.; Wang, D. Growth of p-type Hematite by Atomic Layer Deposition and its Utilization for Improved Solar Water Splitting. *J. Am. Chem. Soc.* 2012**,** *134*, 5508-5511.

[60] Meng, X. Y.; Qin, G. W.; Li, S.; Wen, X. H.; Ren, Y. P.; Pei, W. L.; Zuo, L. Enhanced Photoelectrochemical Activity for Cu and Ti doped Hematite: The first Principles Calculations. *Applied Physics Letters* 2011**,** *98*.

[61] Kumar, P.; Sharma, P.; Shrivastav, R.; Dass, S.; Satsangi, V. R. Electrodeposited Zirconium-Doped α-Fe_2O_3 Thin Film for Photoelectrochemical Water Splitting. *International Journal of Hydrogen Energy* 2011**,** *36*, 2777-2784.

[62] Balko, B. A.; Clarkson, K. M. The Effect of Doping with Ti(IV) and Sn(IV) on Oxygen Reduction at Hematite Electrodes. *J Electrochem Soc* 2001**,** *148*, E85-E91.

[63] Shen, S.; Kronawitter, C. X.; Wheeler, D. A.; Guo, P.; Lindley, S. A.; Jiang, J.; Zhang, J. Z.; Guo, L.; Mao, S. S. Physical and Photoelectrochemical Characterization of Ti-doped Hematite Photoanodes Prepared by Solution Growth. *J. Mater. Chem. A* 2013**,** *1*, 14498-14506.

[64] Zhang, P.; Kleiman-Shwarsctein, A.; Hu, Y. S.; Lefton, J.; Sharma, S.; Forman, A. J.; McFarland, E. Oriented Ti doped Hematite Thin film as Active Photoanodes Synthesized by Facile APCVD. *Energy Environ. Sci.* 2011**,** *4*, 1020-1028.

[65] Lian, X. J.; Yang, X.; Liu, S. J.; Xu, Y.; Jiang, C. P.; Chen, J. W.; Wang, R. L. Enhanced Photoelectrochemical Performance of Ti-doped Hematite Thin Films Prepared by the Sol-Gel Method. *Appl. Surf. Sci.* 2012**,** *258*, 2307-2311.

[66] Ling, Y. C.; Wang, G. M.; Reddy, J.; Wang, C. C.; Zhang, J. Z.; Li, Y. The Influence of Oxygen Content on the Thermal Activation of Hematite Nanowires. *Angew. Chem. Int. Edit.* 2012**,** *51*, 4074-4079.

[67] Yang, T. Y.; Kang, H. Y.; Sim, U.; Lee, Y. J.; Lee, J. H.; Koo, B.; Nam, K. T.; Joo, Y. C. A New Hematite Photoanode Doping Strategy for Solar Water Splitting: Oxygen Vacancy Generation. *Phys. Chem. Chem. Phys.* 2013**,** *15*, 2117-2124.

[68] Forster, M.; Potter, R. J.; Ling, Y.; Yang, Y.; Klug, D. R.; Li, Y.; Cowan, A. J. Oxygen deficient α-Fe2O3photoelectrodes: a balance between enhanced electrical properties and trap-mediated losses. *Chem. Sci.* 2015**,** *6*, 4009-4016.

[69] Zandi, O.; Klahr, B. M.; Hamann, T. W. Highly Photoactive Ti-doped alpha-Fe_2O_3 Thin Film Electrodes: Resurrection of the Dead Layer. *Energy Environ. Sci.* 2013**,** *6*, 634-642.

[70] Kronawitter, C. X.; Zegkinoglou, I.; Shen, S. H.; Liao, P.; Cho, I. S.; Zandi, O.; Liu, Y. S.; Lashgari, K.; Westin, G.; Guo, J. H.; Himpsel, F. J.; Carter, E. A.; Zheng, X. L.; Hamann, T. W.; Koel, B. E.; Mao, S. S.; Vayssieres, L. Titanium incorporation into hematite photoelectrodes: theoretical considerations and experimental observations. *Energy Environ. Sci.* 2014**,** *7*, 3100-3121.

[71] Boumaza, S.; Boudjemaa, A.; Bouguelia, A.; Bouarab, R.; Trari, M. Visible Light Induced Hydrogen Evolution on New Hetero-system $ZnFe_2O_4/SrTiO_3$. *Appl Energ* 2010**,** *87*, 2230-2236.

[72] McDonald, K. J.; Choi, K. S. Synthesis and Photoelectrochemical Properties of $Fe_2O_3/ZnFe_2O_4$ Composite Photoanodes for use in Solar Water Oxidation. *Chem. Mater.* 2011**,** *23*, 4863-4869.

[73] Miao, C.; Ji, S.; Xu, G.; Liu, G.; Zhang, L.; Ye, C. Micro-Nano-Structured Fe_0O_3:Ti/$ZnFe_2O_4$ Heterojunction Films for Water Oxidation. *ACS Appl. Mater. Interfaces* 2012**,** *4*, 4428-4433.

[74] Kim, J. H.; Kim, J. H.; Jang, J.-W.; Kim, J. Y.; Choi, S. H.; Magesh, G.; Lee, J.; Lee, J. S. Awakening Solar Water-Splitting Activity of ZnFe2O4Nanorods by Hybrid Microwave Annealing. *Adv. Energy Mater.* 2015**,** *5*, n/a-n/a.

[75] Rekhila, G.; Bessekhouad, Y.; Trari, M. Visible Light Hydrogen Production on the Novel Ferrite $NiFe_2O_4$. *International Journal of Hydrogen Energy* 2013**,** *38*, 6335-6343.

[76] Townsend, T. K.; Browning, N. D.; Osterloh, F. E. Nanoscale Strontium Titanate Photocatalysts for Overall Water Splitting. *ACS Nano* 2012**,** *6*, 7420-7426.

[77] Hara, S.; Yoshimizu, M.; Tanigawa, S.; Ni, L.; Ohtani, B.; Irie, H. Hydrogen and Oxygen Evolution Photocatalysts Synthesized from Strontium Titanate by Controlled Doping and Their Performance in Two-Step Overall Water Splitting under Visible Light. *J. Phys. Chem. C* 2012**,** *116*, 17458-17463.

[78] Ginley, D. S.; Baughman, R. J. Preparation and Czochralski Crystal-Growth of Iron Titanates, $FeTiO_3$, Fe_2TiO_4, and Fe_2TiO_5. *Mater. Res. Bull.* 1976**,** *11*, 1539-1543.

[79] Gao, B.; Kim, Y. J.; Chakraborty, A. K.; Lee, W. I. Efficient Decomposition of Organic Compounds with $FeTiO_3/TiO_2$ Heterojunction under Visible Light Irradiation. *Appl Catal B-Environ* 2008**,** *83*, 202-207.

[80] Kim, Y. J.; Gao, B.; Han, S. Y.; Jung, M. H.; Chakraborty, A. K.; Ko, T.; Lee, C.; Lee, W. I. Heterojunction of $FeTiO_3$ Nanodisc and TiO_2 Nanoparticle for a Novel Visible Light Photocatalyst. *J. Phys. Chem. C* 2009**,** *113*, 19179-19184.

[81] Truong, Q. D.; Liu, J. Y.; Chung, C. C.; Ling, Y. C. Photocatalytic Reduction of CO_2 on $FeTiO_3/TiO_2$ photocatalyst. *Catal Commun* 2012**,** *19*, 85-89.

[82] Wu, X.; Steinle-Neumann, G.; Narygina, O.; Kantor, I.; McCammon, C.; Pascarelli, S.; Aquilanti, G.; Prakapenka, V.; Dubrovinsky, L. Iron oxidation state of $FeTiO_3$ under high pressure. *Phys. Rev. B* 2009**,** *79*.

[83] Wyckoff, R. W. G., *Crystal Structures*. Wiley: New York, **1964**; Vol. 3, p 297.

[84] Enhessari, M.; Razi, M. K.; Etemad, L.; Parviz, A.; Sakhaei, M. Structural, Optical and Magnetic Properties of the Fe_2TiO_5 Nanopowders. *Journal of Experimental Nanoscience* 2012, 1-10.

[85] Scaife, D. E. Oxide Semiconductors in Photoelectrochemical Conversion of Solar Energy. *Solar Energy* 1980**,** *25*, 41-54.

[86] Courtin, E.; Baldinozzi, G.; Sougrati, M. T.; Stievano, L.; Sanchez, C.; Laberty-Robert, C. New Fe_2TiO_5-based Nanoheterostructured Mesoporous Photoanodes with Improved Visible Light Photoresponses. *J. Mater. Chem. A* 2014**,** *2*, 6567-6577.

[87] Li, Z.; Luo, W.; Zhang, M.; Feng, J.; Zou, Z. Photoelectrochemical Cells for Solar Hydrogen Production: Current State of Promising Photoelectrodes, Methods to Improve their Properties, and Outlook. *Energy Environ. Sci.* 2013**,** *6*, 347-370.

[88] Guijarro, N.; Prevot, M. S.; Sivula, K. Surface modification of semiconductor photoelectrodes. *Phys. Chem. Chem. Phys.* 2015**,** *17*, 15655-15674.

[89] Hu, Y. S.; Kleiman-Shwarsctein, A.; Stucky, G. D.; McFarland, E. W. Improved Photoelectrochemical Performance of Ti-doped alpha-Fe_2O_3 Thin Films by Surface Modification with Fluoride. *Chem. Commun.* 2009, 2652-2654.

[90] Hisatomi, T.; Le Formal, F.; Cornuz, M.; Brillet, J.; Tetreault, N.; Sivula, K.; Gratzel, M. Cathodic Shift in Onset Potential of Solar Oxygen Evolution on Hematite by 13-group Oxide Overlayers. *Energy Environ. Sci.* 2011**,** *4*, 2512-2515.

[91] Barroso, M.; Cowan, A. J.; Pendlebury, S. R.; Gratzel, M.; Klug, D. R.; Durrant, J. R. The Role of Cobalt Phosphate in Enhancing the Photocatalytic Activity of alpha-Fe_2O_3 toward Water Oxidation. *J. Am. Chem. Soc.* 2011**,** *133*, 14868-14871.

[92] Tilley, S. D.; Cornuz, M.; Sivula, K.; Grätzel, M. Light-induced Water Splitting with Hematite: Improved Nanostructure and Iridium Oxide Catalysis. *Angew. Chem., Int. Ed.* 2010**,** *49*, 6405-6408.

[93] Barroso, M.; Mesa, C. A.; Pendlebury, S. R.; Cowan, A. J.; Hisatomi, T.; Sivula, K.; Gratzel, M.; Klug, D. R.; Durrant, J. R. Dynamics of Photogenerated Holes in Surface Modified alpha-Fe_2O_3 Photoanodes for Solar Water Splitting. *P Natl Acad Sci USA* 2012**,** *109*, 15640-15645.

[94] Jiao, F.; Frei, H. Nanostructured Cobalt and Manganese Oxide Clusters as Efficient Water Oxidation Catalysts. *Energy Environ. Sci.* 2010**,** *3*, 1018-1027.

[95] Moniz, S. J. A.; Zhu, J.; Tang, J. 1D Co-Pi Modified BiVO4/ZnO Junction Cascade for Efficient Photoelectrochemical Water Cleavage. *Adv. Energy Mater.* 2014**,** *4*.

[96] Peter, L. M.; Wijayantha, K. G. U.; Tahir, A. A. Kinetics of Light-driven Oxygen Evolution at alpha-Fe_2O_3 Electrodes. *Faraday Discuss* 2012**,** *155*, 309-322.

[97] Barroso, M.; Pendlebury, S. R.; Cowan, A. J.; Durrant, J. R. Charge Carrier Trapping, Recombination and Transfer in Hematite (α-Fe_2O_3) Water Splitting Photoanodes. *Chemical Science* 2013**,** *4*, 2724.

[98] Cherepy, N. J.; Liston, D. B.; Lovejoy, J. A.; Deng, H.; Zhang, J. Z. Ultrafast Studies of Photoexcited Electron Dynamics in γ- and α-Fe_2O_3 Semiconductor Nanoparticles. *The Journal of Physical Chemistry B* 1998**,** *102*, 770-776.

[99] Joly, A. G.; Williams, J. R.; Chambers, S. A.; Xiong, G.; Hess, W. P.; Laman, D. M. Carrier Dynamics in α-Fe_2O_3 (0001) Thin Films and Single Crystals Probed by Femtosecond Transient Absorption and Reflectivity. *Journal of Applied Physics* 2006**,** *99*, -.

[100] Huang, Z.; Lin, Y.; Xiang, X.; Rodriguez-Cordoba, W.; McDonald, K. J.; Hagen, K. S.; Choi, K.-S.; Brunschwig, B. S.; Musaev, D. G.; Hill, C. L.; Wang, D.; Lian, T. In Situ Probe of Photocarrier Dynamics in Water-Splitting Hematite (alpha-Fe_2O_3) Electrodes. *Energy Environ. Sci.* 2012**,** *5*, 8923-8926.

[101] Pendlebury, S. R.; Cowan, A. J.; Barroso, M.; Sivula, K.; Ye, J.; Gratzel, M.; Klug, D. R.; Tang, J.; Durrant, J. R. Correlating Long-lived Photogenerated Hole Populations with Photocurrent Densities in Hematite Water Oxidation Photoanodes. *Energy Environ. Sci.* 2012**,** *5*, 6304-6312.

[102] Bora, D. K.; Braun, A.; Constable, E. C. "In Rust We Trust". Hematite - The Prospective Inorganic Backbone for Artificial Photosynthesis. *Energy Environ. Sci.* 2013**,** *6*, 407-425.

[103] Hou, Y.; Zuo, F.; Dagg, A.; Feng, P. A Three-Dimensional Branched Cobalt-Doped α-Fe_2O_3 Nanorod/$MgFe_2O_4$ Heterojunction Array as a Flexible Photoanode for Efficient Photoelectrochemical Water Oxidation. *Angew. Chem.* 2013**,** *125*, 1286-1290.

[104] Lin, Y. J.; Zhou, S.; Sheehan, S. W.; Wang, D. W. Nanonet-Based Hematite Heteronanostructures for Efficient Solar Water Splitting. *J. Am. Chem. Soc.* 2011**,** *133*, 2398-2401.

[105] Wang, M.; Pyeon, M.; Gonullu, Y.; Kaouk, A.; Shen, S.; Guo, L.; Mathur, S. Constructing Fe_2O_3/TiO_2 core-shell photoelectrodes for efficient photoelectrochemical water splitting. *Nanoscale* 2015**,** *7*, 10094-10100.

[106] Zhao, P.; Kronawitter, C. X.; Yang, X.; Fu, J.; Koel, B. E. WO_3-α-Fe_2O_3 Composite Photoelectrodes with Low Onset Potential for Solar Water Oxidation. *Phys. Chem. Chem. Phys.* 2014**,** *16*, 1327-1332.

[107] Hsu, Y. K.; Chen, Y. C.; Lin, Y. G. Novel ZnO/Fe_2O_3 Core-Shell Nanowires for Photoelectrochemical Water Splitting. *ACS Appl. Mater. Interfaces* 2015**,** *7*, 14157-14162.

[108] Jang, J. W.; Du, C.; Ye, Y.; Lin, Y.; Yao, X.; Thorne, J.; Liu, E.; McMahon, G.; Zhu, J.; Javey, A.; Guo, J.; Wang, D. Enabling unassisted solar water splitting by iron oxide and silicon. *Nat Commun* 2015**,** *6*, 7447.

[109] Su, J.; Guo, L.; Bao, N.; Grimes, C. A. Nanostructured WO_3/$BiVO_4$ Heterojunction Films for Efficient Photoelectrochemical Water Splitting. *Nano Lett.* 2011**,** *11*, 1928-1933.

[110] Leonard, K. C.; Nam, K. M.; Lee, H. C.; Kang, S. H.; Park, H. S.; Bard, A. J. $ZnWO_4$/WO_3 Composite for Improving Photoelectrochemical Water Oxidation. *J. Phys. Chem. C* 2013**,** *117*, 15901-15910.

[111] Bowles, J. F. W.; Deer, W. A.; Howie, R. A.; Vaughan, D. J.; Zussman, J., *Rock-Forming Minerals: Non-Silicates: Oxides, Hydroxides and Sulphides*. Geological Society: 2011.

[112] Liu, Q.; He, J.; Yao, T.; Sun, Z.; Cheng, W.; He, S.; Xie, Y.; Peng, Y.; Cheng, H.; Sun, Y.; Jiang, Y.; Hu, F.; Xie, Z.; Yan, W.; Pan, Z.; Wu, Z.; Wei, S. Aligned Fe_2TiO_5-containing nanotube arrays with low onset potential for visible-light water oxidation. *Nat Commun* 2014**,** *5*, 5122.

[113] Deng, J.; Lv, X.; Liu, J.; Zhang, H.; Nie, K.; Hong, C.; Wang, J.; Sun, X.; Zhong, J.; Lee, S.-T. Thin-Layer Fe_2TiO_5 on Hematite for Efficient Solar Water Oxidation. *ACS Nano* 2015.

[114] van de Krol, R., Photoelectrochemical Measurements. In *Photoelectrochemical Hydrogen Production*, Van de Krol, R.; Grätzel, M., Eds. Springer US: **2012**; Chapter 3, pp 69-117.

[115] Ma, Y. M.; Pendlebury, S. R.; Reynal, A.; Le Formal, F.; Durrant, J. R. Dynamics of Photogenerated Holes in undoped $BiVO_4$ Photoanodes for Solar Water Oxidation. *Chemical Science* 2014**,** *5*, 2964-2973.

[116] Klahr, B.; Gimenez, S.; Fabregat-Santiago, F.; Bisquert, J.; Hamann, T. W. Electrochemical and Photoelectrochemical Investigation of Water Oxidation with Hematite Electrodes. *Energy Environ. Sci.* 2012**,** *5*, 7626-7636.

[117] Dotan, H.; Sivula, K.; Gratzel, M.; Rothschild, A.; Warren, S. C. Probing the Photoelectrochemical Properties of Hematite (alpha-Fe_2O_3) Electrodes using Hydrogen Peroxide as a Hole Scavenger. *Energy Environ. Sci.* 2011**,** *4*, 958-964.

[118] Paracchino, A.; Mathews, N.; Hisatomi, T.; Stefik, M.; Tilley, S. D.; Gratzel, M. Ultrathin Films on Copper(I) Oxide Water Splitting Photocathodes: A Study on Performance and Stability. *Energy Environ. Sci.* 2012**,** *5*, 8673-8681.

[119] Kozuka, K.; Kajimura, M. Sol-gel Preparation and Photoelectrochemical Properties of Fe_2TiO_5 Thin Films. *J Sol-Gel Sci Techn* 2001**,** *22*, 125-132.

[120] Annamalai, A.; Subramanian, A.; Kang, U.; Park, H.; Choi, S. H.; Jang, J. S. Activation of Hematite Photoanodes for Solar Water Splitting: Effect of FTO Deformation. *J. Phys. Chem. C* 2015**,** *119*, 3810-3817.

[121] Wang, D.; Zhang, Y.; Peng, C.; Wang, J.; Huang, Q.; Su, S.; Wang, L.; Huang, W.; Fan, C. Crystallinity Engineering of Hematite Nanorods for High-Efficiency Photoelectrochemical Water Splitting. *Advanced Science* 2015**,** *2*, n/a-n/a.

[122] Moir, J.; Soheilnia, N.; Liao, K.; O'Brien, P.; Tian, Y.; Burch, K. S.; Ozin, G. A. Activation of Ultrathin Films of Hematite for Photoelectrochemical Water Splitting via H2 Treatment. *ChemSusChem* 2015**,** *8*, 1557-1567.

[123] Morrish, R.; Rahman, M.; MacElroy, J. M. D.; Wolden, C. A. Activation of Hematite Nanorod Arrays for Photoelectrochemical Water Splitting. *ChemSusChem* 2011**,** *4*, 474-479.

[124] Liang, Y.; Enache, C. S.; van de Krol, R. Photoelectrochemical Characterization of Sprayed α-Fe_2O_3Thin Films: Influence of Si Doping and SnO_2 Interfacial Layer. *International Journal of Photoenergy* 2008**,** *2008*, 1-7.

[125] Le Formal, F.; Pendlebury, S. R.; Cornuz, M.; Tilley, S. D.; Gratzel, M.; Durrant, J. R. Back Electron-Hole Recombination in Hematite Photoanodes for Water Splitting. *J Am Chem Soc* 2014**,** *136*, 2564-2574.

[126] Li, X.; Bassi, P. S.; Boix, P.; Fang, Y.; Wong, L. H. Revealing the role of TiO2 surface treatment of hematite nanorods photoanodes for solar water splitting. *ACS Appl. Mater. Interfaces* 2015**,** *7*, 16960–16966.

[127] Raghavender, A. T.; Hong, N. H.; Lee, K. J.; Jung, M. H.; Skoko, Z.; Vasilevskiy, M.; Cerqueira, M. F.; Samantilleke, A. P. Nano-ilmenite $FeTiO_3$: Synthesis and characterization. *J Magn Magn Mater* 2013**,** *331*, 129-132.

[128] Bickley, R. I.; Gonzalez-Carreno, T.; Gonzalez-Elipe, A. R.; Munuera, G.; Palmisano, L. Characterization of Iron Titanium-Oxide Photocatalysts .2. Surface Studies. *J Chem Soc Faraday T* 1994**,** *90*, 2257-2264.

[129] Gurudayal; Chee, P. M.; Boix, P. P.; Ge, H.; Fang, Y. N.; Barber, J.; Wong, L. H. Core-Shell Hematite Nanorods: A Simple Method To Improve the Charge Transfer in the Photoanode for Photoelectrochemical Water Splitting. *ACS Appl. Mater. Interfaces* 2015**,** *7*, 6852-6859.

[130] Cowan, A. J.; Barnett, C. J.; Pendlebury, S. R.; Barroso, M.; Sivula, K.; Grätzel, M.; Durrant, J. R.; Klug, D. R. Activation Energies for the Rate-Limiting Step in Water Photooxidation by Nanostructured α-Fe_2O_3 and TiO_2. *J. Am. Chem. Soc.* 2011**,** *133*, 10134-10140.

[131] Bertoluzzi, L.; Lopez-Varo, P.; Jimenez Tejada, J. A.; Bisquert, J. Charge transfer processes at the semiconductor/electrolyte interface for solar fuel production: insight from impedance spectroscopy. *J. Mater. Chem. A* 2015.

[132] Li, J.; Wu, N. Semiconductor-Based Photocatalysts and Photoelectrochemical Cells for Solar Fuel Generation: A Review. *Catalysis Science & Technology* 2015**,** *5*, 1360-1384.

[133] Berera, R.; Van Grondelle, R.; Kennis, J. T. M. Ultrafast Transient Absorption Spectroscopy: Principles and Application to Photosynthetic Systems. *Photosynth Res* 2009**,** *101*, 105-118.

[134] Chen, M.; Shen, X.; Wu, Q. H.; Li, W.; Diao, G. W. Template-assisted Synthesis of Core-shell alpha-Fe_2O_3@TiO_2 Nanorods and their Photocatalytic Property. *Journal of Materials Science* 2015**,** *50*, 4083-4094.

[135] Ramezani, M.; Davoodi, A.; Malekizad, A.; Hosseinpour-Mashkani, S. M. Synthesis and characterization of Fe2TiO5 nanoparticles through a sol-gel method and its photocatalyst applications. *J Mater Sci-Mater El* 2015**,** *26*, 3957-3962.

[136] Arnold, M. S.; Avouris, P.; Pan, Z. W.; Wang, Z. L. Field-Effect Transistors Based on Single Semiconducting Oxide Nanobelts. *J. Phys. Chem. B* 2003**,** *107*, 659-663.

[137] Dou, X.; Sabba, D.; Mathews, N.; Wong, L. H.; Lam, Y. M.; Mhaisalkar, S. Hydrothermal Synthesis of High Electron Mobility Zn-doped SnO_2 Nanoflowers as Photoanode Material for Efficient Dye-Sensitized Solar Cells. *Chem. Mater.* 2011**,** *23,* 3938-3945.

Appendix

Appendix A: Pristine Hematite Nanorods prepared under different annealing profiles

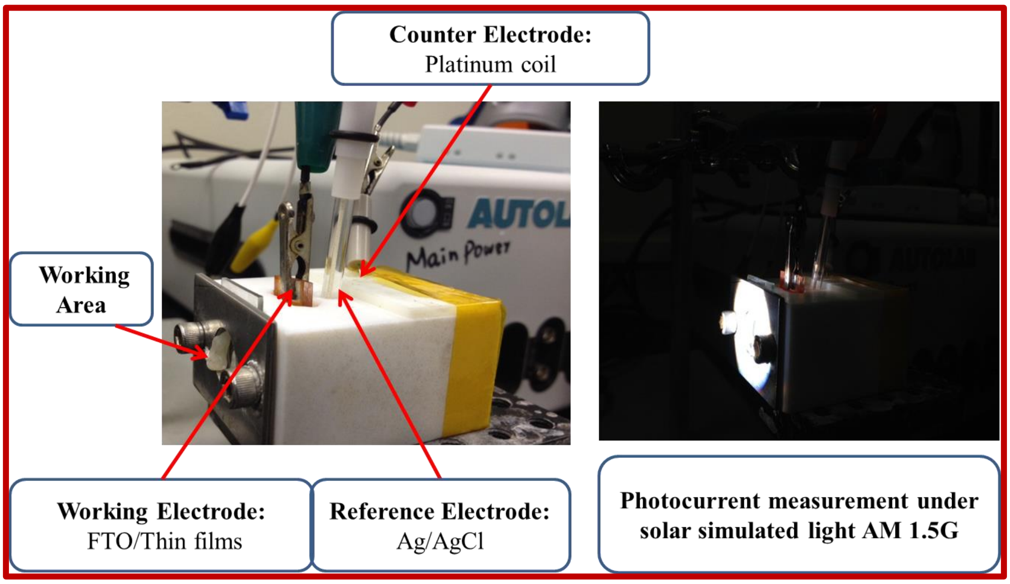

Figure A1: Picture of Photoelectrochemical Setup used for characterization of photoanodes in PEC

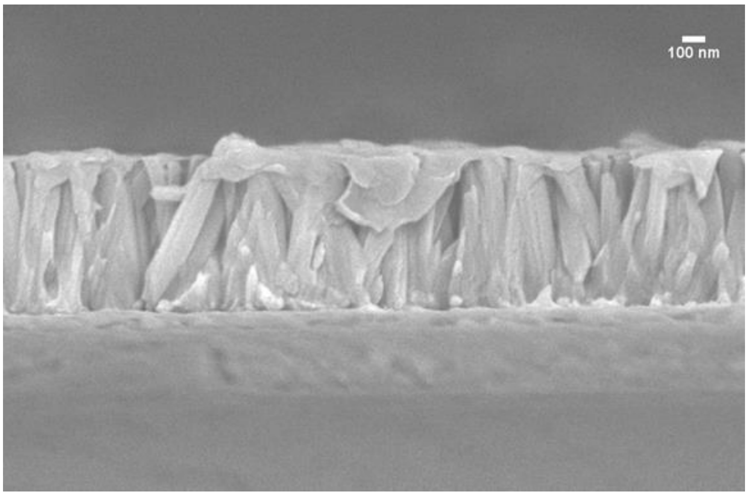

Figure A2: FESEM Cross-section Image of pristine as-grown FeOOH Nanorods fabricated through hydrothermal synthesis at 100°C for 8 hours

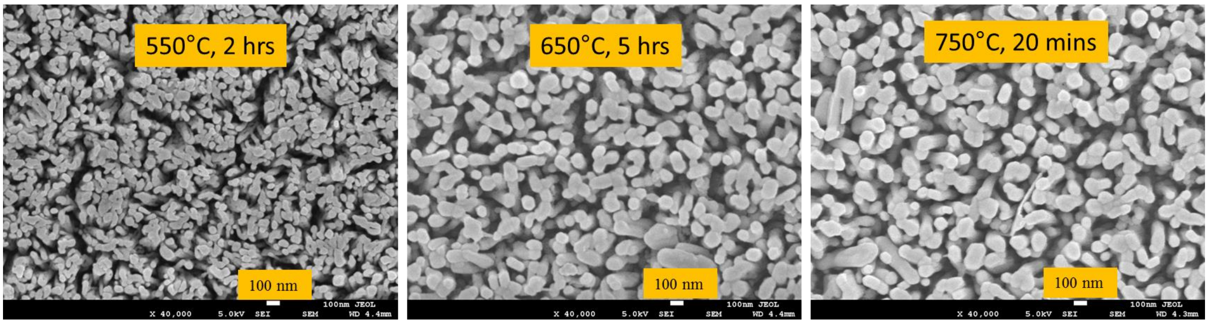

Figure A3: FESEM Top-view Images of Pristine Hematite Nanorods fabricated with different annealing profiles

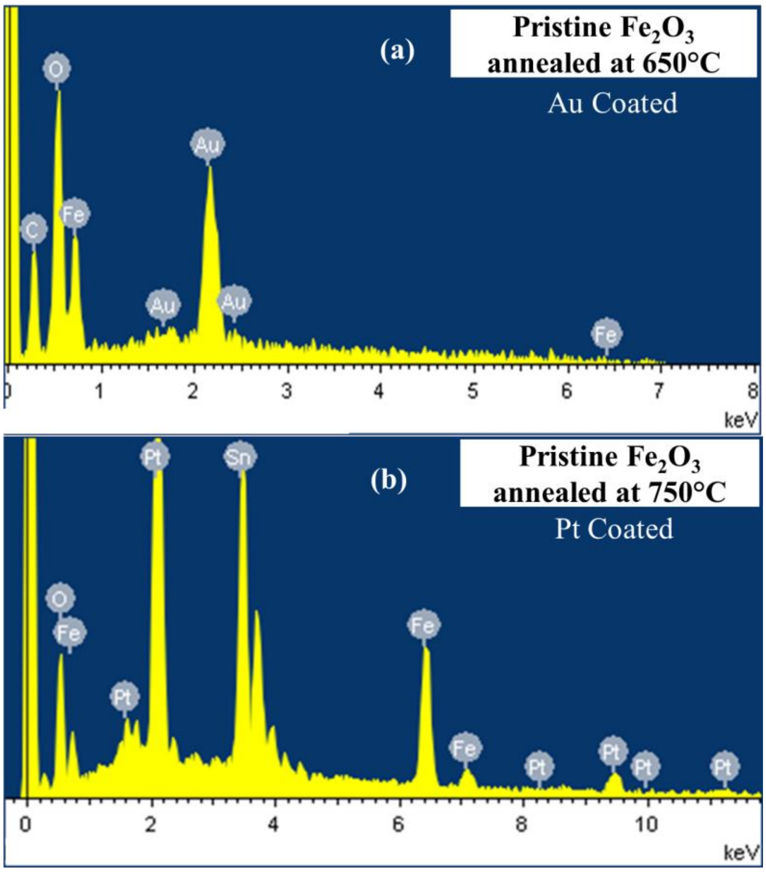

Figure A4: EDAX Spectra of pristine Fe_2O_3 nanorods prepared with annealing profile: (a) 650°C, 5hours and (b) 750C, 20 mins.

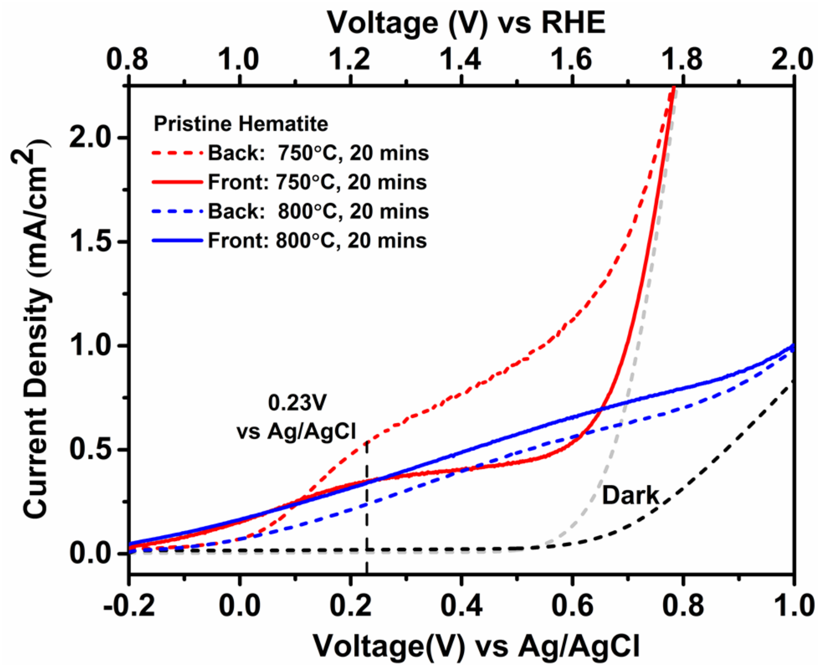

Figure A5: J-V Plots for different annealing profiles measured under standard conditions

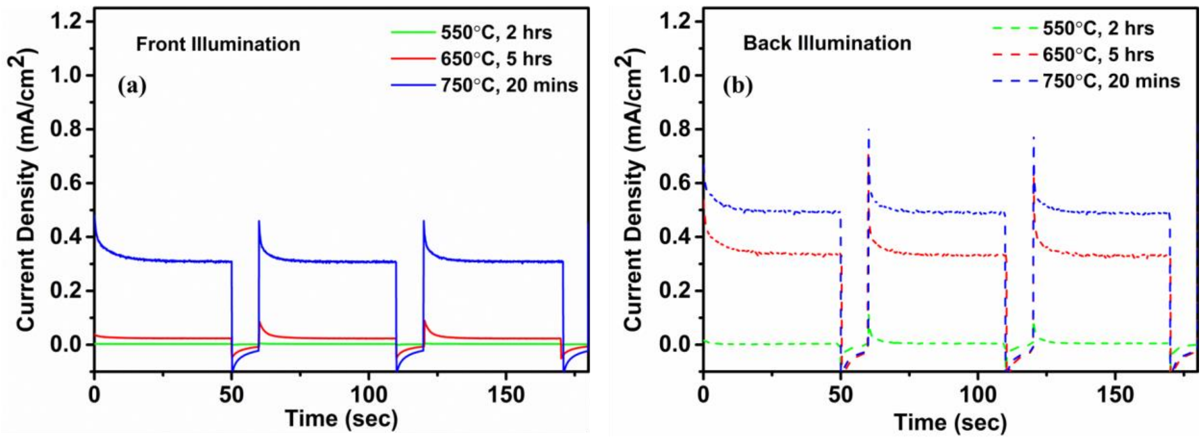

Figure A6: Chopped I-T Amperometric Curve for pristine Fe_2O_3 nanorods prepared with different annealing profiles under frontside and backside illumination

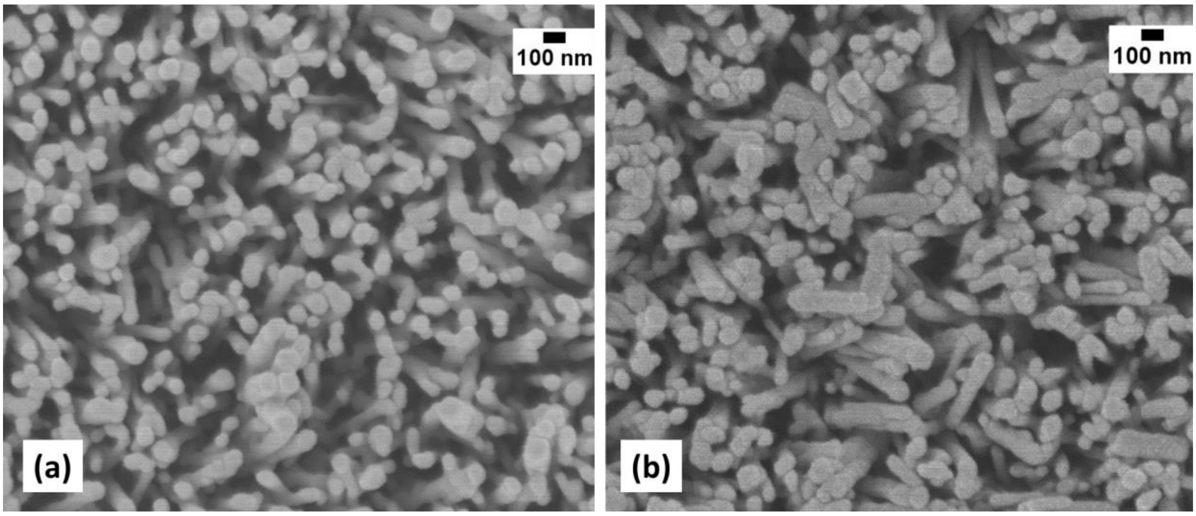

Figure A7: Top-view FESEM Images of (a) pristine, and (b) TiO_x coated Fe_2O_3 nanorods

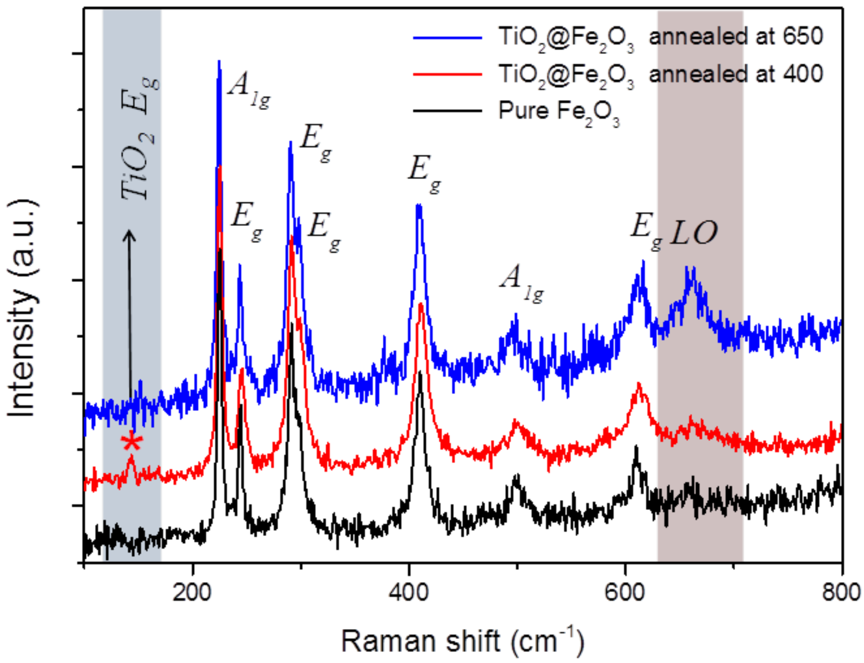

Figure A8: Raman spectra of pristine hematite nanorod arrays (black curve), ALD TiO_x-coated hematite annealed at 400 °C (red curve) and 650 °C (blue curve)

Appendix B: Introduction of pseudobrookite, Fe_2TiO_5 as a photoanode

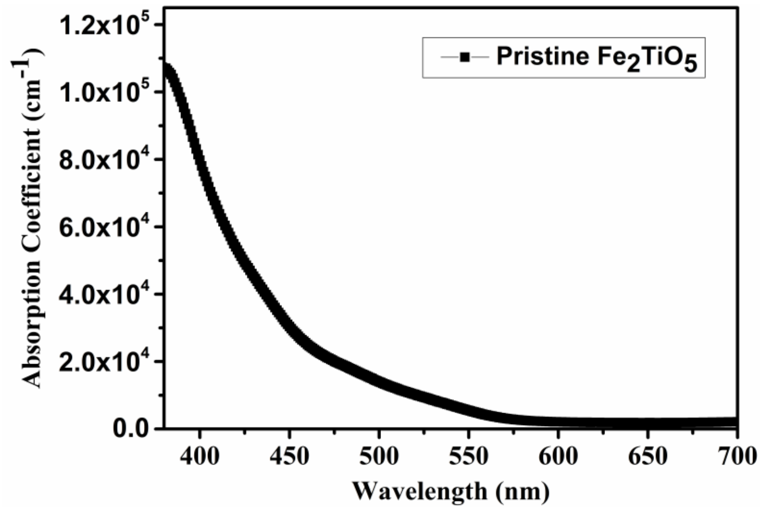

Figure B1: Absorption Coefficient curve for pristine Fe_2TiO_5 films

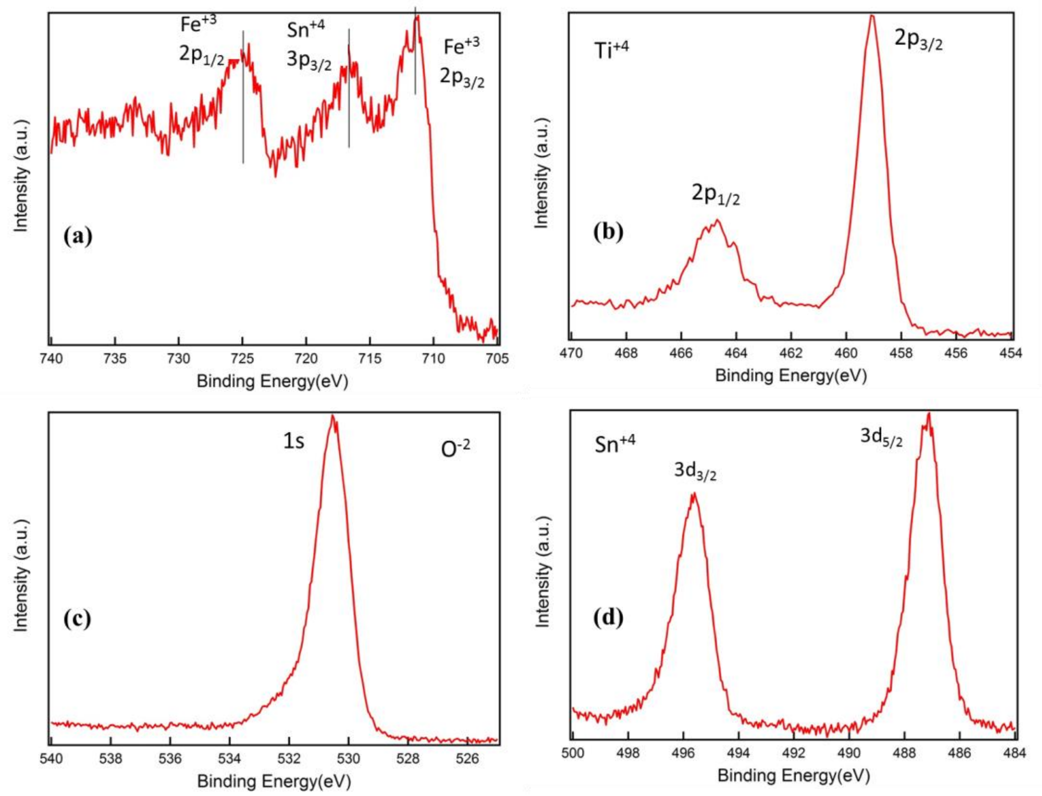

Figure B2: High resolution scans indicating the peaks corresponding to (a) Fe^{+3}, (b) Ti^{+4}, (c) O^{-2} and (d) Sn^{+4} ions in pristine Fe_2TiO_5 thin films

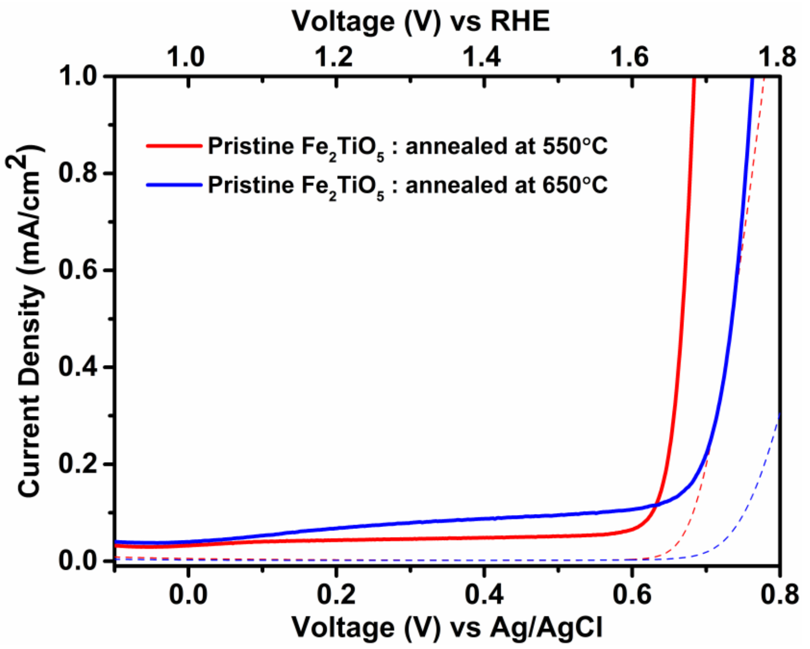

Figure B3: JV curves for pristine Fe_2TiO_5 nanoporous films annealed at 550°C and 650°C

Properties	Fe_2TiO_5 (650 °C) (measured)	Fe_2O_3 (reported)[26]
Resistivity (Ohm*cm)	1289.65	100
Mobility (cm^2/Vs)	6.32	0.01 - 1
Carrier Density (cm^{-3})	7.66×10^{14}	10^{16}
Types of Carriers	Electrons	Electrons

Figure B4: Electrical properties of Fe_2TiO_5 thin films (measured by Hall Measurement) and Fe_2O_3 (reported earlier)

Appendix C: Fe_2O_3/Fe_2TiO_5 Heterojunction as a photoanode with improved charge separation and transport

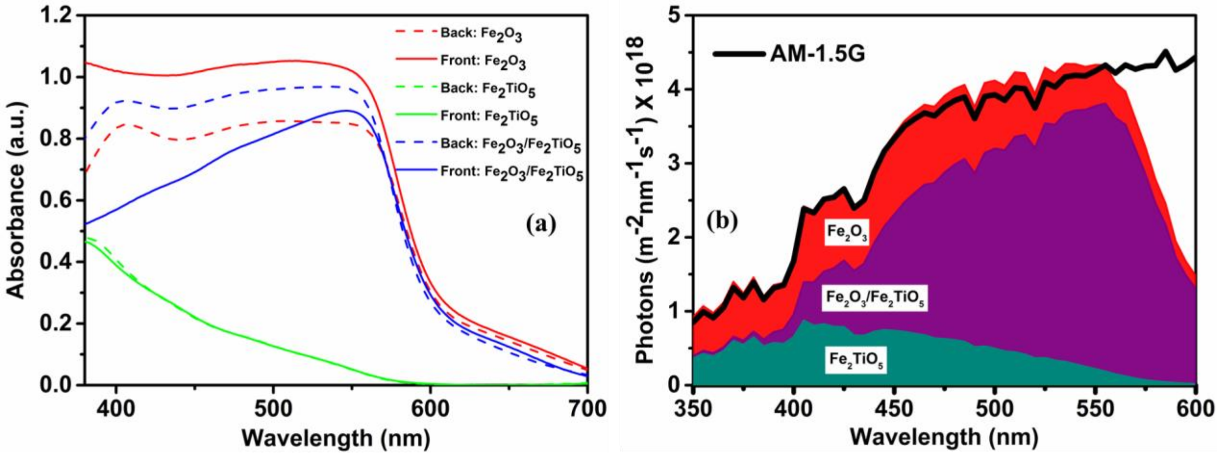

Figure C1: (a) Plots of Absorption Spectra, and (b) Number of Photons absorbed from the solar visible light spectrum, for Pristine and Heterojunction thin films

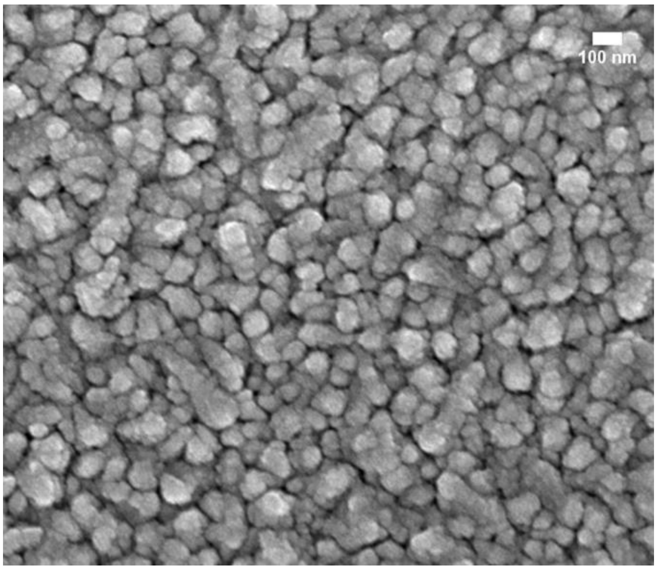

Figure C2: Crystalline nanoporous Fe_2TiO_5 thin films fabricated at 120°C, 12 hrs.

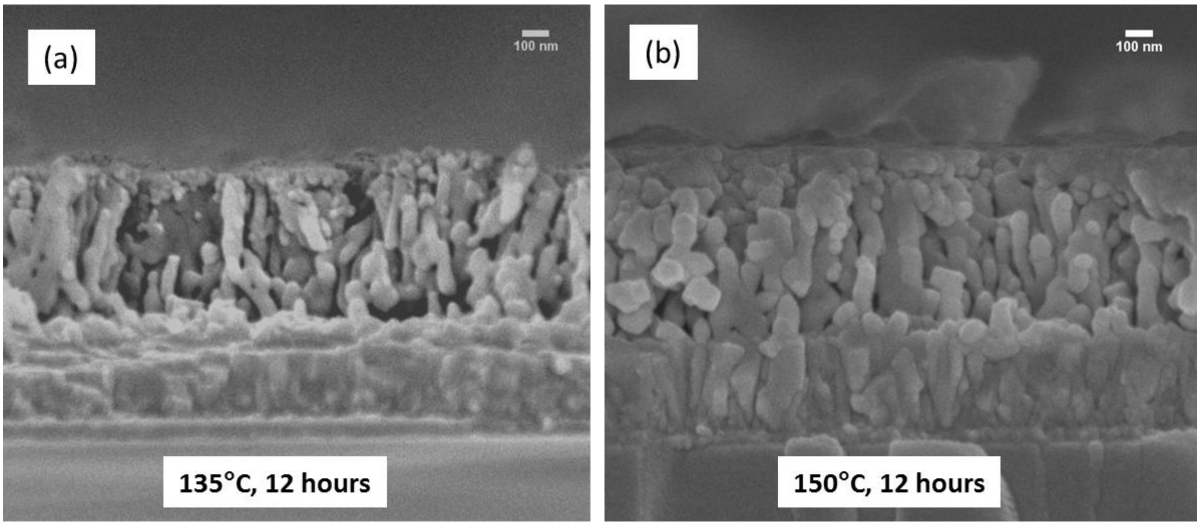

Figure C3: FESEM Cross-section Image of Fe_2O_3/Fe_2TiO_5 thin film deposited at (a) 135ºC, 12 hrs. and (b) 150ºC, 12 hrs.

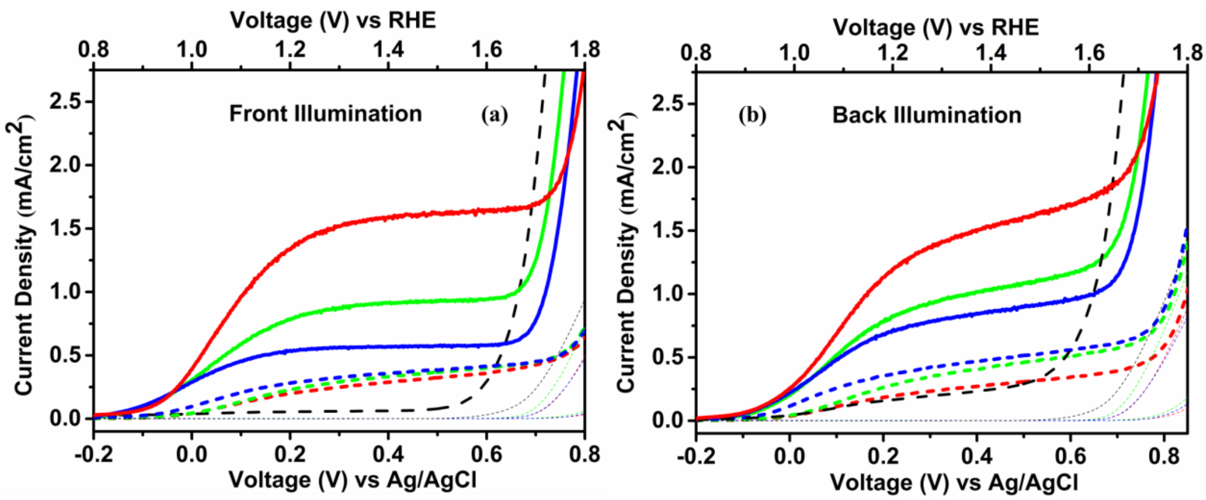

Figure C4: J-V Plots under (a) frontside and (b) backside illumination, for Heterojunction (represented as solid curves), Pristine Fe_2TiO_5 thin films (dashed curves) fabricated at different reaction temperatures of 120ºC (red), 135 ºC (green) and 150 ºC (blue) for 12 hours. Pristine Fe_2O_3 nanorods are represented as dashed black curve

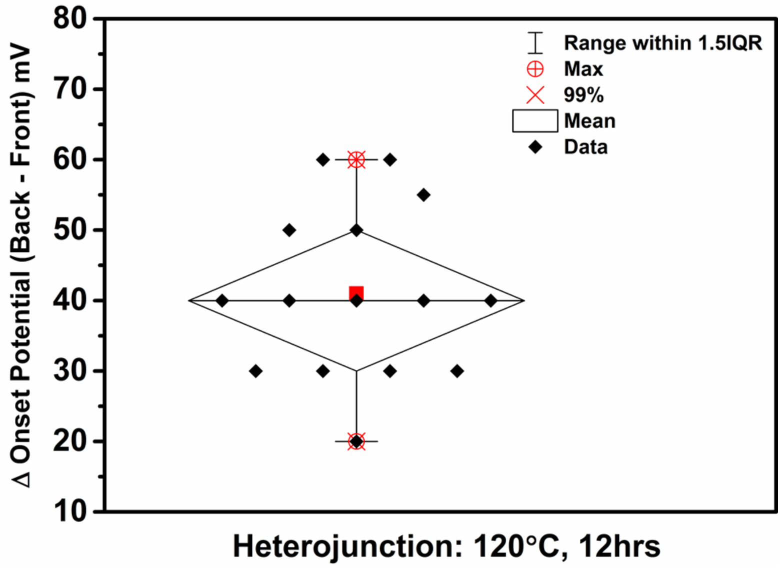

Figure C5: Box chart of onset potential difference for optimized heterojunction samples fabricated at 120°C, 12hrs

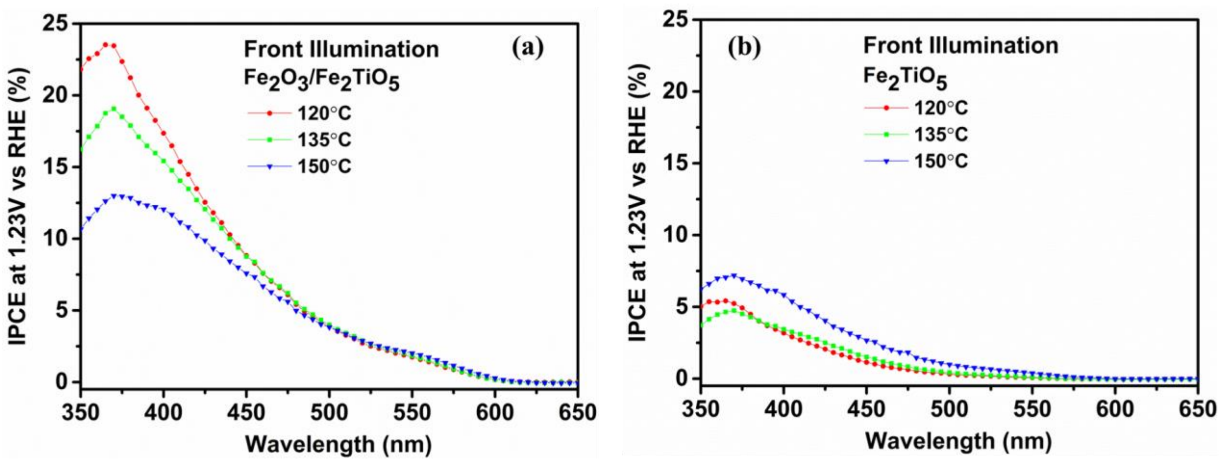

Figure C6: IPCE Spectra of Fe_2O_3/Fe_2TiO_5 heterojunction and pristine Fe_2TiO_5 thin films under front illumination for different reaction temperatures

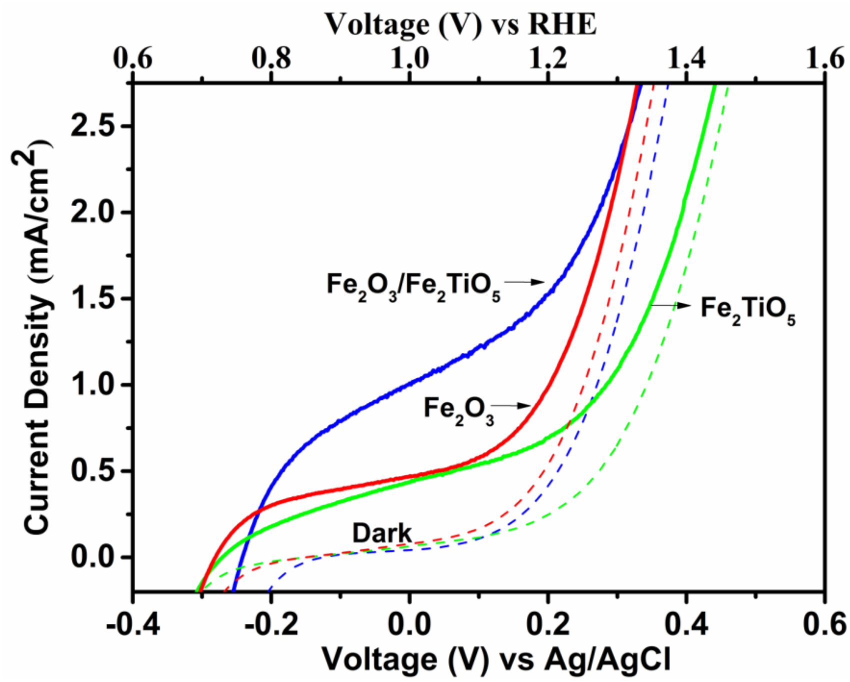

Figure C7: J-V Plots for heterojunction and pristine films under the influence of hole scavenger (H_2O_2) with frontside illumination

List of Publications

- **Prince Saurabh Bassi**, Gurudayal, Lydia Helena Wong and James Barber; "Iron based photoanodes for solar fuel production"; *Phys. Chem. Chem. Phys*., *2014,16, 11834-11842*

- **Prince Saurabh Bassi**, Sing Yang Chiam, Gurudayal, James Barber and Lydia Helena Wong; *"*Hydrothermal Grown Nanoporous Iron Based Titanate, Fe_2TiO_5 for Light Driven Water Splitting"; *ACS Appl. Mater. Interfaces, 2014, 6 (24), pp 22490–22495*

- **Prince Saurabh Bassi**; "Crystalline Fe_2O_3/Fe_2TiO_5 Heterojunction for Solar Water Oxidation: Controllable Synthesis and Efficient Hole Injection into Electrolyte"; *Nano Energy, Volume 22, April 2016, 310–318*

- Xianglin Li, **Prince Saurabh Bassi**, Pablo Boix, Yanan Fang, Lydia H Wong; "Revealing the role of TiO_2 surface treatment of hematite nanorods photoanodes for solar water splitting"; *ACS Appl. Mater. Interfaces*, *2015, 7 (31), 16960–16966*

- Lifei Xi, **Prince Saurabh Bassi**, Sing Yang Chiam, Wai Fatt Mak, Phong D. Tran, James Barber, Joachim Say Chye Loo and Lydia Helena Wong; "Surface treatment of hematite photoanodes with zinc acetate for water oxidation"; *Nanoscale, 2012,4, 4430-4433*

- Lifei Xi, Phong D Tran, Sing Yang Chiam, **Prince Saurabh Bassi**, Wai Fatt Mak, Hemant Kumar Mulmudi, Sudip K Batabyal, James Barber, Joachim Say Chye Loo, Lydia Helena Wong; "Co_3O_4-decorated hematite nanorods as an effective photoanode for solar water oxidation"; *J. Phys. Chem. C, 2012, 116 (26), pp 13884–13889*

- Gurudayal, Sing Yang Chiam, Mulmudi Hemant Kumar, **Prince Saurabh Bassi**, Hwee Leng Seng, James Barber and Lydia Helena Wong; "Improving the efficiency of hematite nanorods for photoelectrochemical water splitting by doping with manganese"; *ACS Appl. Mater. Interfaces, 2014, 6 (8), pp 5852–5859*

- Chen Yang, Phong D Tran, Pablo P Boix, **Prince S Bassi**, Natalia Yantara, Lydia H Wong, James Barber; "Engineering a $Cu_2O/NiO/Cu_2MoS_4$ Hybrid Photocathode for H_2 Generation in Water"; *Nanoscale, 2014,6, 6506-6510*

Conferences

- **Prince Saurabh Bassi**, Lydia Helena Wong; "Investigation into Pseudobrookite (Fe_2TiO_5) as a Photoanode for Solar Water Splitting"; *20th International Conference on Conversion and Storage of Solar Energy, IPS 20, 2014,* Germany
- **Prince Saurabh Bassi**, Lydia Helena Wong; "Investigation of Iron-based Semiconductors for Application as a Photocatalyst for Solar Water Splitting"; *International Conference on Materials for Advanced Technologies (ICMAT), 2013,* Singapore